University of Pennsylvania
ScholarlyCommons

Publicly Accessible Penn Dissertations

1-1-2014

Top-Down Control of Serotonergic Systems in Socioaffective Choices and Depression-Like Behaviors

Collin Challis
University of Pennsylvania, cchallis@mail.med.upenn.edu

Follow this and additional works at: http://repository.upenn.edu/edissertations

 Part of the Neuroscience and Neurobiology Commons

Recommended Citation
Challis, Collin, "Top-Down Control of Serotonergic Systems in Socioaffective Choices and Depression-Like Behaviors" (2014). *Publicly Accessible Penn Dissertations*. 1230.
http://repository.upenn.edu/edissertations/1230

This paper is posted at ScholarlyCommons. http://repository.upenn.edu/edissertations/1230
For more information, please contact libraryrepository@pobox.upenn.edu.

Top-Down Control of Serotonergic Systems in Socioaffective Choices and Depression-Like Behaviors

Abstract
Regulation of social behaviors is necessary to achieve social inclusion, establish relationships and sustain those relationships through adversity. Impairments in socio-emotional function and competence are prominent and debilitating features of major depression, yet are not traditionally recognized as cardinal symptoms of the disease. However, these deficits often persist in patients whose other mood symptoms have remitted and can predict risk of relapse, indicating an important role as a vulnerability factor. Understanding the neurobiology of socioaffective dysfunction in depression is thus important for determining the pathology of the disorder and developing effective treatments. Human imaging studies of depressive patients have consistently reported abnormal activity in the ventromedial prefrontal cortex (vmPFC), an area important for emotional processing and social cognition. Tracing studies in animals and tractography in humans have shown that the dorsal raphe nucleus (DRN) is a major projection target of the vmPFC. The DRN contains the most serotonin (5-HT) producing neurons in the brain and its output has been shown to regulate behaviors along an affiliative-agonistic axis, however it is neuronally heterogeneous. This thesis investigated the cytoarchitecture of the vmPFC-DRN microcircuit and its relevance to socioaffective behaviors using genetic mapping, whole cell electrophysiology and optogenetics. I showed that GABAergic neurons, which are the primary non-serotonergic neuronal population in the DRN, mediated top-down projections from the vmPFC onto mood-regulating 5-HT neurons and demonstrated the relevance of this pathway in mediating socioaffective decisions using the chronic social defeat stress (CSDS) paradigm. In addition, I used deep brain stimulation of the vmPFC as an antidepressant model to show that therapeutic response may rely on restoring the excitatory/inhibitory balance of inputs to 5-HT neurons. Together, these results will provide a better understanding of socioaffective circuitry and could lead to the development of more effective and efficient strategies to treat mood disorders.

Degree Type
Dissertation

Degree Name
Doctor of Philosophy (PhD)

Graduate Group
Neuroscience

First Advisor
Olivier Berton

Keywords
behavior, depression, dorsal raphe, optogenetics, serotonin, socioaffective

Subject Categories
Neuroscience and Neurobiology

This dissertation is available at ScholarlyCommons: http://repository.upenn.edu/edissertations/1230

This dissertation is available at ScholarlyCommons: http://repository.upenn.edu/edissertations/1230

TOP-DOWN CONTROL OF SEROTONERGIC SYSTEMS IN SOCIOAFFECTIVE CHOICES AND DEPRESSION-LIKE BEHAVIORS

Collin M. Challis

A DISSERTATION

in

Neuroscience

Presented to the Faculties of the University of Pennsylvania

in

Partial Fulfillment of the Requirements for the

Degree of Doctor of Philosophy

2014

Supervisor of Dissertation

_____

Olivier Berton, Ph.D.

Assistant Professor of Neuroscience in Psychiatry

Graduate Group Chairperson

_____

Joshua I. Gold, Ph.D.

Professor of Neuroscience

Dissertation Committee:

Sheryl G. Beck, Ph.D., Emeritus Faculty

Gregory C. Carlson, Ph.D., Assistant Professor of Neuroscience in Psychiatry

Christopher M. Fang-Yen, Ph.D., Assistant Professor of Neuroscience

Ming-Hu Han, Ph.D., Assistant Professor of Pharmacology and Systems Therapeutics, and Neuroscience, Icahn School of Medicine at Mount Sinai

TOP-DOWN CONTROL OF SEROTONERGIC SYSTEMS IN SOCIOAFFECTIVE CHOICES AND DEPRESSION-LIKE BEHAVIORS

COPYRIGHT

2014

Collin M. Challis

This work is licensed under the
Creative Commons Attribution-
NonCommercial-ShareAlike 4.0
License

To view a copy of this license, visit:
http://creativecommons.org/licenses/by-nc-sa/4.0/

Acknowledgments

When I came to Philadelphia five years ago I barely knew what a neuron was and now I have a doctorate in neuroscience. This would not have been possible at all without the help from many individuals and so I want to thank everyone who was there to lend a hand along the way.

First and foremost I would like to thank my mentor, Dr. Olivier Berton, for guiding me throughout an amazing project. Our meetings usually resulted in ten new ideas for experiments, but you provided a great atmosphere to help me accomplish as many of those as I could. Without your advising I would not be ready to start the next chapter in my professional life.

I would like to thank the members of my thesis committee – Dr. Greg Carlson, Dr. Sheryl Beck and Dr. Chris Fang-Yen – for all of the advice given during our meetings and for helping finish the donut holes of which I always managed to bring too many. A special thanks goes to Sheryl, who often acted as a second mentor by training me in everything electrophysiology related.

I would like to thank the Neuroscience Graduate Group at UPenn for creating an environment that has been accommodating, collaborative and exciting. It would be difficult to find another group of people that is as bright, fun and weird as you all.

I would like to thank my former advisor, Dr. Cary Lai, for taking a chance on me. Relocating with your lab from California to Indiana for a "change in scenery" sparked my interest in neuroscience and had a positive impact I could not have known at the time.

I would like to thank my parents, Dalia and Graham, and sister, Laura, for all the encouragement and guidance you've given me over the years. Everything you've provided and done for me has fueled my passions and ambitions and has shaped me into the person I am today.

Finally, I would also like to thank my fiancée – and shortly after this document is deposited, my wife – Rosemary, for being supportive, patient and understanding. Completing this dissertation would not have been possible without you.

ABSTRACT

TOP-DOWN CONTROL OF SEROTONERGIC SYSTEMS IN SOCIOAFFECTIVE CHOICES AND DEPRESSION-LIKE BEHAVIORS

Collin M. Challis

Olivier Berton

Regulation of social behaviors is necessary to achieve social inclusion, establish relationships and sustain those relationships through adversity. Impairments in socio-emotional function and competence are prominent and debilitating features of major depression, yet are not traditionally recognized as cardinal symptoms of the disease. However, these deficits often persist in patients whose other mood symptoms have remitted and can predict risk of relapse, indicating an important role as a vulnerability factor. Understanding the neurobiology of socioaffective dysfunction in depression is thus important for determining the pathology of the disorder and developing effective treatments. Human imaging studies of depressive patients have consistently reported abnormal activity in the ventromedial prefrontal cortex (vmPFC), an area important for emotional processing and social cognition. Tracing studies in animals and tractography in humans have shown that the dorsal raphe nucleus (DRN) is a major projection target of the vmPFC. The DRN contains the most serotonin (5-HT) producing neurons in the brain and its output has been shown to regulate behaviors along an affiliative-agonistic axis, however it is neuronally heterogeneous. This thesis investigated the cytoarchitecture of the vmPFC-DRN microcircuit and its relevance to socioaffective behaviors using genetic

mapping, whole cell electrophysiology and optogenetics. I showed that GABAergic neurons, which are the primary non-serotonergic neuronal population in the DRN, mediated top-down projections from the vmPFC onto mood-regulating 5-HT neurons and demonstrated the relevance of this pathway in mediating socioaffective decisions using the chronic social defeat stress (CSDS) paradigm. In addition, I used deep brain stimulation of the vmPFC as an antidepressant model to show that therapeutic response may rely on restoring the excitatory/inhibitory balance of inputs to 5-HT neurons. Together, these results will provide a better understanding of socioaffective circuitry and could lead to the development of more effective and efficient strategies to treat mood disorders.

Table of contents

List of tables

List of figures

Chapter 1

Introduction

Depression is a major public health concern that has been recognized as a distinct and serious condition for over 2000 years (Radden, 2003). Although definitions have varied, the core construct of depression has remained intact: a condition that is characterized by a negative affective state that resembles sadness but is crucially distinct in its severity, duration and lack of an identified trigger. In modern psychiatry, major depressive disorder (MDD) is broadly defined as a syndrome that includes recurring episodes of persistent dysphoria (decreased mood), anhedonia (loss of interest in pleasurable activities) and social withdrawal, and is associated with a combination of additional emotional, psychological and neurovegetative symptoms, highlighted in Table 1.1 (Fava and Kendler, 2000). For diagnosis, at least 5 symptoms in this constellation must persist for at least 2 weeks independent from normal grief and not be secondary to an obvious medical condition, use of a substance or other psychiatric disorder.

It is important to note that MDD is, by its very nature, a heterogeneous disorder. Although current textbook diagnostic classifications such as by the International Classification of Diseases (ICD) and Diagnostic and Statistical Manual of Mental Disorders (DSM) were developed to provide a common language based on observable signs, real-life depression presents in such a wide variety of forms related to polarity (unipolar, bipolar), symptoms (melancholic, atypical, psychotic, anxious), onset (specific events, seasons, age), recurrence and severity. This suggests that two patients that are clinically diagnosed with MDD may have only few symptoms in common. Furthermore,

although there is a substantial list of identified risk factors associated with MDD such as stressful life events and endocrine or immune abnormalities (hyperthyroidism and hypercortisolism), most depression episodes occur idiopathically and the current limited understanding of MDD etiology suffers from a lack of genuine biomarkers or depression genes. The multidimensionality and inter-individual heterogeneity of the depressive spectrum makes it illusory to develop a preclinical MDD model that reproduces the human syndrome in its entirety.

Table 1.1. Symptoms associated with MDD.

Psychological symptoms*	**Physical symptoms***	**Social symptoms**
Guilt, self-doubt or loss of self-esteem	Disturbances in sleep – insomnia or hypersomnia	Poor performance at work or school
Lack of interest, pleasure or enthusiasm	Abnormal psychomotor activity	Interpersonal difficulties at home or with family
Concentration or attention span is reduced	Fatigue or loss of energy	Avoidance of social contact
Recurring thoughts of death or suicide	Impaired appetite resulting in weight loss or gain	Neglecting hobbies or interests

In addition to depressed mood and sadness, listed are the core symptoms associated with MDD. It is important to note that only symptoms in the categories marked with an asterisk are used to clinically diagnose MDD.

For MDD diagnosis, most core symptoms are subjective and clinical evaluation is language-based. In combination with the multidimensionality of the disease, modeling MDD in animals is a difficult task. Many animal paradigms that have been developed only capture a single domain of the disease (Berton et al., 2012; Buckholtz and Meyer-Lindenberg, 2012). This is in line with the Research Domain Criteria (RDoC) project

established by the National Institute of Mental Health that aims to redefine psychiatric illnesses using dimensional rather than categorical definitions (Insel, 2014). Given this general goal of understanding the core symptomatic domains of MDD, most neurobiological studies to date have focused on low mood and anhedonia. These studies have identified brain systems implicated in punishment and reward such as the amygdala and ventral tegmental area (VTA), where function is largely conserved between human and animal models. In contrast, little attention has been paid to the alterations in social functioning associated with depression. Humans suffering from MDD often either withdraw socially or excessively seek reassurance from others (Willner et al., 2013).

Clinical research has also focused on determining the neural circuits the underlie MDD as it is thought that abnormal interactions between brain structures that regulate emotion trigger onset (Drevets et al., 2008; Hamilton et al., 2012). Using functional imaging, clinicians have detected several brain regions in depressive patients that appear to be dysfunctional when compared to healthy controls (Drevets et al., 2008; Liao et al., 2011; Mayberg, 1997; Mayberg, 2003) and are normalized when treated with pharmacologic antidepressants (Bellani et al., 2011; Delaveau et al., 2011; Drevets et al., 2002). In particular, these networks are primarily composed of frontal areas (i.e. anterior cingulate, prefrontal cortex) and limbic structures (i.e. amygdala, hippocampus). Recent studies have identified specific networks that are consistently recruited when individuals must make social approach or avoidance decisions (Billeke et al., 2013; Frith, 2007) and it is likely that dysfunction in these networks gives rise to the social symptoms observed in MDD (Derntl et al., 2011). The focus of this thesis is to increase our understanding of

the neurobiological circuits and mechanisms that contribute to social function and susceptibility to social stress.

Social interaction and impairment in MDD

Humans are social by nature, with almost all of our actions being directed towards or generated in response to other individuals. The ability to regulate the expression of social behavior in order to optimize social relationships and capitalize on opportunities in the social environment is referred to as social competence (Taborsky and Oliveira, 2012). Social competence depends on a multitude of cognitive abilities and is necessary to achieve social inclusion, establish nurturing interpersonal relationships and sustain these relationships in the face of adverse or threatening conditions. Critical to this is the ability to rapidly detect, appraise and interpret the emotional state of others using non-verbal socioemotional signals from a potential social partner. This allows adaptation through flexible social decision-making and efficient voluntary control of one's own instinctive avoidant and aggressive impulses. These mechanisms require the central nervous system to process available sensory cues, many of which are non-verbal such as body posture, movement and facial features (Cahn and Frey, 1992; Chang et al., 2013). Successful interactions are determined by the correct recognition, evaluation and reaction to these cues, a process that is often performed unconsciously (Morris et al., 1998). For humans, since face-to-face interactions are an important part of daily human visual communication, facial features are the most salient of these social cues that are recognized and can convey the emotional state and behavioral intentions of a social partner (Oosterhof and Todorov, 2009). Studies have shown that it can take under 50ms for an individual to observe, process and evaluate a facial stimulus (Todorov, 2008) and

that emotional sensory cues can rapidly activate behavioral tendencies in the perceiver, specifically approach or avoidance behaviors (Volman et al., 2011).

More than a third of the world's population is affected by mental illnesses at some point in life, with impairments in social competence being one of the most prominent and disabling features. Clinical research has shown that systems involved in social processing are dysfunctional in MDD and when these systems malfunction, the resulting deficits in social skills are a severely debilitating symptom (Romera et al., 2010). Central to the understanding of social perception in MDD is a cognitive bias where those diagnosed tend to view even neutral stimuli more negatively (Beck, 2008). This can lead to serious interpersonal difficulties or an extreme fear of judgment that results in social isolation (Derntl et al., 2011). Although these social deficits are well acknowledged as a domain of MDD, they are traditionally not viewed as a cardinal symptom of the disease, but rather as a secondary consequence of the depressive state (Table 1.1). However, clinical studies that included psychosocial stress as a measurable outcome have actually shown that impairment of social function persisted in MDD patients that had remitted of other depressive symptoms (Paykel, 2008). Therefore, the social deficits observed in depressed patients may indicate a susceptible endophenotype, while the ability to maintain sociability and affiliation, especially in the aftermath of traumatic interpersonal experiences, is one of the strongest early predictors of a resilient trajectory (Mathews and MacLeod, 2005).

Modeling social competence and MDD in animals

Social interaction is an extremely complex behavioral component and is important for many species, but is also a potential source of harm and danger. In social species,

animals interact frequently with their conspecifics and must adjust the expression of their social behavior according to previous social experiences and context. This behavioral flexibility in the social domain allows animals to navigate daily changes in the social environment and should be viewed as an adaptive performance trait that impacts Darwinian fitness such as avoiding risky social interactions or being ejected from a social group (Oliveira, 2009, 2012). Consequently, dealing with social complexity requires the evolution of cognitive mechanisms that allow individuals to assess the internal (i.e. emotional) state of other organisms and the social context in order to generate perceptual information meaningful for that moment in time. Thus, more than any other behavioral domain, it is expected that social behavior should exhibit high levels of plasticity.

There are major challenges when it comes to modeling social competence in animals and even larger challenges in modeling MDD, specifically whether symptoms of social withdrawal observed in humans can also be demonstrated in animals. Several rodent models have been developed for this purpose that use various stressors to induce behavioral adaptations that recapitulate MDD symptoms. These include learned helplessness, which capitalizes on despair through inescapable situations paired with foot or tail shocks (Chourbaji et al., 2005), and chronic mild stress, which exposes subjects to repeated unpredictable stressors (Willner, 2005). While subjects in these paradigms are responsive to pharmacologic antidepressant treatments, the behavioral readouts are often only one-dimensional. Additionally, these models use foreign, artificial stressors, which have shown to have biological dissimilarities compared to more natural stressors (Vinkers et al., 2009).

The social defeat paradigm takes advantage of inherent animal behaviors to induce a depression-like state (Kudryavtseva et al., 1991). It uses social stress by exposing an insubordinate subject to a dominant one and is reflective of observations in humans where "bullies" prey on "victims" (Björkqvist, 2001). The model has been adapted for different species including rats (Koolhaas et al., 1997; Rygula et al., 2005), mice (Berton et al., 2006; Krishnan et al., 2007), hamsters (Cooper and Huhman, 2007; Kollack-Walker et al., 1997) and primates (Kaplan et al., 2002; Shively et al., 1997) and has been shown to have strong predictive validity for MDD (Golden et al., 2013; Krishnan and Nestler, 2008). Social defeat sets itself apart from other models of MDD with the heterogeneous distribution of behavioral responses following social stress, which, as mentioned above, may be predictive criteria for the vulnerability to develop MDD in humans. The majority of animal subjects put through a standardized defeat protocol will display subsequent long lasting, generalized social avoidance while a smaller subpopulation will maintain social approach and are considered resilient (Krishnan et al., 2007). Complicating matters though is resilient subjects do appear to function normally in social situations, they are not devoid of symptoms as both vulnerable and resilient populations have been shown to exhibit metabolic syndromes and increased anxiety- and anhedonia-like behaviors (Krishnan et al., 2007; Lutter et al., 2008). Technical advances in neuroscience have allowed for the discrimination between the two subpopulations anywhere from a behavioral to a molecular level and with these tools, researchers can begin to probe the question of how adverse social experiences differentially modify neural circuits that result in susceptible or resilient phenotypes.

Serotonin influences social behaviors

Serotonin (5-HT) is a neuromodulator that has been shown to have a wide range of effects on the brain and behavior. The dorsal raphe nucleus (DRN) is one of the largest serotonergic nuclei in the brain and provides 5-HT to numerous other structures. Early characterization of the effects of 5-HT on behavior led it be synonymous with mood, however its actual role appears to be much more complex (Graeff et al., 1996). Studies across species have shown that altering levels of 5-HT has varying behavioral effects that consistently fall on an affiliative-agonistic axis (Young and Leyton, 2002). These observations have been made in a wide range of organisms including drosophila (Alekseyenko et al., 2010), lobsters (Kravitz, 2000), crickets (Stevenson and Schildberger, 2013) and zebrafish (Teles et al., 2013).

In humans, clinical researchers have found that artificially depleting or boosting 5-HT in healthy individuals can induce negative or positive shifts in social perception respectively (Bilderbeck et al., 2011; Crockett et al., 2013; Crockett et al., 2012; Geurts et al., 2013; Harmer et al., 2004; Robinson et al., 2013; Young, 2013). Patients suffering from MDD have been shown to have dysfunctional 5-HT systems. Functional imaging studies have shown decreased grey matter in the DRN of MDD patients (Lee et al., 2011) while post-mortem tissue from MDD suicide victims revealed differences in levels of 5-HT receptors (Stockmeier et al., 1997) and tryptophan hydroxylase, the 5-HT synthesizing enzyme, in the DRN (Boldrini et al., 2005). Thus, it is likely that a dysfunctional DRN and 5-HT systems can induce significant negative shifts in social perception, similar to those observed in tryptophan depletion studies performed in humans (Passamonti et al., 2012; Rogers, 2011). Complicating matters is that despite being the largest serotonergic nucleus, over half of the neuronal population in the DRN is

non-serotonergic (Fu et al., 2010). The DRN has been shown to contain glutamatergic (Xie et al., 2012), GABAergic (Gocho et al., 2013) and dopaminergic (Dougalis et al., 2012) neurons in addition to the 5-HT population. It still remains to be determined how these cellular populations interact with each other and also with a 5-HT population that has differential physiological properties dependent on anatomical location (Calizo et al., 2011; Crawford et al., 2010, 2011).

Ventromedial prefrontal cortex and socioemotional processing

The ventromedial prefrontal cortex (vmPFC) is a cluster of anatomically defined brain regions located in the frontal lobe. These areas include Brodmann areas 10, 11, 12, 13, 14, 25 and 32 though there is not a universal agreement on the delineation of vmPFC borders (Haber and Knutson, 2010). The vmPFC was identified based on functional imaging data in humans that shows activation of these regions in response to the same stimuli (Der-Avakian and Markou, 2012; Finger et al., 2008; Phan et al., 2002). From this, the vmPFC has been classically described as a control center for executive function, emotional processing, autonomic control and social cognition and is thought to orchestrate thoughts and actions in accordance with internal goals (Fuster, 2000; Miller and Cohen, 2001). Further PET and fMRI imaging has shown that the vmPFC is activated during the recall of emotional memories and when done in conjunction with eye tracking, suggests its importance in social attention and the processing of social sensory information (Adolphs, 2014; Winecoff et al., 2013; Wolf et al., 2014). It is likely that the vmPFC coordinates this information with subcortical and limbic structures to initiate social behavioral decisions. This is supported by more recent studies that have correlated

neural function via EEG or fMRI and the assessment of social approach or avoidance (Boksem et al., 2012; Quirin et al., 2013).

In 1990, Damasio and colleagues characterized the behaviors of 6 patients that were suffering from frontal lesions. They found these individuals to be sociopathic as they had abnormal autonomic responses to presented images of social stimuli (Damasio et al., 1990). More recent functional imaging has shown metabolic and activity changes in the vmPFC of patients with MDD. Decreases in vmPFC activity have been reported using PET and fMRI imaging in MDD patients compared to healthy controls, while a separate study found an increase in glutamate levels in the vmPFC (Drevets et al., 1997; Liao et al., 2011; McEwen et al., 2012). Meanwhile, antidepressant treatments have been able to reverse these functional changes. Two converging studies have demonstrated using PET imaging that MDD patients exhibited higher metabolism in the prefrontal cortex versus healthy controls, which was reduced by treatment with pharmacologic antidepressants or interpersonal cognitive therapy (Brody et al., 2001; Drevets et al., 2002). Morphological abnormalities have also been found in the prefrontal cortex of MDD patients, with several groups reporting decreases in grey matter that were also reduced by treatment with sertraline (Smith et al., 2013; Vasic et al., 2008). These morphological changes have likewise been observed in the vmPFC of rodents that were put through stressful conditions reflective of precipitating factors for MDD (Brown et al., 2005; Izquierdo et al., 2006; Muhammad et al., 2012). Lastly, experimental use of vmPFC-targeted deep brain stimulation (DBS) has been shown to be effective in improving the mood of MDD patients who were previously resistant to the effects of pharmacologic treatments (Lozano et al., 2008; Mayberg et al., 2005), though the effects

on social behaviors have not been fully explored. Interestingly, preclinical work by Hamani and colleagues has shown that DBS of the vmPFC recruits and alters the plasticity of the DRN and serotonergic projections (Hamani et al., 2010; Hamani et al., 2011; Hamani et al., 2012) and thus, it is likely that the vmPFC coordinates with the DRN to influence affective states and social behaviors.

vmPFC-DRN pathways

Probabilistic tractography uses diffusion tensor imaging to characterize the microstructure and organization of white matter fiber tracts and studies seeking to identify key downstream regions mediating vmPFC DBS therapeutic activity have identified the DRN as a required structure (Gutman et al., 2009; Lehman et al., 2011). There have been a number of retrograde and anterograde tracing studies that have shown that the vmPFC sends direct afferents to the DRN (detailed in Tables 1.2 and 1.3), however questions remain pertaining to the cytoarchitecture of the circuit. For one, there is no consensus on the definition of the vmPFC and its anatomical location varies across studies. In lower mammals in which these tracing studies were performed, the vmPFC is often defined as a combination of the infralimbic (IL) and prelimbic (PL) cortex, however these two regions appear to have opposing functions. Fear studies have shown that IL is important for extinction consolidation and retrieval while the PL plays a role in fear expression and resistance to extinction (Quirk et al., 2000; Senn et al., 2014). In mice, it is difficult to isolate the IL from the PL, as there are no neurochemical markers that distinguish each region and physical manipulations are often not precise enough to target one region over the other. A few of the tracing studies that used rats or non-human primates to differentiate between the two regions presented strong evidence showing the

PL to be the primary region of the vmPFC that provides input to the DRN (Chiba et al., 2001; Gabbott et al., 2005; Vertes, 2004) (Tables 1.2 and 1.3). These studies also find that these projecting neurons localize to layer V (Aghajanian and Wang, 1977; Gabbott et al., 2005) where excitatory pyramidal neurons are typically found (Hattox and Nelson, 2007).

It has been shown that the majority of vmPFC projections to the DRN are glutamatergic (Commons et al., 2005; Soiza-Reilly and Commons, 2011), however several studies suggest that these afferents target GABAergic rather than 5-HT neurons (Jankowski and Sesack, 2004; Varga et al., 2001). While the basic properties of these neurons have been characterized (Gocho et al., 2013; Shikanai et al., 2012), how they fit into vmPFC-DRN circuitry is not fully understood. Local release of GABA within the DRN has been observed, but it was not determined whether this was from local or projecting neurons, though it is strongly suggested that GABA is released from interneurons (Pan and Williams, 1989; Wilson and Gallager, 1988). If this were the case, GABAergic neurons in the DRN would be positioned to gate the top-down projections from the vmPFC onto mood regulating 5-HT neurons (Fig. 1.1). Pharmacologic activation of GABA-B receptors in the DRN increases aggression (Takahashi et al., 2012; Takahashi et al., 2010) and the local GABA population in the DRN responds to stress (Ishida et al., 2002; Roche et al., 2003). Thus, DRN GABAergic neurons represent a population that may be critical for socioemotional perception. The work described in this thesis will probe the function of these DRN GABA neurons as well as descending excitatory inputs from the vmPFC to the DRN in the context of socioaffective decisions and depression-like behaviors.

I hypothesized that DRN GABAergic neurons were preferential targets of glutamatergic vmPFC afferents and were critically positioned to gate these influences onto mood-regulating 5-HT neurons. Based on this, I also hypothesized that silencing DRN GABA neurons directly or vmPFC projections to the DRN would disinhibit 5-HT neuronal activity and produce an antidepressant-like effect during social defeat paradigm, preventing social avoidance.

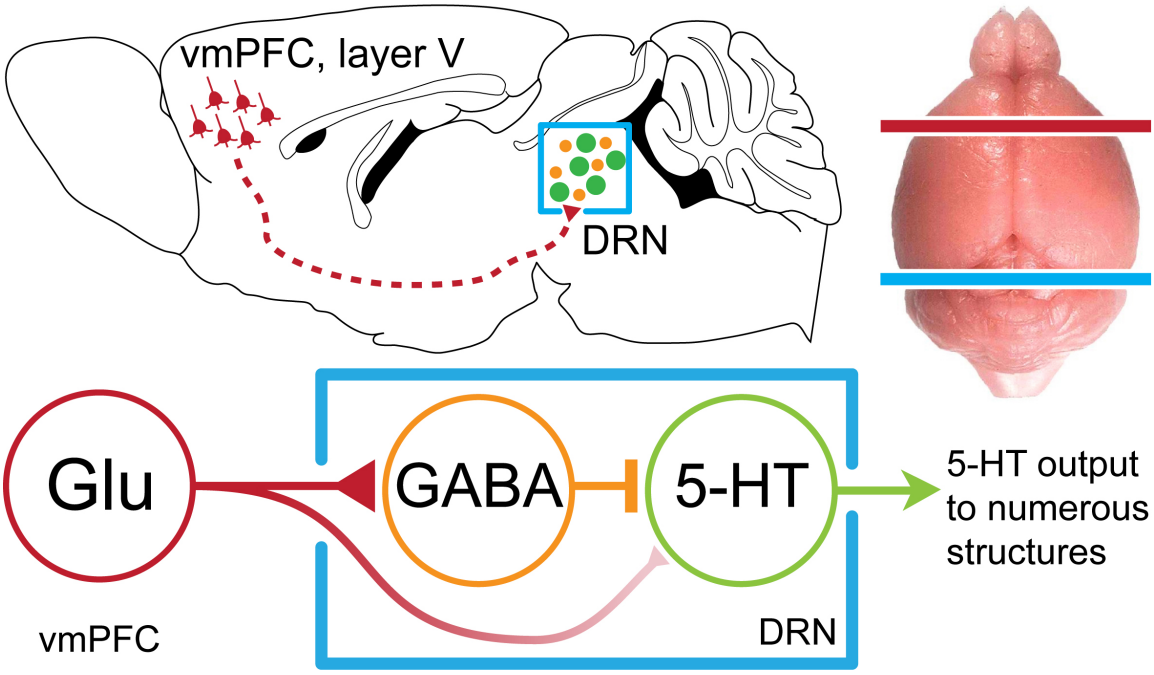

Figure 1.1. Overview of vmPFC-DRN circuitry.

Based on data from previous tracing studies, glutamatergic layer V vmPFC neurons send afferents to the DRN that preferentially synapse on GABA interneurons, which then locally inhibit 5-HT neurons and gate serotonergic output.

Table 1.2. List of anterograde tracing studies originating in the vmPFC.

Citation	Tracer	Injection site	Species
Chiba et al., 2001 *Brain Res*	BDA	IL (weak), PL (medium), Cg3 (medium)	Macaca fuscata (Japanese monkey)
Freedman et al., 2000, *J Comp Neurol*	PHA-L, BDA, RDA	Subgenual cortex (area 25, medium)	Rhesus monkey
Hajos et al., 1998, *Neurosci*	PHA-L	IL (strong), DP (strong)	Sprague-Dawley rat
Hurley et al., 1991, *J Comp Neurol*	PHA-L	IL	Sprague-Dawley rat
Jankowski and Sesack, 2004, *J Comp Neurol*	BDA	vmPFC	Sprague-Dawley rat
Lee et al., 2003, *Brain Res*	PHA-L	PL, IL, DP	Long-Evans hooded rat
Peyron et al., 1998, *Neurosci*	PHA-L	IL (medium), DP (strong), Cg (strong)	OFA rat
Sesack et al., 1989, *J Comp Neurol*	PHA-L	mPFC (strong)	Sprague-Dawley rat
Takagishi et al., 1991, *Brain Res*	PHA-L	IL	Sprague-Dawley rat
Vertes, 2007, *Synapse*	PHA-L	PL (strong), IL (weak)	Sprague-Dawley rat

Selected tracing studies looking at downstream targets of the vmPFC. Injection sites are verbatim from cited article as well as strength of signal if reported. BDA – biotinylated dextran amine, PHA-L – *Phaseolus vulgaris* leukoagglutinin, RDA – rhodamine-labeled dextran amine, vmPFC – ventromedial prefrontal cortex, IL – infralimbic cortex, PL – prelimbic cortex, DP – dorsal peduncular cortex, Cg – cingulate cortex

Table 1.3. List of retrograde tracing studies originating in the DRN.

Citation	Tracer	Retrograde targets	Species
Aghajanian and Wang, 1977, *Brain Res*	HRP	PFC (layer V, medium)	Albino rat
Gabbott et al., 2005, *J Comp Neurol*	WGA-HRP	PL (layer V, strong), IL (weak)	Sprague-Dawley rat
Goncalves et al., 2009, *Brain Res Bull*	CTb	PL (strong), IL (medium)	Wistar rat
Hajos et al., 1998, *Neurosci*	WGA-HRP, CTb	IL (strong), DP (strong), Cg3 (weak)	Sprague-Dawley rat
Lee et al., 2003, *Brain Res*	WGA-HRP (variant)	mPFC (strong)	Long-Evans hooded rat
Peyron et al., 1998, *Neurosci*	CTb	IL	OFA rat
Vazquez-Borsetti et al., 2009, *Cereb Cortex*	CTb	PL, IL, Cg	Wistar rat

Selected tracing studies looking at upstream inputs to the DRN. Injection sites are verbatim from cited article as well as strength of signal if reported. HRP – horseradish peroxidase, WGA – wheat germ agglutinin, CTb – cholera toxin B subunit, vmPFC – ventromedial prefrontal cortex, IL – infralimbic cortex, PL – prelimbic cortex, DP – dorsal peduncular cortex, Cg – cingulate cortex

Chapter 2

Raphe GABAergic neurons mediate the acquisition of avoidance following social defeat

Collin Challis[1,2], Janette Boulden[1], Avin Veerakumar[1], Julie Espallergues[1], Fair M. Vassoler[1], R. Christopher Pierce[1], Sheryl G. Beck[2,3], Olivier Berton[1,2]

[1]Department of Psychiatry, [2]Neuroscience Graduate Group, University of Pennsylvania Perelman School of Medicine, and [3]Department of Anesthesiology, Children's Hospital of Philadelphia and University of Pennsylvania Perelman School of Medicine, Philadelphia, PA 19104

Acknowledgments

This work was supported by grants from the National Institute of Mental Health (MH087581 to OB and MH0754047, MH089800 to SGB), from the International Mental Health Research Organization (IMHRO) to OB, from NARSAD to OB, and by NRSA (T32MH014654 and F31MH097386) to CC.

The work in this chapter was published in the *Journal of Neuroscience* in 2013:

Challis, C., Boulden, J., Veerakumar, A., Espallergues, J., Vassoler, F. M., Pierce, R. C., Beck, S. G., Berton, O. (2013). Raphe GABAergic neurons mediate the acquisition of avoidance after social defeat. *J Neurosci*, *33*(35), 13978–88.

Abstract

Serotonin (5-HT) modulates neural responses to socioaffective cues and can bias approach or avoidance behavioral decisions, yet the cellular mechanisms underlying its contribution to the regulation of social experiences remain poorly understood. We hypothesized that GABAergic neurons in the dorsal raphe nucleus (DRN) may participate in socioaffective regulation by controlling serotonergic tone during social interaction. We tested this hypothesis using whole-cell recording techniques in genetically identified DRN GABA and 5-HT neurons in mice exposed to chronic social defeat stress (CSDS), a model that induces long lasting avoidance behaviors in a subset of mice responsive to serotonergic antidepressants. Our results revealed that CSDS engaged DRN GABA neurons and drove GABAergic sensitization that strengthened inhibition of 5-HT neurons in mice that were susceptible, but not resilient to CSDS. Furthermore, optogenetic silencing of DRN GABA neurons disinhibited neighboring 5-HT neurons and prevented the acquisition of social avoidance in mice exposed to a social threat, but did not affect a previously acquired avoidance phenotype. We provide the first characterization of GABA neurons in the DRN that monosynaptically inhibit 5-HT neurons and reveal their key role in neuroplastic processes underlying the development of social avoidance.

Introduction

Studies in numerous species support a conserved role for the neurotransmitter serotonin (5-HT) in the modulation of social approach or avoidance behaviors (Canli and Lesch, 2007). In humans, pharmacological manipulations of 5-HT have been shown to shift appraisal and responses to social cues along an "affiliative-aggressive" axis (Young, 2013), with 5-HT depletion consistently facilitating socially defensive responses such as avoidance and aggression (Liu et al., 2010; Passamonti et al., 2012). In contrast, enhancement of 5-HT has been shown to induce rapid positive shifts in the perception of socioaffective stimuli, often promoting affiliation and dominance (Bilderbeck et al., 2011; Raleigh et al., 1991). These 5-HT-mediated effects could contribute to the therapeutic action of monoaminergic antidepressants by facilitating interpersonal function and promoting resilience to psychosocial threats such as social rejection, a common precipitant of the onset or relapse of affective disorders in vulnerable individuals (Charuvastra and Cloitre, 2008; Cusi et al., 2012; Hames et al., 2013; Meyer-Lindenberg and Tost, 2012; Phan et al., 2013; Slavich et al., 2010). Despite the existence of a large body of research on 5-HT, surprisingly little is known about the precise circuitry through which 5-HT neurons regulate cognitive processes associated with social approach or avoidance behaviors in mammals. Most ascending 5-HT neurons are found in the median and dorsal raphe nuclei (DRN) of the brainstem, however these two nuclei are neuronally heterogeneous and a large proportion of raphe neurons are non-serotonergic (Bang and Commons, 2012; Bang et al., 2012). Local GABAergic neurons in the DRN are thought to provide an inhibitory relay for converging inputs that exert top-down control over 5-HT function (Amat et al., 2005; Celada et al., 2001; Chiba et al., 2001; Freedman et al.,

2000; Varga et al., 2003; Varga et al., 2001). Pharmacological evidence further suggests that modulating GABA activity in the DRN has a dramatic impact on affiliative or aggressive behaviors (Takahashi et al., 2012; Takahashi et al., 2010), however our understanding of these mechanisms on a microcircuit level remains limited.

To analyze the interplay between GABAergic and 5-HT neurons in the DRN microcircuit and their regulation during social stress adaptative processes, we used transgenic mouse lines for genetic identification of these neuronal populations and selective targeting of optogenetic effectors for functional studies. We examined these mechanisms in the context of chronic social defeat stress (CSDS), a model of psychosocial stress that results in long lasting social avoidance and is sensitive to the effects of antidepressants (Berton et al., 2006; Tsankova et al., 2006). Our results provide direct functional evidence for the existence of DRN GABA neurons that monosynaptically inhibit 5-HT neurons and implicate experience-driven neuroplastic adaptations in these GABA neurons during the development of social avoidance. By providing novel insights about the cellular underpinnings of social approach or avoidance decision biases, our results have important implications for the understanding and treatment of affective disorders.

Materials and Methods

Animal subjects

Eight- to twelve-week old male mice bred onto a C57BL/6 background were used for all experiments. Mice were housed on a 12-hour light/dark cycle with food and water available *ad libitum*. All studies were conducted according to protocols approved by the University of Pennsylvania Institutional Animal Care and Use Committee. All procedures were performed in accordance with institutional guidelines. To generate a mouse line with fluorescently labeled *GAD65*-containing GABAergic or serotonergic neurons, male knockin *GAD2-Cre* mice (*Gad2*$^{tm2(cre)Zjh}$*/J*; JAX stock number 010802) (Taniguchi et al., 2011) or BAC transgenic *Pet1-Cre* mice (*B6.Cg-Tg(Fev-cre)*1Esd/J; JAX stock number 012712) (Scott et al., 2005) were respectively crossed to floxed-stop controlled *tdTomato* (RFP variant) mice (*B6.Cg-Gt(ROSA)26Sor*$^{tm9(CAG-tdTomato)Hze}$*/J*; JAX stock number 007908) (Madisen et al., 2010) to achieve fluorescent labeling of *Cre* containing cells. We also obtained BAC transgenic *GAD1-GFP* mice (*CB6-Tg(Gad1-EGFP)G42Zjh/J*; JAX stock number 007677) (Chattopadhyaya et al., 2004) for fluorescent labeling of *GAD67*-containing GABAergic neurons. In our behavioral experiments, we use the *GAD2-Cre* mice as well as the generated *GAD2-tdTomato* and *Pet1-tdTomato* mice, with the exception of the limited sensory contact defeat experiment where we use C57BL/6J (JAX stock number 000664) mice. All strains were procured from The Jackson Laboratory (Bar Harbor, ME).

Viruses and surgery

To express optogenetic or fluorescent proteins in GABAergic neurons, adeno-associated virus (AAV) vectors were produced by and purchased from the University of

Pennsylvania vector core (Philadelphia, PA) and injected into *GAD2-Cre* mice. In this work we used AAVs for the *Cre*-inducible expression of the inhibitory optogenetic probe *Archaerhodopsin* (AAV2/9.flex.CBA.Arch-GFP.W.SV40; Addgene #22222) and *Cre*-inducible expression of the fluorescent protein *tdTomato* (AAV2/1.CAG.FLEX.tdTomato.WPRE.bGH; Allen Institute #864). For tracing of excitatory vmPFC terminals in the DRN we used an AAV for the *CaMKIIa*-driven expression of *YFP* fused to *Channelrhodopsin* (AAV2/9.CaMKII.ChR2-YFP.SV40; Stanford) (Mattis et al., 2012).

For viral injections, mice were anesthetized with isofluorane and stereotaxically injected unilaterally in the DRN (from Lambda, in mm: 0.0 AP, +0.8 ML, -3.3 DV, 15° angle) or prelimbic region of the vmPFC (from Bregma, in mm: +1.8 AP, +0.8 ML, -2.7 DV, 15° angle) with 1µl of virus. Viral yields (in GC) were 6.962×10^{11} for *Arch-GFP*, 2.049×10^{12} for *tdTomato* and 4.347×10^{12} for *CaMKIIa-ChR2-YFP*. CSDS began 4 weeks post-surgery for non-cannulated mice to allow time for recovery and viral expression.

For *in vivo* optical stimulation, precut guide cannulae (Plastics One, Roanoke, VA) targeting the DRN were secured to the skull using the coordinates mentioned above. Cannulae were secured using stainless steel skull screws and acrylic cement. A fitted dustcap dummy was secured atop the guide cannula and mice were placed back in homecages and allowed 6 weeks to recover. Body weight and behavior was monitored during recovery. Three days before the start of experiment, a homemade fiber optic with ferrule connector (described below) was inserted into the guide cannula and secured with acrylic cement.

Preparation of optical fibers

A 200 μm core, 0.37 NA standard multimode fiber (Thorlabs, Newton, NJ) was stripped of cladding, passed through a 230 μm multimode ceramic zirconia ferrule (Precision Fiber Products, Milpitas, CA), and secured in place using fiber optic connector epoxy (Fiber Instrument Sales, Oriskany, NY). Ferrules were then polished and cut to length to target the DRN. They were tested for light output and sterilized with 70% ethanol.

Repeated social defeat training and interaction testing

The chronic social defeat (CSDS) paradigm consisted of alternating periods of physical contact with a trained CD1 aggressor (5 minutes) and protected sensory contact via separation by a perforated Plexiglass partition (24 hours). In trials where sensory contact was limited, mice were separated for only 20 minutes before returning to home cages overnight. This continued for 10 consecutive days with exposure to a novel aggressor each day as has been previously described (Espallergues et al., 2012; Golden et al., 2011). Control animals were housed in similarly partitioned cages with a paired mouse from the same genotype and were switched to opposite sides of the partition daily. On day 11, social approach or avoidance behavior toward an unfamiliar CD1 social target was assessed in a two-trial social interaction task. In the first 2.5-minute trial ("no target"), experimental mice explored a dimly lit (55 lux) open-field arena containing an empty wire mesh cage on one edge of the arena (see Figure 6A). In the second 2.5-minute trial ("target present"), experimental mice were reintroduced to the arena now with an unfamiliar CD1 aggressor positioned in the mesh cage. TopScan video tracking software (CleverSys, Reston, VA) was used to measure the time spent in the interaction zone

surrounding the target box. Interaction ratios (IR) were calculated as the time spent in the interaction zone in the "target present" condition as a percent of the time spent in the zone in the "no target" condition. Susceptible (SUS, IR<100) and Resilient (RES, IR>100) mice were determined as previously described (Krishnan et al., 2007).

Open Field Test and Elevated Plus Maze

For the open field test (OFT), mice were placed in the center of an arena identical to that which was used for the social interaction test described before, but lacking the mesh wire cage. The test lasted for 5 min and TopScan video tracking software was used to determine the amount of time spent in the center of the arena. OFT was conducted under 55 lux illumination. The elevated plus maze (EPM) consisted of two perpendicular, intersecting platforms, each 7.6 cm wide and 60 cm long positioned on a pedestal 30 cm from the floor. TopScan was also used to measure the time spent and number of entries in open and closed arms. Illumination of the open arms of the EPM was measured to be 10 lux.

Immunohistochemistry

Animals were transcardially perfused with 4% paraformaldehyde and brains were processed for standard single or dual immunolabeling methods as previously described (Espallergues et al., 2012). For detection of *cFos*, we used an affinity purified rabbit polyclonal antibody raised against the N-terminus of human *cFos* (SC-52, Santa Cruz Biotechnology, Santa Cruz, CA). To label 5-HT neurons we used a sheep anti-*TPH* antibody (AB1541, Millipore, Temecula, CA). For dual–labeling of *cFos* and Δ*FosB*, we used affinity purified goat anti-*cFos* (SC-52, Santa Cruz Biotechnology) and rabbit anti-Δ*FosB* (SC-48, Santa Cruz Biotechnology) antibodies. To enhance *GFP* expression we

used a chicken anti-*GFP* antibody (GFP-1020, Aves Labs, Inc., Tigard, OR). Primary antibodies were detected using fluorescent secondary antibodies obtained from Jackson ImmunoResearch Laboratories (West Grove, PA). For the processing of the brain slices from electrophysiology we used mouse anti-*TPH* (T067, Sigma-Aldrich, St. Louis MO) along with either a donkey anti-mouse Alexa Fluor 488 (A21202, Invitrogen, Grand Island, NY) or donkey Anti-mouse Alexa Fluor 647 (A31571, Invitrogen), and the biocytin was visualized by streptavidin Alexa fluor 647 (S32357, Invitrogen) or streptavidin 594 (S11227, Invitrogen).

Cell counting

To quantify *cFos* or Δ*FosB* colocalization with *tdTomato*$^+$ or *GFP*$^+$ neurons, 30 µm serial sections of the DRN were collected every 120 µm between -4.36 mm and -4.96 mm from Bregma. Slices were stained for *cFos* or Δ*FosB* and labeled neurons were manually counted in the DRN of each section. Colocalization with *tdTomato* or *GFP* was defined as nuclear localization of the *cFos* or Δ*FosB* signal and was manually counted. There was not a significant variation of total number of *tdTomato*$^+$ or *GFP*$^+$ cells within each strain.

Electrophysiology

Brain slices were prepared as previously described (Calizo et al., 2011; Crawford et al., 2010; Crawford et al., 2013; Espallergues et al., 2012). The 200 µm coronal slices containing DRN were placed in aCSF (in mM, NaCl 124, KCl 2.5, NaH_2PO_4 1.25, $MgSO_4$ 2.0, $CaCl_2$ 2.5, dextrose 10, $NaHCO_3$ 26) at 37°C, aerated with 95% O_2/5% CO_2. After one hour, slices were kept at room temperature. Tryptophan (2.5 mM) was included in the holding chamber to maintain 5-HT synthesis, but was not in the aCSF perfusing the

slice in the recording chamber. Individual slices were placed in a recording chamber (Warner Instruments, Hamden, CT) and perfused with aCSF at 2 ml/min maintained at 32°C by an in-line solution heater (TC-324, Warner Instruments). Neurons were visualized using a Nikon E600 upright microscope fitted with a 60X water immersion objective and targeted under DIC or fluorescent filters. Resistance of electrodes was about 8-10 MOhms when filled with a recording solution composed of (in mM) K-gluconate (130), NaCl (5), Na phosphocreatine (10), $MgCl_2$ (1), EGTA (0.02), HEPES (10), MgATP (2) and Na_2GTP (0.5) with 0.1% biocytin and a pH of 7.3. Whole-cell recordings were obtained using a Multiclamp 700B amplifier (Molecular Devices, Sunnyvale, CA). Cell characteristics were recorded using current clamp techniques as previously described (Crawford et al., 2010; Espallergues et al., 2012). Signals were collected and stored using Digidata 1320 analog-to-digital converter and pClamp 9.0 software (Molecular Devices). Collection of EPSC data was as previously described (Crawford et al., 2011) and performed with bath application of 20 μM bicuculline to block GABA synaptic activity. Collection of IPSC data was performed as previously described (Crawford et al., 2013) with bath application of 20 μM DNQX to block AMPA/Kainate synaptic activity. All drugs were made in stock solutions, diluted on the day of the experiment and added directly to the ACSF.

Electrophysiology data analysis

Cellular characteristics were analyzed using Clampfit 9.0 (Molecular Devices). Synaptic properties were analyzed using MiniAnalysis (Synaptosoft, Decatur, GA) as previously described (Crawford et al., 2011; Crawford et al., 2013). Frequency-intensity plots were generated by measuring the number of action potentials generated by

depolarizing current steps ranging from 0 to 100 pA for *GAD2-tdTomato* or 0 to 120 pA for *Pet1-tdTomato* neurons in 20 pA increments. Average firing rate for each condition was determined by the number of action potentials generated over the 500 ms current pulse. Synaptic events were analyzed using parameters optimized for each cell with the detection threshold set beyond the maximum values of the all-points noise histogram for a portion of the trace containing no detectable synaptic events. This threshold generally ranged from 5 to 8 pA. MiniAnalysis generates a summary table containing the mean and median values for the frequency, amplitude, rise time (10-90%), decay time and event half width (50%). For each cell, at least 200 events were chosen at random and manually filtered to exclude multiple peaks then combined to obtain an averaged EPSC or IPSC for each cell to obtain values for decay time, event area, and event time half-width. The Kolmogorov-Smirnov test was used to determine whether the histograms and cumulative probability plots of the synaptic activity characteristics were different between each group. Additional statistical analysis is described below. Data reported are means ± SEM.

Optical stimulation

For *in vivo* stimulation, mice with previously implanted fiber optic ferrules were connected to a 200 μm, 0.37 NA patch cord via zirconia sleeve that was then connected to a diode-pumped solid-state (DPSS) laser through an FC/PC adaptor and rotary joint. We used a yellow (561 nm, GR-561-00100-CWM-SD-05-LED-F) DPSS laser obtained from OEM Laser Systems (Bluffdale, UT). For stimulation of *Arch* expressing *GAD2* neurons in the DRN we performed constant yellow light stimulation for 20 minutes. Power output was measured using an optical sensor (Thorlabs, Newton, NJ) to be about

10 mW. Intensity was calculated using a model predicting irradiance in mammalian tissues (http://www.stanford.edu/group/dlab/cgi-bin/graph/chart.php). From a 200 μm tip, estimated intensity was 7.05 mW mm^{-2} for yellow laser stimulation.

For stimulation of brain slices expressing *Arch* in *GAD2* neurons, a prepared 200 μm core, 0.37 NA standard multimode fiber was lowered into the recording chamber and submerged below ACSF. The tip of the fiber was positioned approximately 1 mm from the DRN, illuminating the entire region. Constant 10 mW yellow light stimulation was performed in 5 second epochs every 20 seconds. Laser intensity was estimated to be 10.01 mW mm^{-2}.

Data analysis and statistics

For multiple group comparisons, all variables were distributed normally based on Bartlett's test and analyzed using parametric statistics (i.e. one-, two-way ANOVAs, between group or with repeated measures, followed by Fisher's PLSD test where appropriate). Comparisons between two groups were performed using Student's t-test. Statistical analysis was performed using Statistica (StatSoft, Tulsa, OK). Statistical significance was defined as a p value < 0.05. All data are presented as the mean ± SEM. Outlying values (3 standard deviations from the mean) were excluded from group means.

Results

Induction of *FOS* proteins in the DRN by CSDS predominates in *GAD2*-containing GABA neurons

Prior studies using immediate early gene mapping have documented the activation of DRN neurons by stress (Paul et al., 2011; Roche et al., 2003). Our previous multilabel studies combining *in situ* hybridization detection of cell-type specific mRNA markers and immunohistochemical labeling of *FOS* family proteins, showed that 5-HT neurons represent only a minority (<10%) of DRN cells undergoing *FOS*-mediated neuroadaptations after repeated exposure to two models of depression (learned helplessness and CSDS) while a comparatively higher proportion of *FOS* labeled cells expressed *GAD* mRNA (Berton et al., 2007). Here we tested whether transgenic mouse lines with genetically labeled neurons would reveal a comparable distribution of *cFos* in the DRN after being subjected to CSDS. To assess the engagement of two major GABA neurons subtypes (i.e., $GAD1^{+}$ and $GAD2^{+}$) in the DRN, we examined CSDS-induced *cFos* in *GAD1-GFP* BAC transgenic mice that have fluorescently labeled *GAD67* neurons (Chattopadhyaya et al., 2004) (Fig. 2.1A) and also *GAD2-tdTomato* mice that were generated by crossing mice expressing *Cre* recombinase at the *GAD2 (GAD65)* locus (Taniguchi et al., 2011) with a double-floxed *tdTomato* reporter strain (Madisen et al., 2010) (Fig. 2.1D). A *Pet1-tdTomato* line was similarly generated to label 5-HT neurons (Scott et al., 2005) (Fig. 2.1G).

We subjected cohorts of adult male mice from these three lines to 10 consecutive days of CSDS as previously described (Berton et al., 2006; Golden et al., 2011). No differences were observed between *GAD1-GFP*, *GAD2-tdTomato* and *Pet1-tdTomato*

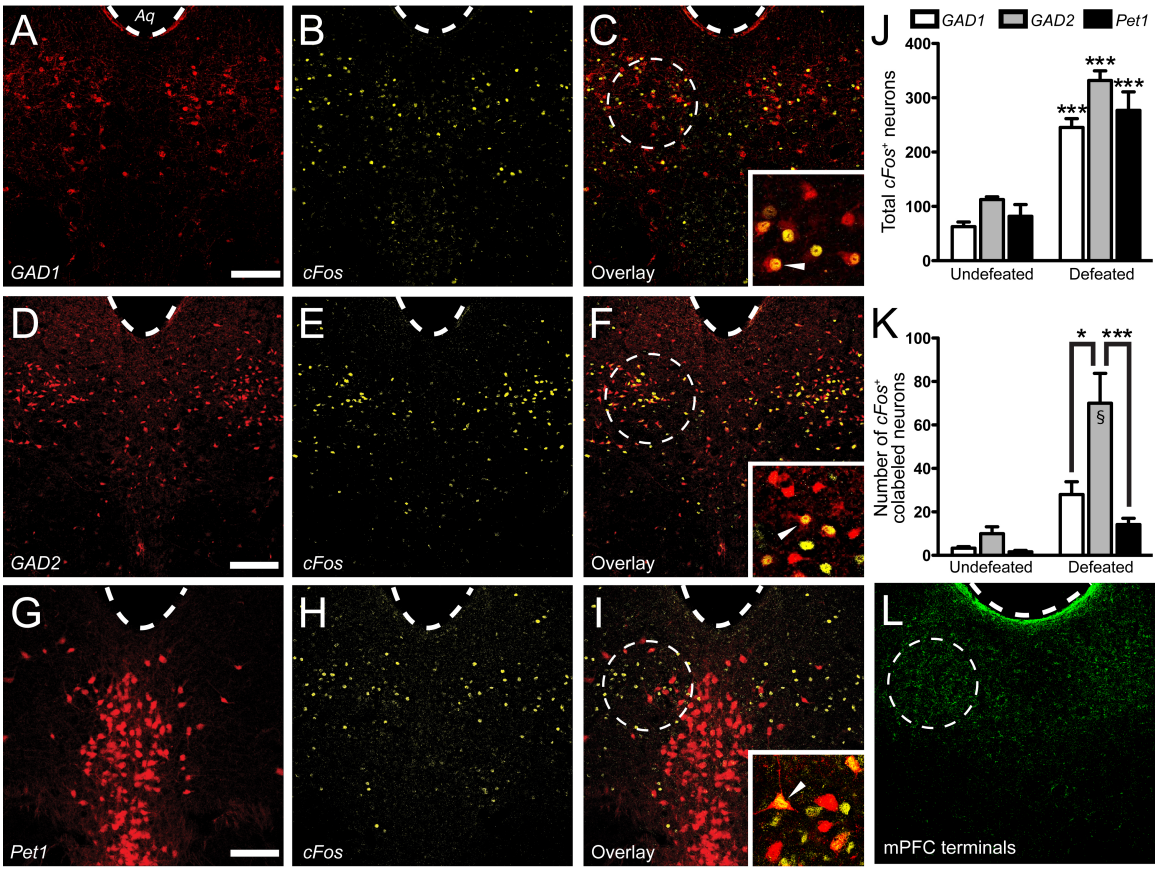

Figure 2.1. CSDS induced *cFos* expression predominated in *GAD2*-expressing GABAergic neurons in the DRN.

(A-I) Distribution of defeat-induced *cFos* in the DRN of **(A-C)** *GAD1-GFP* mice with fluorescently tagged *GAD67*$^+$ GABA neurons (pseudo-colored red for consistency) (D-F) *GAD2-tdTomato* mice with fluorescently tagged *GAD65*$^+$ GABA neurons, or **(G-I)** *Pet1-tdTomato* mice with fluorescently tagged 5-HT neurons. Note the striking overlap between *cFos* and *GAD2*-labeled GABAergic neurons. *Aq*, aqueduct; scale bar 50µm. High magnification (63X) images depicting *cFos* colocalization with fluorescently labeled neurons can be found in the insets of **(C)**, **(F)** and **(I)**. Examples of colocalized neurons are marked with a solid arrowhead.
(J) Lack of overall difference in total number of *cFos*$^+$ labeled DRN neurons after CSDS between *GAD2-tdTomato*, *Pet1-tdTomato* and *GAD1-GFP* mouse lines. Within strains there was a significant increase in total *cFos*$^+$ neurons after defeat compared to controls (Two-way ANOVA, Fisher post-hoc; *GAD2* ***p < 0.001; *Pet1* ***p < 0.001; *GAD1* ***p < 0.001; per genotype n = 3-5 for undefeated, n = 3-7 for defeat).
(K) Quantitation of *cFos* colocalization in GABA and 5-HT neurons of control and defeated mice. The defeated mice demonstrated significantly higher GABAergic *cFos* induction over controls. Overall *cFos* induction in *GAD2*-labeled neurons was significantly greater than in *Pet1*- or *GAD1*-labeled neurons. (Two-way ANOVA, Fisher post-hoc; *GAD2*/defeat vs *GAD1*/defeat *p = 0.033; *GAD2*/defeat vs *Pet1*/defeat ***p < 0.001; *GAD2*/defeat vs *GAD2*/undefeated §p < 0.001; n = 3-7 per group).
(L) Confocal image depicting the distribution of vmPFC axon terminals in the DRN after anterograde tracing of excitatory vmPFC neurons using AAV-mediated expression of *ChR2-YFP* driven by the *CaMKIIa* promoter. Note the dense clustering of tagged terminals in the lateral portion of DRN corresponding to the areas rich in *cFos* expressing GABAergic neurons after CSDS (dashed circles).

lines regarding their expression of social avoidance following CSDS (data not shown). Twenty-four hours after testing, mice were exposed to an additional CSDS experience and perfused one hour later. DRN slices from each strain were immunolabeled for *cFos* (Fig. 2.1B, 2.1E, 2.1H). A significant increase in total number of *cFos* labeled cells was observed in the DRN of defeated mice versus undefeated controls (Two-Way ANOVA, main effect of CSDS, $F_{(1,26)} = 60.22$, $p < 0.001$; for *GAD1*-labeled mice n = 3 for undefeated, 3 for defeated; for *GAD2*-labeled mice n = 4 for undefeated, 7 for defeated; for *Pet1*-labeled mice n = 3 for undefeated, 7 for defeated), without a significant difference between strains (Fig. 2.1J). Topographic distribution of *cFos* after repeated CSDS, which was circumscribed to the ventrolateral portions of the DRN where 5-HT cells are sparse, resembled the previously reported distribution of Δ*FosB*, which is another *FOS* variant induced by stress and is particularly enriched in DRN substance P neurons (Berton et al., 2007). Because topographical similarity suggests the same cell population may be expressing both *cFos* and Δ*FosB* after CSDS, we examined the level of colocalization between these two proteins in DRN neurons using immunolabeling. We found that 77.3 ± 6.9% of $cFos^+$ cells also expressed Δ*FosB* (n=3), making it likely that the CSDS-activated cells identified in this study overlap with the cellular population identified in our previous study (Berton et al., 2007). The relatively restricted localization of *cFos* to the lateral areas of the DRN also suggests it may be driven by descending inputs that are topographically distributed in this area. Viral tracing studies from the Allen Brain Atlas (Sunkin et al., 2013), corroborated by our own anterograde tracing data (Fig. 2.1L), indicate that one such afferent input originates from the ventromedial prefrontal cortex (vmPFC), an area thought to be important for social cognition (Roy et

al., 2012). Indeed, we observed a striking similarity between the distribution of anterogradely traced vmPFC axons and defeat induced *cFos* in the DRN (Fig. 2.1C, 2.1F, 2.1I, 2.1L).

Quantification of *cFos* colocalization with native *GAD1-GFP* (Fig. 2.1C), *GAD2-tdTomato* (Fig. 2.1F) or *Pet1-tdTomato* (Fig. 2.1I) fluorescence revealed significantly greater *cFos* induction in *GAD2*- compared to *GAD1*- and *Pet1*-labeled cells (Two-Way ANOVA, genotype x condition, $F_{(2,24)} = 12.79$, $p = 0.004$; Fig. 2.1K). Taken together, these results reinforce the notion that CSDS induces activation of DRN neurons and further demonstrates that GABAergic neurons, more specifically $GAD2^{+}$ neurons, are a predominant social stress-activated cell type in the DRN.

Sensitization of DRN GABA neurons in SUS mice after CSDS coincides with increased 5-HT inhibition

Given the significant increase in *GAD2*-specific GABAergic *cFos* induction after CSDS, we next examined functional adaptations following CSDS in this cell type by conducting whole-cell patch clamp recordings in midbrain slices from control and defeated mice. The use of the *GAD2-tdTomato* mouse line allowed us to unequivocally identify GABA cells for recordings. After defeating *GAD2-tdTomato* mice, we determined their social interaction, distinguishing between resilient (high social interaction, RES) and susceptible (low social interaction, SUS) subpopulations, and prepared brain slices for whole-cell patch clamp electrophysiology. We focused recordings in the ventrolateral area (i.e. lateral wings; Fig. 2.2A) of the DRN that show the highest density GABA cell distribution and *cFos* induction after CSDS (Fig. 2.1D-F)

and is also a region that receives strong excitatory input from the vmPFC (Fig 2.1L and inset of Fig. 2.2A) (Jankowski and Sesack, 2004).

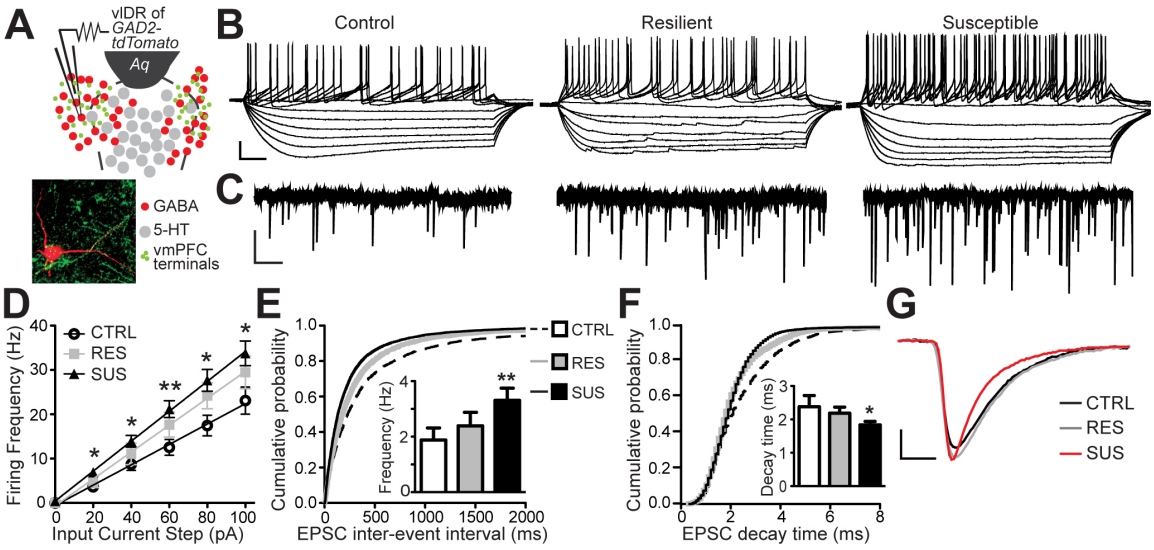

Figure 2.2. CSDS sensitized excitatory input and excitability of vmPFC-innervated DRN GABAergic neurons in SUS mice, but not in RES mice.

(A) Schematic of DRN topography in recorded slices from *GAD2-tdTomato* mice. *vlDR* – ventrolateral DRN, *Aq* – aqueduct. Recorded neurons were purposely selected in ventrolateral subregions of the DRN that are rich in afferents from the vmPFC. Inset depicts a high magnification confocal image of a biocytin-filled recorded *GAD2-tdTomato* neuron (red) in close contact with axon terminals from vmPFC neurons (green) anterogradely traced using AAV-*CaMKIIa-ChR2-YFP*.
(B) Raw data traces of membrane potential changes recorded from DRN GABA neurons in response to hyperpolarizing and depolarizing injection of current in control, Resilient, and Susceptible mice. Scale bar 20mV, 50ms.
(C) Representative voltage clamp traces of mEPSC synaptic activity in DRN GABA neurons from control, Resilient, and Susceptible mice. Scale bar 20pA, 500ms.
(D) Frequency-intensity plots showed increased excitability of DRN GABA neurons in Susceptible mice (Repeated measures ANOVA, Fisher post-hoc; SUS vs CTRL, 20pA *p = 0.030, 40pA *p = 0.034, 60pA **p = 0.008, 80pA *p = 0.012, 100pA *p = 0.025; Number of mice (number of neurons) = 7(29) for control, 4(20) for Resilient, 10(37) for Susceptible).
(E) Cumulative probability plot shows a shift to shorter inter-stimulus intervals of mEPSC synaptic activity in DRN GABA neurons of Susceptible mice versus control or Resilient mice (Kolmogorov-Smirnov test, $Z = 7.1402$, $p < 0.001$). Inset displays summary histogram showing significantly higher average mEPSC frequency in Susceptible mice (One-way ANOVA, Fisher post-hoc; SUS vs CTRL **p = 0.006).
(F) Cumulative probability plot of mEPSC decay time shows the shift to faster decay times in DRN GABA neurons of Susceptible mice (Kolmogorov-Smirnov test, $Z = 6.4021$, $p < 0.001$). Inset shows summary histogram depicting the significantly lower average mEPSC decay times in Susceptible mice versus control and Resilient mice (One-way ANOVA, Fisher post-hoc; SUS vs CTRL *p = 0.014).
(G) Enlarged depiction of averaged individual EPSC synaptic events in GABA neurons for each group. Scale bar 4pA, 2ms.

The intrinsic properties of DRN *GAD2*$^{+}$ GABA neurons were distinct from those of identified 5-HT cells (Crawford et al., 2010); notably they displayed a higher membrane resistance (*GAD2* = 944 ± 75 MOhms vs. *Pet1* = 583 ± 39 MOhms; *GAD2* Number of mice (number of cells) = 7(29), *Pet1* = 3(16)) and had shorter duration action potentials (*GAD2* = 1.68 ± 0.11 ms vs. *Pet1* = 2.4 ± 0.1). The GABA characteristics were similar to those of previously reported recordings from GABA neurons (Brown et al., 2008; McKenna et al., 2013; Wierenga et al., 2010). Furthermore, in contrast to 5-HT cells, which are silent in brain slice preparations, approximately 40% of recorded GABA neurons displayed spontaneous firing activity at an average rate of 6.6 ± 1.1 Hz. We next determined the membrane responses of these cells to 20 pA steps of depolarizing injected current (Fig. 2.2B) and found that DRN GABA neurons in SUS mice had a significant increase in the number of action potentials elicited versus controls. In contrast, cell excitability of GABA neurons in RES mice did not significantly differ from undefeated mice (Repeated measures ANOVA, defeat x input current, $F_{(2,460)} = 2.40$, $p = 0.010$; N(n)=7(29) for control, 4(20) for RES, 10(37) for SUS; Fig. 2.2B and 2.2D). We then asked whether excitatory synaptic inputs to these neurons had been changed by CSDS using voltage clamp techniques (Crawford et al., 2011). Recording of spontaneous glutamatergic EPSC activity from *GAD2-tdTomato* neurons in each behavioral group revealed a significant increase in the overall EPSC frequency in DRN GABA neurons of SUS mice compared to controls, but not in RES mice (One-way ANOVA, $F_{(2,78)}=4.08$, $p = 0.021$; Fig. 2.2C and inset histogram of Fig. 2.2E). This was confirmed by a significant shift in the cumulative probability plot of interstimulus intervals (Kolmogorov-Smirnov test, $Z = 7.14$, $p < 0.001$, Fig. 2.2E). In the presence of tetrodotoxin (TTX), mEPSC

frequency was not altered implying that the recorded excitatory events were not due to local, actively firing neurons (data not shown; N(n)=3(13)). Analysis of synaptic current kinetics for individual events revealed a significant decrease in event decay time in SUS mice leading to the possibility of altered AMPA receptor conformation or phosphorylation (One-way ANOVA, $F_{(2,78)} = 3.13$, $p = 0.049$; inset histogram in Fig. 2.2F and 2.2G). This was also confirmed by a significant shift in the cumulative probability plot of decay times (Kolmogorov-Smirnov test, $Z = 6.40$, $p < 0.001$, Fig. 2.2F).

To determine whether CSDS also induced adaptations in 5-HT neurons, we next conducted recordings in slices from defeated *Pet1-tdTomato* mice, focusing on neurons in the dorsomedial and ventromedial DRN (Fig. 2.3C). Similar to DRN GABA neurons, we found that CSDS altered membrane properties and synaptic activity of genetically identified 5-HT neurons, with differences between SUS and RES subgroups. In contrast to the sensitization observed in GABA neurons, we found that 5-HT neurons of SUS mice had reduced intrinsic excitability (Repeated measures ANOVA, defeat x input current, $F_{(12,228)} = 2.79$, $p = 0.001$; N(n) = 3(15) for control, 3(16) for RES, 3(21) for SUS; Fig. 2.3A and 2.3D). In the 5-HT neurons, IPSC activity was measured as previously described (Crawford et al., 2013). In SUS mice, mIPSC frequency was increased as compared to controls (One-way ANOVA, $F_{(2,28)} = 3.52$, $p = 0.043$; Fig. 2.3B and inset of Fig. 2.3E). The change in frequency was confirmed by a significant shift in the cumulative probability plot of inter-IPSC intervals (Kolmogorov-Smirnov, $Z = 8.65$, $p < 0.001$; Figure 2.3E). Additionally, there was a trend towards a significant increase in EPSC frequency in *Pet1-tdTomato* neurons of RES mice compared to controls (One-Way ANOVA, $F_{(2,28)} = 2.82$, $p = 0.076$; data not shown). Collectively, these results support the

hypothesis that expression of social avoidance in stress SUS mice was associated with sensitized descending excitatory input onto DRN GABAergic neurons, which in turn carried into an enhanced inhibition of neighboring 5-HT neurons.

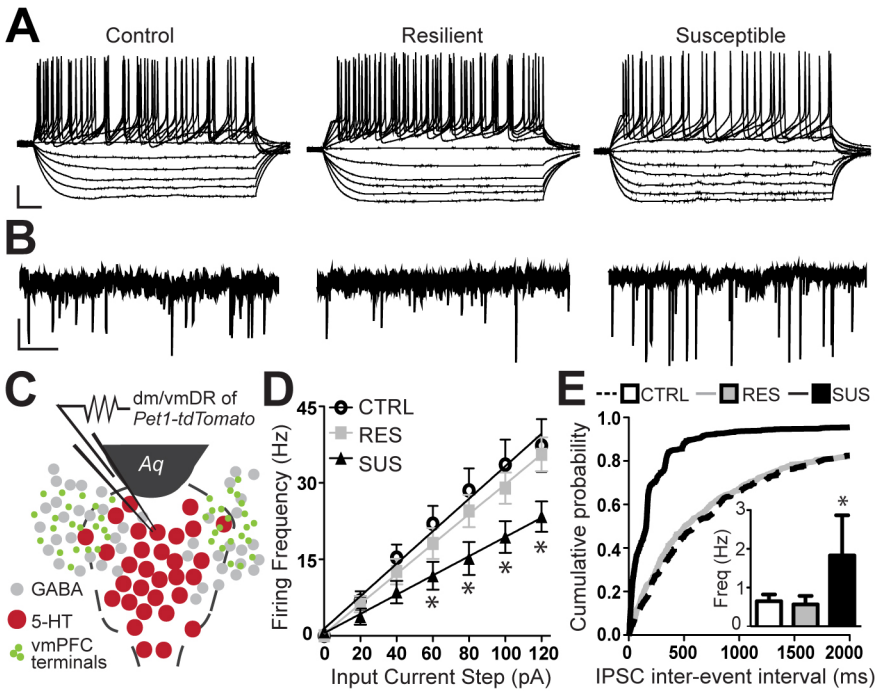

Figure 2.3. CSDS decreased excitability and enhanced inhibitory input of DRN 5-HT neurons of SUS mice.

(A) Raw data traces of membrane potential changes recorded from DRN 5-HT neurons in response to hyperpolarizing and depolarizing current injection in control, Resilient, and Susceptible mice. Scale bar 20mV, 50ms.
(B) Representative traces of mIPSC activity in DRN 5-HT neurons from control, Resilient, and Susceptible mice. Scale bar 20pA, 2s.
(C) Schematic of DRN topography in recorded slices from *Pet1-tdTomato* mice. *dm/vmDR* – dorsomedial/ventromedial DRN, *Aq* – aqueduct.
(D) Frequency-intensity plots show decreased excitability of DRN 5-HT neurons in Susceptible mice (Repeated measures ANOVA, Fisher post-hoc; SUS vs CTRL, 60pA *p = 0.043, 80pA *p = 0.024, 100pA *p = 0.023, 120pA *p = 0.033; N(n)=3(15) for control, 3(16) for Resilient, 3(21) for Susceptible).
(E) Cumulative probability plots show the shift to shorter inter-stimulus intervals of mIPSC activity in DRN 5-HT neurons of Susceptible mice versus control or Resilient mice (Kolmogorov-Smirnov test, $Z = 8.652$, $p < 0.001$). Inset displays summary histogram depicting the significantly higher average mIPSC frequency in Susceptible mice (One-way ANOVA, Fisher post-hoc; SUS vs CTRL *p = 0.035).

Optogenetic silencing of ventrolateral DRN GABA neurons disinhibits midline 5-HT neurons

To test the causal involvement of DRN GABA neuron sensitization in the expression of behaviors associated with the SUS phenotype, we adopted an optogenetic silencing approach that we applied in slices and in freely moving animals. To achieve GABA neuron silencing, we expressed a *GFP*-tagged version of the inhibitory optogenetic effector *Archaerhodopsin* (*Arch-GFP*) (Chow et al., 2010). We infused a *Cre*-recombinase inducible AAV vector into the DRN of *GAD2-Cre* mice to selectively target *Arch-GFP* to GABA neurons. In mice perfused six weeks after injection, counting of GFP^+ cells along the entire rostro-caudal extent of the DRN showed that approximately 21% of $GAD2^+$ DRN neurons (248.5 ± 8.8 per field of view) were transduced and expressed *Arch-GFP* (51.75 ± 8.7; n = 4). No $Arch\text{-}GFP^+/GAD2^-$ cells were detected, confirming the selectivity of viral targeting (Student's t-test, $t_{(6)} = 6.37$, $p < 0.001$; data not shown). Numerous $GAD2^+/Arch\text{-}GFP^+$ neurons were found in ventrolateral portions of the DRN (Fig. 2.4Ai). These cells were clearly distinct from, but in close proximity to 5-HT neurons identified using immunolabeling of tryptophan hydroxylase (*TPH*) (Figure 2.4Aii-iv). To validate *Arch*-mediated silencing of GABA neurons, we conducted whole-cell recordings in DRN slices six weeks after viral stereotaxic injection. When recording from visually identified GABA neurons that were spontaneously firing (Fig. 2.4D), application of 543 nm light at an irradiance of about 10.01 mW mm^{-2} resulted in time-locked silencing (Fig. 2.4B). Firing was completely abolished when the laser was on and returned upon cessation of illumination, with

activity often rebounding at an increased firing rate (Repeated measures ANOVA, $F_{(2,53)} = 3.53$, $p < 0.001$; N(n)=3(18); Fig. 2.4E).

We then asked whether identified *GAD2*$^{+}$ cells in the ventrolateral DRN form local connections with nearby 5-HT neurons present on the same slice. To our knowledge, despite multiple references in the literature indicating that DRN GABA

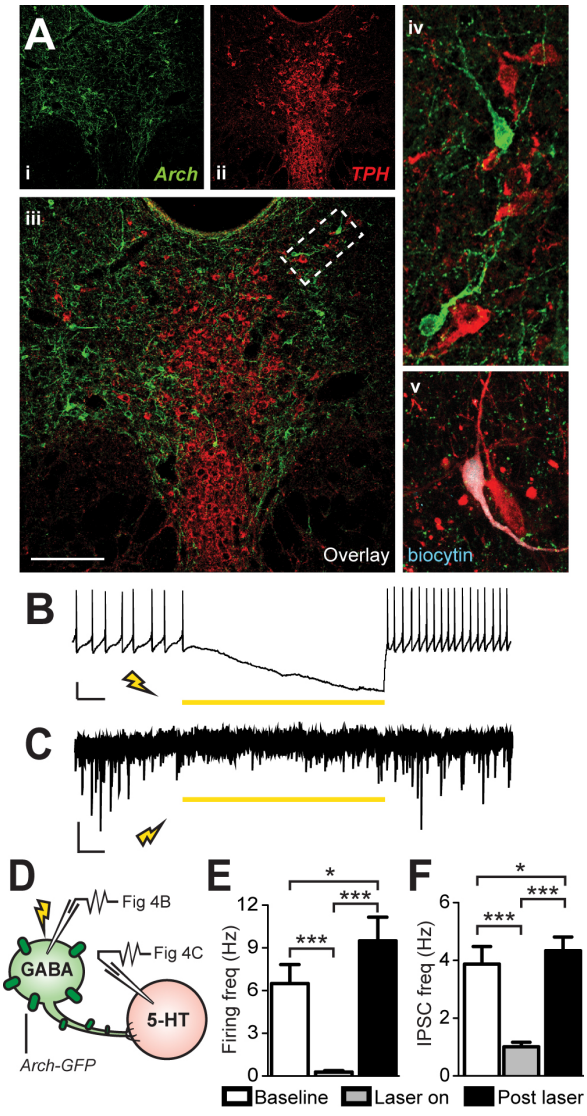

Figure 2.4. *Archaerhodopsin*-mediated photoinhibition of DRN GABAergic neurons silenced their spontaneous firing and decreased IPSC activity of neighboring 5-HT neurons.

(A) i-iv: confocal image of *Arch-GFP* expressing GABAergic neurons (green) and *TPH* labeled 5-HT neurons (red) in the DRN. Scale bar 50µm. v: Example of a 5-HT neuron recorded in the DRN that was filled with biocytin and its neurochemical identity was confirmed a posteriori using *TPH* immunostaining. **(B)** Current clamp trace of a spontaneously firing, *Arch*-expressing *GAD2*$^{+}$ GABA neuron. Exposure to 318mW mm^{-2} of 593nm light inhibited the tonic firing. Scale bar 20mV, 1s. **(C)** Voltage clamp recording from a later identified 5-HT neuron. Illumination of the DRN with 318mW mm^{-2} of 593nm light resulted in a reduction of IPSC frequency that returned upon laser stimulation cessation. Scale bar 10pA, 1s. **(D)** Schematic of recording experiments. Whole-cell patch clamp was performed on either GABA or 5-HT neurons while *Arch*-expressing GABA neurons were photoinhibited via laser stimulation. **(E)** Summary histogram showing that laser illumination resulted in complete silencing of spontaneous firing of *GAD2*$^{+}$ GABA neurons (N(n) = 3(18)) that was restored upon laser cessation (Repeated measures ANOVA, Fisher post-hoc; baseline vs laser, ***$p < 0.001$; laser vs post-stim ***$p < 0.001$; baseline vs post-stim *$p = 0.030$). **(F)** Summary histogram showing that laser stimulation reduced IPSC frequency in 5-HT neurons (N(n)=2(5)) that was restored after laser cessation (Repeated measures ANOVA, Fisher post-hoc; baseline vs laser ***$p < 0.001$; laser vs post-stim ***$p < 0.001$; baseline vs post-stim *$p = 0.047$).

neurons synapse with 5-HT neurons (Celada et al., 2001; Hou et al., 2012; Varga et al., 2001), there is currently no direct evidence that demonstrates monosynaptic inhibition of DRN 5-HT cells by neighboring GABA neurons. To test this we applied the same silencing protocol as above, but recorded from *tdTomato*$^{-}$/*GFP*$^{-}$ neurons located in the 5-HT-rich midline area of the DRN (Fig. 2.4D). For this experiment, 5-HT cell type was predicted primarily based on identification of firing patterns typical of 5-HT neurons (Crawford et al., 2010). However, since this electrophysiological criterion is not entirely reliable, neurochemical identity was also confirmed *a posteriori* using biocytin filling and *TPH* immunolabeling (Fig. 2.4Av). Laser illumination resulted in a significant decrease in IPSC frequency in 17% of recorded 5-HT cells and, as noted previously for GABA neurons, rebounded to levels greater than baseline upon cessation of laser illumination (Repeated measures ANOVA, $F_{(2,14)} = 7.33$, $p < 0.001$; N(n)=2(5); Fig. 2.4C, 2.4F). Those 5-HT neurons responsive to the laser inhibition of GABA synaptic activity were located in the dorsomedial DRN. Taken together, these results provide definitive evidence of DRN GABA neurons that locally synapse on and inhibit 5-HT neurons.

Silencing DRN GABA neurons interferes with the development, but not the expression of social aversion

DRN circuits might contribute to the development of social avoidance in SUS mice by affecting a number of different processes. For example, DRN output could mediate negative perceptive biases where detection and processing of threatening socioemotional information (e.g. body postures, auditory and olfactory cues) become sensitized after defeat (Passamonti et al., 2012; Roy et al., 2012; Todorov, 2008). Alternatively, these circuits could also affect the threshold for the execution of

approach/avoidance responses through effects on decisions to engage in actions (i.e. execution of approach) (Miller and Cohen, 2001; Rogers, 2011; Volman et al., 2011). To dissociate these two potentially distinct roles, we manipulated DRN GABA neurons optogenetically, either during the phase corresponding to the associative encoding of social threat (physical defeat/sensory contact; Fig. 2.6A, top row) or execution of a previously acquired social avoidance response (social interaction testing; Fig. 2.6A, bottom row).

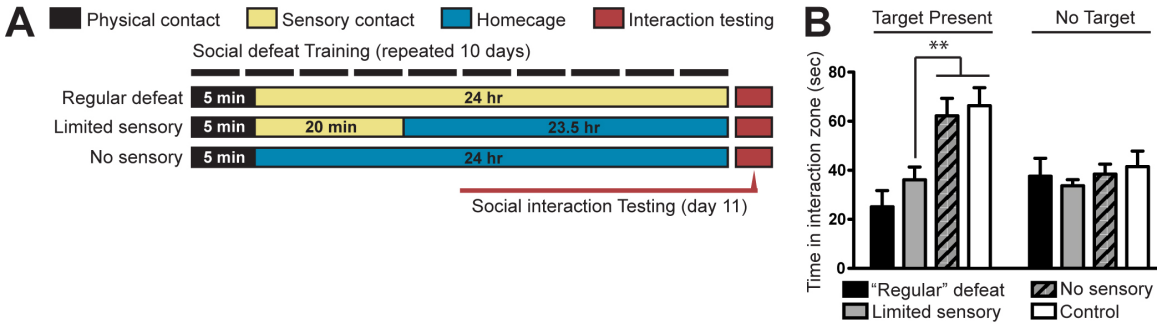

Figure 2.5. Sensory contact was necessary for encoding of avoidance behavior.

(A) Experimental conditions used to evaluate the contribution of sensory contact to acquisition of social avoidance behavior. During CSDS, all groups received 5 min of physical contact with an aggressor followed by variable durations of sensory exposure through a Plexiglass divider. The "Regular defeat" group remained in sensory contact overnight with the aggressor, while the "Limited sensory" group was maintained in sensory contact only for 20 min, before being transferred into single housing overnight. In the "No sensory" group, mice were individually housed immediately after physical contact. These conditions were repeated for 10 days, with exposure to a novel aggressor each day. Social avoidance was tested on day 11, 24h after last physical defeat exposure.
(B) Compared to undefeated controls, mice from the "limited sensory" group displayed a level of social avoidance comparable to the "regular defeat" group. In contrast, mice from the "no sensory" group did not display a significant decrease in interaction compared to undefeated controls (One-way ANOVA, Fisher post-hoc; limited vs. no sensory **p = 0.005; limited vs. control **p = 0.005; n = 8-13 per group). Without a novel target present, durations in the interaction zone did not differ between groups.

We hypothesized that a critical encoding period may be when mice are maintained in sensory contact with their aggressor after physical aggression. To test this we compared avoidance behavior of mice that underwent 10 days of standard defeat (5

minutes of physical contact + 24 hours of sensory contact with aggressor through a Plexiglass partition) to mice that experienced a physical defeat experience without subsequent sensory contact with the aggressor (5 minutes of physical contact + 24 hours home cage) (Fig. 2.5A). This comparison revealed that a sensory contact period is required for the subsequent expression of the avoidance response (One-Way ANOVA, $F_{(3,37)} = 8.34$, $p = 0.002$; n = 9-12 per group; Fig. 2.5B). We then determined the minimal duration of sensory contact necessary for the expression of social avoidance. Comparing various durations we found that 20 minutes of post-defeat sensory exposure to the aggressor is sufficient to allow full expression of avoidance behavior (Fig. 2.5B). These results reveal the existence of a critical period following physical defeat during which key sensory and associative processes establish the intensity and stability of subsequent avoidance behaviors.

We next tested the role of DRN GABA neurons by silencing them either during the daily sensory contact period (encoding) or during the 5-minute interaction test when mice were evaluated for approach-avoidance decisions in the presence of an unfamiliar social target (execution). Cohorts of mice injected with AAV vectors coding for *Cre*-dependent expression of *Arch-GFP* or *tdTomato* in DRN GABA neurons as described above were implanted chronically with a fiber optic ferrule used to subsequently connect to an external light source. Mice were exposed to 5 minutes of physical contact with aggressors followed by 20 minutes of sensory contact during which they were connected to the light source. For the entire duration of the sensory contact period, DRN GABA neurons were silenced (543 nm, 10 mW) and then returned to their home cages overnight (Fig. 2.6A, top row). A cohort of mice expressing *tdTomato* in GABA neurons was

exposed to the identical defeat and laser illumination protocol. Groups of undefeated control mice, injected with *Arch-GFP* or *tdTomato* and exposed to identical procedures apart from the 5 minutes of physical contact, were also included as controls in subsequent tests to evaluate possible effects of GABA silencing independent of defeat experience. This procedure was conducted for 10 days like the CSDS procedure described above.

When subsequently tested for social interaction, defeated mice receiving the *tdTomato* virus showed typical social avoidance responses indicating that the laser illumination procedure *per se* does not influence development of social avoidance. In contrast, defeated mice exposed to DRN GABA silencing during sensory contact exhibited similar levels of social interaction as undefeated mice. (Two-way ANOVA, virus x defeat, $F_{(7,38)} = 8.07$, $p < 0.001$; n = 6-8 per group; Fig. 2.6B, left panel). Importantly, the effects of DRN GABA silencing were specific to the regulation of social experience since neither virus nor laser condition had significant effects on total movement (data not shown) or the time spent in the interaction zone in the absence of a social target (Figure 2.6B, right panel).

Having shown that DRN GABA neurons contribute to the encoding of avoidance behavior, we lastly asked whether they also influence processes related to the execution of social avoidance responses (i.e., decision or ability to avoid social interaction). We tested this by silencing DRN GABA neurons after defeat-induced social avoidance had already been established (Fig. 2.6A, bottom row). In contrast to our previous observation, we found that the time spent in the social interaction zone after defeat remained low in both *Arch* and *tdTomato* groups (Two-way ANOVA, main effect of defeat, $F_{(3,13)} = 24.39$, $p < 0.001$; n = 5-6 per group; Fig. 2.6C). These results indicate that the activity of DRN

GABA neurons is critical during the appraisal or neural encoding of social threat, but is dispensable during the execution of previously established social avoidance responses.

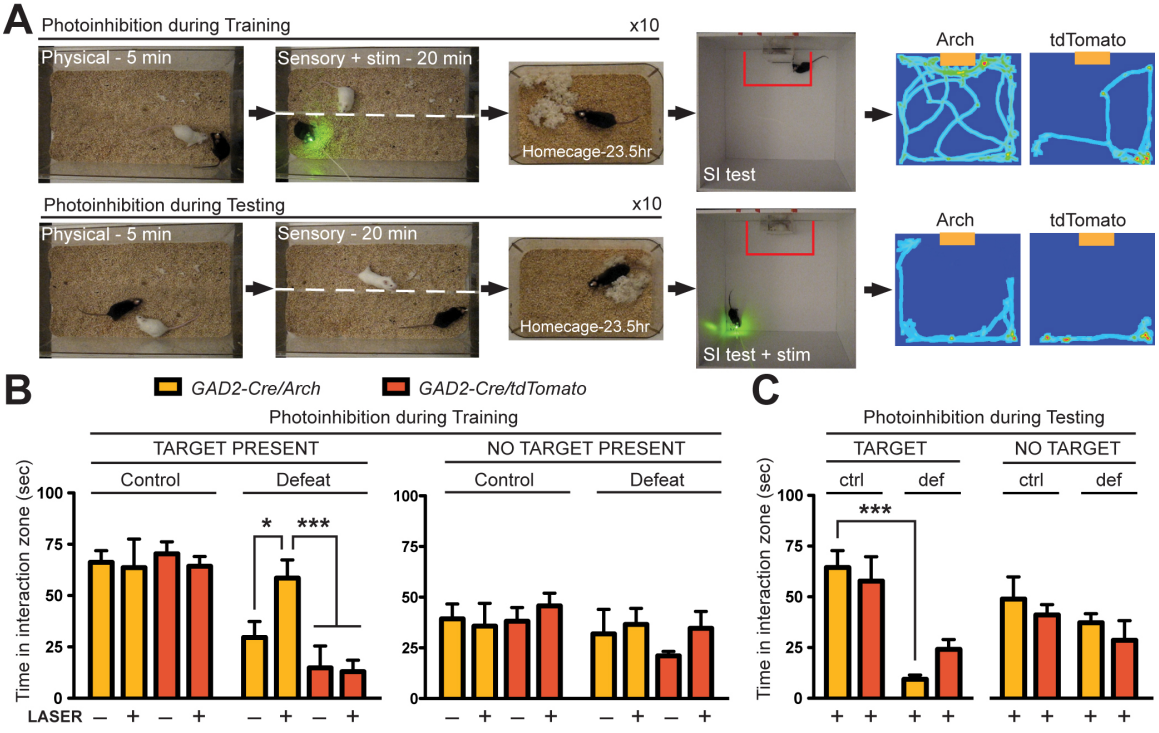

Figure 2.6. Photoinhibition of DRN GABA neurons prevented the acquisition, but not expression of social avoidance behavior.

Two cohorts of *GAD2-Cre* mice were injected in the DRN with *Cre*-dependent AAV vectors, driving expression of *Arch-GFP* or a sham *tdTomato* protein selectively in DRN GABA neurons. The first cohort **(A**, Top row: Photoinhibition during training**)** received daily photoinhibition during 20 min of sensory contact following physical aggression. The second cohort **(A**, Bottom row: Photoinhibition during testing**)** received photoinhibition only during the social interaction task. Heat maps depict representative behavioral effects of DRN GABA photoinhibition. Corresponding group averages are shown for the time spent in the interaction zone **(B)** in Control and Defeated mice receiving photoinhibition during the sensory contact period, or **(C)** during social interaction task. Light application during daily sensory contact period abrogated social avoidance in *Arch-GFP,* but not in *tdTomato* targeted mice (Two-way ANOVA, Fisher post-hoc; defeated *Arch*/stim vs. defeated *Arch*/no stim *p = 0.011; defeated *Arch*/stim vs. defeated *tdTomato* ***p < 0.001; n = 6-8 per group). In contrast, no significant effects were observed when light was applied during the social interaction task (Two-way ANOVA, Fisher post-hoc; *Arch* CTRL vs. DEF ***p < 0.001). Note that GABA photoinhibition had no effect on the behaviors of mice tested in the absence of a social target, and that laser illumination *per se* was devoid of effect in mice expressing *tdTomato*.

DRN GABA neurons do not mediate increased anxiety-related behaviors after CSDS

Studies have reported a high rate of comorbidity between depression and anxiety disorders (Pollack, 2005). Because GABA activity within the DRN has been implicated in anxiety-related behaviors (Crawford et al., 2013; Ettenberg et al., 2011) we also tested whether GABA inhibition during the sensory contact phase of CSDS blocked the anxiogeneic effect of CSDS, which is another known consequence of the CSDS paradigm (Krishnan et al., 2007). We tested this using the open field test (OFT) and elevated plus maze (EPM). In agreement with previous studies, CSDS had an anxiogenic effect in both tests as defeated mice spent less time in the center of the OFT arena compared to undefeated controls (Two-Way ANOVA, main effect of CSDS, $F_{(1,46)} = 21.60$, $p < 0.001$; n=6-8 per group; Table 2.1). However, there was no distinction between mice receiving DRN GABA neuron inhibition during CSDS and unstimulated mice. A similar lack of effect of optogenetic stimulation was also observed in the EPM where both stimulated and unstimulated mice display similar levels anxiety-like behaviors (i.e., decreased time spent in open arms, increased entries into closed arms) (Table 2.2). This suggests that DRN GABA neurons play a specific role in social avoidance, but are dispensable for the encoding of CSDS-mediated anxiety-related behaviors.

Table 2.1. DRN GABA inhibition effects on anxiety-related behaviors: Open field test.

	Open field test – time in center of arena (s)			
	GAD2-Cre/Arch		*GAD2-Cre/tdTomato*	
Stim (+/–)	+	–	+	–
Defeated	28.94 ± 7.19***	28.89 ± 6.61***	25.56 ± 7.38***	25.54 ± 9.34***
Control	56.09 ± 10.47	46.86 ± 8.59	50.50 ± 4.13	42.81 ± 8.79

Data are expressed as mean (time in the center of arena) ± SEM.
The asterisks indicate a significant difference in defeated mice from undefeated controls of the same virus (*GAD2-Cre/Arch* or *GAD2-Cre/tdTomato*) and stimulation (+ or –) condition (Two-Way ANOVA, Fisher post-hoc, Control vs Defeated ***$p < 0.01$).

Table 2.2. DRN GABA inhibition effects on anxiety-related behaviors: Elevated plus maze.

	Elevated plus maze – defeated mice			
	GAD2-Cre/Arch		*GAD2-Cre/tdTomato*	
Stim (+/–)	+	–	+	–
Time in open arms (s)	6.30 ± 2.27	5.66 ± 3.77	4.69 ± 1.48	4.77 ± 2.94
Time in closed arms (s)	267 ± 6.5	254.50 ± 7.76	273.42 ± 6.86	271.65 ± 8.00
Open arm entries	6 ± 1	4 ± 1	5 ± 2	3 ± 1
Closed arm entries	15 ± 2	11 ± 2	13 ± 4	11 ± 3

Data are expressed as mean (time spent in arms, number of arm entries) ± SEM.
There was no significant difference between conditions.

Discussion

Our primary finding showed that CSDS sensitized DRN GABA neurons and increased GABA-mediated inhibition of 5-HT neurons in SUS mice. In contrast, RES mice escaped this effect and displayed unaltered GABA and 5-HT neuronal excitability. Furthermore, GABA silencing dishinibited 5-HT cells and promoted a RES phenotype in mice exposed to CSDS. Thus, we established a role for DRN GABA neurons in the neural encoding of social threats. By identifying cellular mechanisms underlying stable social approach/avoidance decision biases in mice exposed to CSDS, our results contribute to a better neurobiological understanding of the neural circuitry underlying socio-emotional deficits increasingly conceived as part of the cognitive core of mood and anxiety disorders (Beck, 2008; Cusi et al., 2012; Roiser et al., 2012).

GABAergic neurons provide inhibitory control of 5-HT neurons in the DRN microcircuit

Aside from 5-HT neurons, the DRN contains a large proportion (estimated 50–75%) of non-5-HT cells, comprised primarily of GABA- and glutamate-producing neurons (Bang and Commons, 2012; Fu et al., 2010). Pharmacological and neuroanatomical evidence supports the notion that, in concert with 5-HT autoreceptor-mediated mechanisms, GABA neurons are key to the inhibitory control of 5-HT systems (Liu et al., 2000; Varga et al., 2001). Based on converging data from previous *in vivo* recording and tracing studies, GABA neurons located within the DRN may serve as local inhibitory relays for several major descending excitatory inputs converging onto the DRN, including those originating from the vmPFC and lateral habenula (Celada et al., 2001; Varga et al., 2003; Varga et al., 2001). Using *Archaerhodopsin*–mediated silencing we

showed that DRN *GAD2*$^{+}$ GABA neurons connect monosynaptically to local 5-HT neurons, providing a source of postsynaptic inhibitory currents to roughly 20% of 5-HT cells probed in the medial DRN. This proportion, however, is almost certainly an underestimate considering that the brain slice preparation used for electrophysiology likely disrupted axonal connections for at least some GABA neurons. Our results provide evidence confirming that this hypothetical organization of DRN microcircuits exists and confirms the role of GABA neurons in affective regulation.

Defeat drives adaptations in DRN GABA and 5-HT neurons that discriminate RES from SUS mice

Our previous study demonstrated that DRN 5-HT neurons identified using post-recording immunolabeling underwent CSDS-induced physiological adaptations (Espallergues et al., 2012), however it did not reveal clear distinctions between RES and SUS subpopulations. Here, using a genetic labeling method that facilitated cell-typing, we observed differences between behavioral subgroups and found that DRN neurons in SUS mice undergo clear adaptations, while the properties of the neurons in RES mice more closely resemble those of undefeated controls. In SUS mice, the DRN 5-HT neuronal population had decreased excitability and increased inhibitory input. The source of this inhibitory synaptic activity is likely from local DRN GABA neurons, which we found were hyperexcitable and also driven by increased excitatory input in SUS mice. These adaptations in both GABA and 5-HT neurons, when coupled together, suggest an overall decrease in 5-HT excitability in SUS mice, which is consistent with literature describing the role of 5-HT in socioaffective regulation (Bilderbeck et al., 2011; Liu et al., 2010; Passamonti et al., 2012; Raleigh et al., 1991).

Though we did not formally demonstrate the source of the increased excitatory input on DRN GABAergic neurons, our tracing results indicate that a likely driving brain region is the ventral mPFC. Indeed the distribution of *CaMKIIa*-driven *YFP* labeling of vmPFC axonal terminals in the DRN shows a striking overlap with the distribution of CSDS-activated GABA neurons. Furthermore, ultrastructural studies of vmPFC axons in the DRN have shown that they to preferentially target GABA neurons over 5-HT neurons (Jankowski and Sesack, 2004). The vmPFC is thought to play a role in determining social valence (Roy et al., 2012) and thus it is plausible that vmPFC afferents to the DRN modulate 5-HT tone via GABAergic neurons, affecting socioaffective judgment. Our results are in line with the antidepressant-like effects of vmPFC DBS in rats, which increases 5-HT output in certain forebrain projection areas (Hamani et al., 2010; Hamani et al., 2011). However, recent studies further emphasized the complex role of vmPFC-DRN pathways in depression-related behaviors by reporting similar antidepressant-like effects in the forced swim test (FST) in rats after direct optogenetic activation of glutamatergic vmPFC terminals in the DRN or direct stimulation of a mixed GABA/5-HT DRN neuronal population (Warden et al., 2012). Based on this it is likely that partially distinct vmPFC-DRN sub-circuits modulate escape behaviors to noxious stimuli versus social approach/avoidance and antagonistic behaviors. This view is supported by the fact that a regimen of chronic optogenetic stimulation of *Thy1*$^{+}$ layer V vmPFC neurons in mice that enhanced DRN activity did not influence social avoidance after CSDS, even though this treatment produced long lasting antidepressant-like effects in the FST (Kumar et al., 2013).

DRN GABAergic neurons mediate associative encoding of social aversion, but are dispensable for the execution of avoidance decisions.

Social defeat is a model of psychosocial stress with predictive validity that has proved useful in examining modes of action of antidepressant therapeutics and the neurobiology of depression-like behaviors (Golden et al., 2011; Krishnan et al., 2008; Kudryavtseva et al., 1991). An essential aspect of the specific paradigm used in the present study is the application of a daily sensory exposure period during which mice are maintained in protected sensory contact with an aggressor after a brief, but severe experience of physical aggression (Berton et al., 2006). Following this associative process, an initially positively valenced social stimulus (i.e. an unfamiliar CD1 social target that unconditionally induces approach in control mice) acquires aversive motivational value and triggers social avoidance in the social interaction testing for most defeated mice. Importantly, this social avoidance response after CSDS observed in SUS mice is generalized and is observed independent of the degrees of familiarity, physical appearance or genetic strain of the social target (Berton et al., 2006). Although the specific sensory modalities of salient social cues involved during the acquisition and expression of avoidance behavior have yet to be determined, our previous studies have shown that the social target actively emits these cues, since the use of an anesthetized target leads to a complete loss of the avoidance response (Krishnan et al., 2007).

In the present study we identify the critical period during which sensory associations necessary for subsequent expression of social avoidance were established. We showed that these associations occurred during a defined time lapse that spans the first 20 minutes after the end of physical contact with the aggressor and we demonstrated

that this period is both necessary and sufficient for the development of long lasting social avoidance. Further, we demonstrated using *Arch*-mediated optogenetic silencing of DRN *GAD2*$^{+}$ neurons *in vivo,* that activation of DRN GABA neurons was required for acquiring the avoidance response, but were not involved in the expression of a previously acquired avoidance response. The mechanism by which silencing DRN GABA neurons impaired the socioaffective encoding without influencing the execution of social avoidance response remains uncertain. Increases in 5-HT output in the vmPFC after GABA-B receptor activation in the DRN and dishinibition of 5-HT neurons has consistently been shown to promote social approach and offensive behaviors of defeated mice (Takahashi et al., 2012; Takahashi et al., 2010). This is in general agreement with data linking enhancement of forebrain 5-HT output with resilience to social stress and maintenance of dominant social status in various species (Alekseyenko et al., 2010; Bruchas et al., 2011; Malatynska et al., 2005; Penn et al., 2010; Raleigh et al., 1991). Our study identifies the role of GABAergic neurons embedded within DRN microcircuits as that of a pivotal cellular population to regulate mood-affecting 5-HT neurons. By revealing a striking influence of social experiences on the basic neurophysiological characteristics and synaptic properties of these GABA neurons, our results introduce a novel circuitry relevant to affective resilience and the treatment of affective disorders.

Chapter 3

Optogenetic modulation of descending prefrontocortical inputs to the dorsal raphe bidirectionally bias socioaffective decisions after social defeat

Collin Challis[1,2], Sheryl G. Beck[2,3], Olivier Berton[1,2]*

[1]Department of Psychiatry, [2]Neuroscience Graduate Group, University of Pennsylvania Perelman School of Medicine, and [3]Department of Anesthesiology, Children's Hospital of Philadelphia and University of Pennsylvania Perelman School of Medicine, Philadelphia, PA 19104

Acknowledgments

This work was supported by grants from the National Institute of Mental Health (MH087581 to OB and MH0754047, MH089800 to SGB), from the International Mental Health Research Organization (IMHRO) to OB, from NARSAD to OB, and by NRSA (T32MH014654 and F31MH097386) to CC.

The work in this chapter was published in *Frontiers in Behavioral Neuroscience* in 2014: Challis, C., Beck, S. G., & Berton, O. (2014). Optogenetic modulation of descending prefrontocortical inputs to the dorsal raphe bidirectionally bias socioaffective choices after social defeat. *Front Behav Neurosci*, 8, 43.

Abstract

It has been well established that modulating serotonin (5-HT) levels in humans and animals affects perception and response to social threats, however the circuit mechanisms that control 5-HT output during social interaction are not well understood. A better understanding of these systems could provide groundwork for more precise and efficient therapeutic interventions. Here we examined the organization and plasticity of microcircuits implicated in top-down control of 5-HT neurons in the dorsal raphe nucleus (DRN) by excitatory inputs from the ventromedial prefrontal cortex (vmPFC) and their role in social approach-avoidance decisions. We did this in the context of a social defeat model that induces a long lasting form of social aversion that is reversible by antidepressants. We first used viral tracing and *Cre*-dependent genetic identification of vmPFC glutamatergic synapses in the DRN to determine their topographic distribution in relation to 5-HT and GABAergic subregions and found that excitatory vmPFC projections primarily localized to GABA-rich areas of the DRN. We then used optogenetics in combination with *cFos* mapping and slice electrophysiology to establish the functional effects of repeatedly driving vmPFC inputs in DRN. We provide the first direct evidence that vmPFC axons drive synaptic activity and immediate early gene expression in genetically identified DRN GABA neurons through an AMPA receptor-dependent mechanism. In contrast, we did not detect vmPFC-driven synaptic activity in 5-HT neurons and *cFos* induction in 5-HT neurons was limited. Finally we show that optogenetically increasing or decreasing excitatory vmPFC input to the DRN during sensory exposure to an aggressor's cues enhances or diminishes avoidance bias, respectively. These results clarify the functional organization of vmPFC-DRN pathways

and identify GABAergic neurons as a key cellular element filtering top-down vmPFC influences on affect-regulating 5-HT output.

Introduction

The capacity to detect and interpret the affective state of others using non-verbal social cues (e.g. facial expression, vocal prosody, posture, body movement and olfactory cues) is a necessary survival skill shared by many animal species (Chang et al., 2013; Oliveira, 2012). It allows individuals to anticipate harmful intentions of others and adapt through rapid approach or avoidance decisions (O'Connell and Hofmann, 2012). The capacity to conduct social-cognitive appraisal is also a determining aspect of human social competence (Todorov, 2008; Volman et al., 2011) and dysfunction of the neural systems that mediate socioaffective decisions are thought to contribute to excessive reassurance-seeking behaviors and social withdrawal, which are two symptomatic dimensions shared across several affective disorders, including major depression and social phobia (Cusi et al., 2012; Derntl et al., 2011; Heuer et al., 2007; Moser et al., 2012; Seidel et al., 2010; Stuhrmann et al., 2011).

Serotonin (5-HT) is a neurotransmitter system that plays an evolutionarily conserved role in regulating affiliative and antagonistic behaviors (Canli and Lesch, 2007; Dayan and Huys, 2009). Increases in 5-HT output, such as resulting from treatment with SSRI antidepressants, have consistently been shown to positively bias socioaffective appraisals and facilitate social affiliation and dominance in human and animals (Bond, 2005; Harmer and Cowen, 2013; Knutson et al., 1998; Raleigh et al., 1991; Tse and Bond, 2004). In contrast, 5-HT depletion facilitates socially defensive behaviors and aggression (Munafò et al., 2006; Young and Leyton, 2002). The fact that the output of ascending 5-HT neurons located in the dorsal raphe nucleus (DRN) is under top-down control by multiple forebrain areas (Celada et al., 2002) suggests a potentially key role for DRN

afferent systems in the modulation of socioaffective responses. Studies conducted *in vivo* in anesthetized rodents combining electrical stimulation of the ventromedial prefrontal cortex (vmPFC) and extracellular recordings in the DRN demonstrated the rapid inhibition of putative 5-HT neurons (Celada et al., 2002; Varga et al., 2001). Parallel histological tracing studies demonstrated that DRN GABAergic neurons that are preferential targets of vmPFC projections could mediate the inhibitory responses recorded *in vivo* (Jankowski and Sesack, 2004). However, due to the limited specificity of electrophysiological signatures to predict neurochemical cell-type (Calizo et al., 2011), the identities of neuronal populations that compose the vmPFC-DRN microcircuit have not been fully elucidated. Furthermore, there is a lack of information about the possible topographical distribution of various DRN cellular populations thereby limiting the progress of studies assessing their causal role in socioaffective responses and other behaviors.

In recent studies we used a murine model of chronic social defeat stress (CSDS) that induces long lasting avoidance bias responsive to antidepressants to characterize the role of DRN microcircuits in the development and expression of social aversion (Challis et al., 2013; Crawford et al., 2013; Espallergues et al., 2012; Veerakumar et al., 2013). In mice susceptible to CSDS, but not in ones resilient, we detected a sustained sensitized synaptic inhibition of DRN 5-HT neurons, associated with a state of dramatically reduced intrinsic excitability of 5-HT neurons. Furthermore, we identified a subset of $GAD2^{+}$ GABA neurons with sensitized excitatory synaptic input and intrinsic excitability, which monosynaptically inhibits nearby 5-HT neurons. Using optogenetic photosilencing we provided evidence of their key role in the associative process that underlie the

development of social avoidance in susceptible mice (Challis et al., 2013). Interestingly, we noted that these sensitized GABAergic neurons appear to be located in circumscribed lateral subregions of the DRN heavily innervated by the vmPFC. These observations suggest a potentially unique role of inputs from the vmPFC in driving stress-induced plasticity of GABA neurons within the DRN that underlie the stabilization of avoidance bias after CSDS.

In the present study, we set out to test this hypothesis. We used *in vivo* optogenetics to drive or inhibit the synaptic inputs from vmPFC axons locally within the DRN during the sensory contact phase of CSDS. We also used viral tracing, whole-cell recordings and optogenetic methods in slice preparations to further characterize the anatomical and functional organization of the vmPFC-DRN pathway. Our results directly show that excitatory projections from the vmPFC preferentially target and synaptically activate GABA neurons that are topographically distributed within the DRN. We also show that activation of these terminals paired temporally with exposure to social cues potentiates negative socioaffective bias and social avoidance, while inhibition of these inputs facilitates the maintenance of social engagement after defeat, a characteristic of resilient individuals. These results provide fundamentally novel insights about neural mechanisms implicated in the top-down control of 5-HT during socioaffective tasks and have important implications for the understanding and treatment of affective disorders.

Materials and Methods

Animals

Eight- to twelve-week old male mice bred onto a C57BL/6 background were used for all experiments. Mice were housed on a 12-hour light/dark cycle with food and water available *ad libitum*. All studies were conducted according to protocols approved by the University of Pennsylvania Institutional Animal Care and Use Committee. All procedures were performed in accordance with institutional guidelines. The large cohort of defeated mice used to determine social choice consisted of male C57 Black mice (*C57BL/6J*: JAX stock number 000664). Trained aggressor mice were retired CD-1 male breeder mice (*Crl:CD1*; Charles River Laboratories, Malvern, PA).To generate a mouse line with fluorescently labeled *GAD65*-containing GABAergic or serotonergic neurons, male knockin *GAD2-Cre* mice (*Gad2*$^{tm2(cre)Zjh}$*/J*; JAX stock number 010802) (Taniguchi et al., 2011) or BAC transgenic *Pet1-Cre* mice (*B6.Cg-Tg(Fev-cre)*1Esd/J; JAX stock number 012712) (Scott et al., 2005) were respectively crossed to female floxed-stop controlled *tdTomato* (RFP variant) mice (*B6.Cg-Gt(ROSA)26Sor*$^{tm9(CAG-tdTomato)Hze}$*/J*; JAX stock number 007908) (Madisen et al., 2010) to achieve fluorescent labeling of *Cre* containing cells. To achieve expression of optogenetic probes or fluorescent tracers in glutamatergic vmPFC neurons we used *CaMKIIa-Cre* mice (*B6.Cg-Tg(CamK2a-Cre)T29-1Stl/J*; JAX stock number 005359) (Tsien et al., 1996). With the exception of the CD-1 strain, all mice were procured from the Jackson Laboratory (Bar Harbor, ME).

Virus and surgery

To express optogenetic or fluorescent proteins in glutamatergic neurons, adeno-associated virus (AAV) vectors were produced by and purchased from the University of

Pennsylvania vector core (Philadelphia, PA) and injected into *CaMKIIa-Cre* mice. In this work we used AAVs for the *Cre*-inducible expression of the excitatory optogenetic probe *Channelrhodopsin* (AAV2/9.EF1a.DIO.hChR2(H134R)-EYFP.WPRE.hGH; Addgene #20298), inhibitory optogenetic probe *Archaerhodopsin* (AAV2/9.flex.CBA.Arch-GFP.W.SV40; Addgene #22222), fluorescent protein *tdTomato* (AAV2/1.CAG.FLEX.tdTomato.WPRE.bGH; Allen Institute #864) and *GFP* tagged Synaptophysin (AAV2/9.CMV.FLEX.Synaptophysin-Venus.WPRE.hGH; plasmid kindly provided by Anton Maximov, PhD, Department of Molecular and Cellular Neuroscience, The Scripps Research Institute). For stimulation of excitatory vmPFC terminals in the DRN of *GAD2-tdTomato* or *Pet1-tdTomato* mice we used an AAV for the *CaMKIIa*-driven expression of *Channelrhodopsin* fused to *YFP* (AAV2/9.CaMKII.ChR2-YFP.SV40; Stanford) (Mattis et al., 2012).

For viral injections, mice were anesthetized with isofluorane and stereotaxically injected unilaterally in the prelimbic region of the vmPFC (from Bregma, in mm: +1.8 AP, +0.8 ML, -2.7 DV, 15° angle) with 0.5µl of virus. Viral yields (in GC) were 3.54 x 10^{12} for *ChR2-YFP,* 6.962 x 10^{11} for *Arch-GFP*, 2.049 x 10^{12} for *tdTomato* and 4.347 x 10^{12} for *CaMKIIa-ChR2-YFP*. Social defeat began 4 weeks post-surgery for non-cannulated mice to allow time for recovery and viral expression.

For *in vivo* optical stimulation, precut guide cannulae (Plastics One, Roanoke, VA) targeting the DRN (from Lambda, in mm: 0.0 AP, +0.8 ML, -3.3 DV, 15° angle) were secured to the skull using stainless steel skull screws and acrylic cement. A fitted dustcap dummy was secured atop the guide cannula and mice were placed back in homecages and allowed 6 weeks to recover. Body weight and behavior was monitored

during recovery. Three days before the start of experiment, a homemade fiber optic with ferrule connector (described below) was inserted into the guide cannula and secured with acrylic cement.

Preparation of optical fibers

A 200 μm core, 0.37 NA standard multimode fiber (Thorlabs, Newton, NJ) was stripped of cladding, passed through a 230 μm multimode ceramic zirconia ferrule (Precision Fiber Products, Milpitas, CA), and secured in place using fiber optic connector epoxy (Fiber Instrument Sales, Oriskany, NY). Ferrules were then polished and cut to length to target the DRN. They were tested for light output and sterilized with 70% ethanol.

Chronic Social Defeat Stress

We use a modified chronic social defeat stress (CSDS) paradigm to induce social avoidance (Challis et al., 2013; Golden et al., 2011). Our model consists of exposing male mice to alternating periods of physical contact with a trained CD1 aggressor male mouse (5 minutes) and protected sensory contact via separation by a perforated Plexiglass partition (20 minutes) before returning to home cages overnight. The 20 minutes of sensory contact is sufficient to induce a significant decrease in social interaction compared to undefeated mice or mice that were not exposed to a sensory period after physical contact. This effect has been previously described (Challis et al., 2013). This continued for 10 consecutive days with exposure to a novel aggressor each day. Control animals were also singly housed and were only exposed to daily sensory contact with novel aggressors. On day 11, social approach or avoidance behavior toward an unfamiliar CD1 social target was assessed in a two-trial social interaction task. In the first 2.5-

minute trial ("no target"), experimental mice explored a dimly lit (55 lux) open-field arena containing an empty wire mesh cage on one edge of the arena (see Fig. 3.6A). In the second 2.5-minute trial ("target present"), experimental mice were reintroduced to the arena now with an unfamiliar CD1 aggressor positioned in the mesh cage. TopScan video tracking software (CleverSys, Reston, VA) was used to measure the time spent in the interaction zone surrounding the target box.

Immunohistochemistry

Animals were transcardially perfused with 4% paraformaldehyde and brains were processed for standard single or dual immunolabeling methods as previously described (Espallergues et al., 2012). For detection of *cFos*, we used an affinity purified rabbit polyclonal antibody raised against the N-terminus of human *cFos* (1:1000 dilution; SC-52, Santa Cruz Biotechnology, Santa Cruz, CA). To enhance *GFP* expression we used a chicken anti-*GFP* antibody (1:1000 dilution; GFP-1020, Aves Labs, Inc., Tigard, OR). Primary antibodies were detected using fluorescent secondary antibodies obtained from Jackson ImmunoResearch Laboratories (1:500 dilution; West Grove, PA).

Cell counting

To map neuronal populations in the DRN, 30 μm serial sections of the DRN were collected every 120 μm between -4.36 mm and -4.96 mm from Bregma. Native *tdTomato* fluorescence and immuno-enhanced *GFP* fluorescence of *SynP* labeled vmPFC terminals were visualized using confocal microscopy. Slices from corresponding rostro-caudal levels between mice were aligned on a map based on location of the aqueduct. Neurons and terminals were manually drawn for each level of the DRN.

To quantify *cFos* colocalization with *tdTomato*$^+$ neurons, slices were stained for *cFos* and labeled neurons were manually counted in the DRN of each section. Colocalization with *tdTomato* was defined as nuclear localization of the *cFos* signal and was manually counted by an experimenter blind to the experimental condition of the mice from which the slices originated. There was not a significant variation of total number of *tdTomato*$^+$ cells within each strain.

To determine whether spatial distribution of synaptic vmPFC inputs traced using *SynP-GFP* correlated with the distribution of *GAD2-tdTomato* or *Pet1-tdTomato* neurons, we divided corresponding coronal views of the DRN in *GAD2-tdTomato*, *Pet1-tdTomato* and *SynP-GFP* injected *CaMKIIa-Cre* mice into 10 x 10 grids and tested for correlations between *SynP-GFP* and *tdTomato* fluorescence across the grid. This was done at each of the 6 rostro-caudal levels across the DRN. Fluorescent intensity within each grid box was calculated using the ImageJ "Measure" function which converts red, green, and blue (RGB) pixel values to brightness using the formula V=(R+G+B)/3. These intensity values were then normalized to the grid box with the highest intensity. Correlations were tested using the Pearson coefficient and plotted using linear regression.

Electrophysiology

Brain slices were prepared as previously described (Calizo et al., 2011; Challis et al., 2013; Crawford et al., 2010; Crawford et al., 2013; Howerton et al., 2013). The 200 μm coronal slices containing DRN were placed in aCSF (in mM, NaCl 124, KCl 2.5, NaH_2PO_4 1.25, $MgSO_4$ 2.0, $CaCl_2$ 2.5, dextrose 10, $NaHCO_3$ 26) at 37°C, aerated with 95% O_2/5% CO_2. After one hour, slices were kept at room temperature. Tryptophan (2.5 mM) was included in the holding chamber to maintain 5-HT synthesis, but was not in the

aCSF perfusing the slice in the recording chamber. Individual slices were placed in a recording chamber (Warner Instruments, Hamden, CT) and perfused with aCSF at 2 ml/min maintained at 32°C by an in-line solution heater (TC-324, Warner Instruments). Neurons were visualized using a Nikon E600 upright microscope fitted with a 60X water immersion objective and targeted under DIC or fluorescent filters. Resistance of electrodes was about 8-10 MOhms when filled with a recording solution composed of (in mM) K-gluconate (130), NaCl (5), Na phosphocreatine (10), $MgCl_2$ (1), EGTA (0.02), HEPES (10), MgATP (2) and Na_2GTP (0.5) with 0.1% biocytin and a pH of 7.3. Whole-cell recordings were obtained using a Multiclamp 700B amplifier (Molecular Devices, Sunnyvale, CA). Cell characteristics were recorded using current clamp techniques as previously described (Crawford et al., 2010; Espallergues et al., 2012). Signals were collected and stored using Digidata 1320 analog-to-digital converter and pClamp 9.0 software (Molecular Devices). Collection of EPSC data was as previously described (Crawford et al., 2011) and performed with bath application of 20 μM bicuculline to block GABA synaptic activity. To characterize light-evoked ESPC activity, 20 μM DNQX was applied to the bath to block AMPA receptor activity. All drugs were made in stock solutions, diluted on the day of the experiment and added directly to the ACSF.

Electrophysiology data analysis

Synaptic properties were analyzed using MiniAnalysis (Synaptosoft, Decatur, GA) as previously described (Crawford et al., 2011; Crawford et al., 2013). Synaptic events were analyzed using parameters optimized for each cell with the detection threshold set beyond the maximum values of the all-points noise histogram for a portion of the trace containing no detectable synaptic events. This threshold generally ranged

from 5 to 8 pA. MiniAnalysis generates a summary table containing the mean and median values for the frequency, amplitude, rise time (10-90%), decay time and event half width (50%). For each cell, at least 200 events were chosen at random and manually filtered to exclude multiple peaks then combined to obtain an averaged EPSC or IPSC for each cell to obtain values for decay time, event area, and event time half-width. Additional statistical analysis is described below. Data reported are means ± SEM.

Optical stimulation

For *in vivo* stimulation, mice with previously implanted fiber optic ferrules were connected to a 200 μm, 0.37 NA patch cord via zirconia sleeve that was then connected to a diode-pumped solid-state (DPSS) laser through an FC/PC adaptor and rotary joint. We used blue (473 nm, BL-473-00100-CWM-SD-05-LED-0) and yellow (561 nm, GR-561-00100-CWM-SD-05-LED-F) DPSS lasers obtained from OEM Laser Systems (Bluffdale, UT). Power output was measured using an optical sensor (Thorlabs, Newton, NJ) to be about 10 mW. Intensity was calculated using a model predicting irradiance in mammalian tissues (http://www.stanford.edu/group/dlab/cgi-bin/graph/chart.php). From a 200 μm fiber optic tip, estimated intensity was 7.33 mW mm^{-2} for blue laser stimulation and 7.05 mW mm^{-2} for yellow laser stimulation. For stimulation of vmPFC terminals expressing *ChR2* to determine DRN neuronal activation, the day before the stimulation mice were connected to the laser and housed in home cages overnight. The following day we performed sustained blue light stimulation at 25 Hz with 10 ms pulse width for 20 minutes without disturbing the mouse. For stimulation of *ChR2* during CSDS mice were connected to the laser after physical defeat and we performed sustained blue light stimulation at 25 Hz and 10 ms pulse width during 20 minutes of sensory contact. For

stimulation of *Arch* during CSDS we performed constant yellow light stimulation for 20 minutes.

For stimulation of brain slices expressing *ChR2* in vmPFC terminals, a prepared 200 μm core, 0.37 NA standard multimode fiber was lowered into the recording chamber and submerged below ACSF. The tip of the fiber was positioned approximately 1 mm from the vmPFC or DRN, illuminating the entire region. Stimulation of the DRN was either performed at 0.5 Hz with a 10 ms pulse width for an 8 second epoch with 22 seconds between sweeps or at 25 Hz with a 5 ms pulse width for a 20 second epoch with 10 seconds between sweeps. Stimulation of the vmPFC was performed at either 5 Hz, 25 Hz or 100 Hz with a 5 ms pulse width for a 2 second epoch with 18 seconds between sweeps. Laser intensity was estimated to be 18.07 mW mm-2.

Data analysis and statistics

For multiple group comparisons, all variables were distributed normally based on Bartlett's test and analyzed using parametric statistics (i.e. one-, two-way ANOVAs, between group or with repeated measures, followed by Fisher's PLSD test where appropriate). Comparisons between two groups were performed using Student's t-test. Statistical analysis was performed using Statistica (StatSoft, Tulsa, OK). To calculate spatial correlation between *SynP* and *tdTomato* fluorescence, the Pearson correlation coefficient (Pearson's r) was calculated. To determine rate of cumulative time spent per second, the slope of the linear regression and goodness of fit (r^2) was calculated. Statistical significance was defined as a p value < 0.05. All data are presented as the mean ± SEM. Outlying values (3 standard deviations from the mean) were excluded from group means.

Results

Excitatory vmPFC terminals and GABAergic neurons in the DRN have overlapping topographic distributions

To assess the distribution of vmPFC axon terminals in the DRN we performed viral mediated tracing using a *Cre*-dependent AAV vector coding for a *GFP*-tagged variant of the synaptic protein *Synaptophysin* (*SynP*) (Veerakumar et al., 2013). To selectively target excitatory neurons in the vmPFC the vector was injected in male mice of the *CaMKIIa-Cre* line (Calhoun et al., 1996) (Fig. 3.1A). We then assessed the distribution of excitatory vmPFC terminals by visualizing *SynP-GFP* fluorescence in the DRN (Fig. 3.1B). The distribution pattern of vmPFC terminals shows a striking similarity to images from the Allen Brain Connectivity Atlas after injetion of an AAV

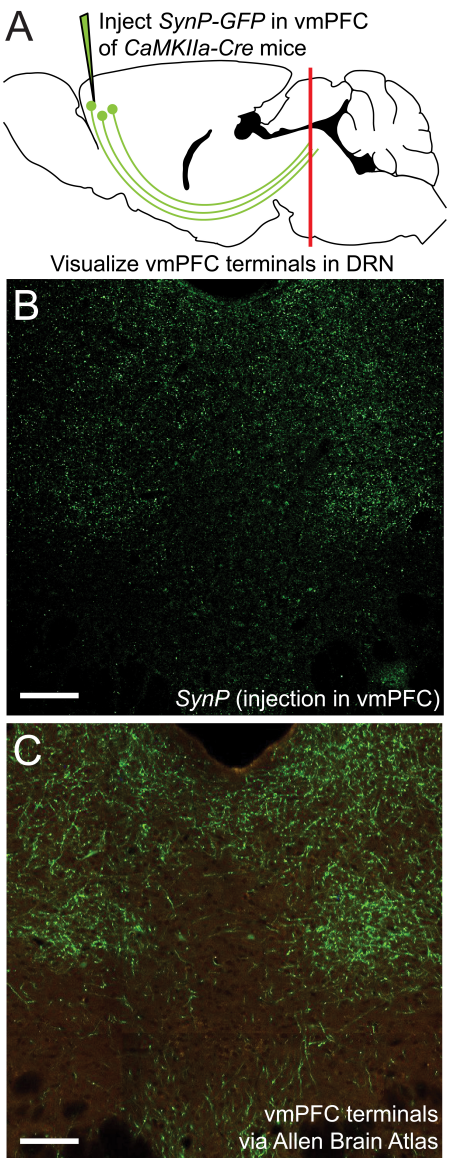

Figure 3.1. Visualization of vmPFC axon terminals in the DRN.

(A) An AAV vector coding for the *Cre*-dependent expression of the fluorescently tagged synaptic protein *Synaptophysin* (*SynP-GFP*) was injected in the vmPFC of *CaMKIIa-Cre* mice. Topographic distribution of vmPFC axon terminals in the DRN was visualized using confocal microscopy. **(B)** Distribution of vmPFC terminals as determined by *SynP-GFP* expression as reported in this study. Scale bar 50µm. **(C)** Anterograde tracing using an AAV-GFP vector injected in the vmPFC as reported by the Allen Brain Connectivity Atlas. Picture is courtesy of the Allen Mouse Brain Atlas [Internet]. ©2012 Allen Institute for Brain Science (Seattle, WA). Available from: http://mouse.brain-map.org. Despite use of different tracing methods, the pattern of innervation revealed is strikingly similar, with sparse innervation of the midline area of the DRN, classically containing 5-HT neurons, and denser innervation of lateral portions of the DRN. Scale bar

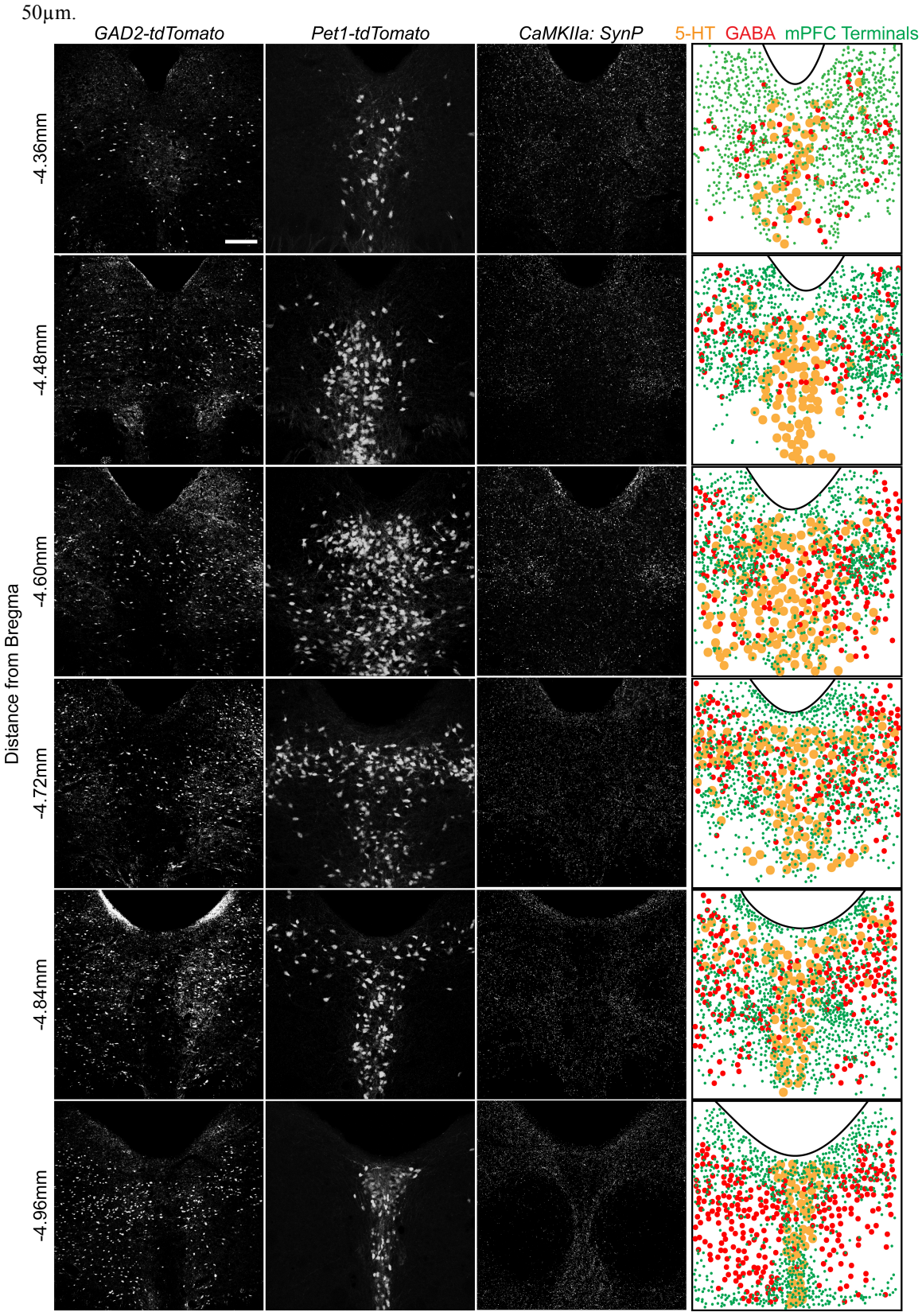
50µm.
GAD2-tdTomato
Pet1-tdTomato
CaMKIIa: SynP
5-HT GABA mPFC Terminals
Distance from Bregma
-4.36mm
-4.48mm
-4.60mm
-4.72mm
-4.84mm
-4.96mm

Figure 3.2. Spatial organization of 5-HT and GABA neurons and vmPFC terminals in the DRN.

Native fluorescence of GABA (*GAD2-tdTomato*, column 1) and 5-HT (*Pet1-tdTomato*, column 2) neurons as well as antibody enhanced glutamatergic vmPFC terminal fluorescence (*CaMKIIa*: *SynP-GFP*) is visualized in serial sections of the DRN. Individual cellular or synaptic localization was overlaid on a map using the aqueduct as a reference. Scale bar 50μm.

expressing *EGFP* in the vmPFC (Fig. 3.1C). To determine whether synapses formed by these terminals occur preferentially in areas enriched in 5-HT or GABA neuron subtypes, we compared the topographic distribution of *SynP-GFP* punctas with that of genetically labeled GABA (*GAD2-tdTomato*) or 5-HT (*Pet1-tdTomato*) neurons at similar rostro-caudal levels (Challis et al., 2013) (Fig. 3.2). We found that GABA neurons tended to be primarily distributed in the lateral aspects of the DRN, while 5-HT neurons were concentrated in the midline in the anterior and posterior DRN and were in the midline as well as branched to the dorsolateral DRN, or lateral wings (Crawford et al., 2010), in the mid DRN. Glutamatergic vmPFC terminals on the other hand clustered in the dorsolateral and ventrolateral DRN in the anterior to mid DRN before gathering in the dorsomedial and ventromedial DRN of the most posterior slices. We compared the relative fluorescent intensity of *SynP-GFP* with the intensities of *GAD2-tdTomato* or *Pet1-tdTomato* signals to determine if there was a topographic correlation in the DRN (Fig. 3.3). Scatter plots summarize the correlation found between *SynP-GFP* intensity and either *GAD2-tdTomato* (Fig. 3.3B) or *Pet1-tdTomato* (Fig. 3.3C) intensity. We found that throughout the DRN, distribution of vmPFC terminals correlated more strongly with GABA neurons than with 5-HT neurons except in the most caudal extent of the DRN as determined by calculation of Pearson correlation coefficients (Fig. 3.3D).

Figure 3.3. Topographic distribution of vmPFC terminals correlates with GABAergic populations in the DRN.

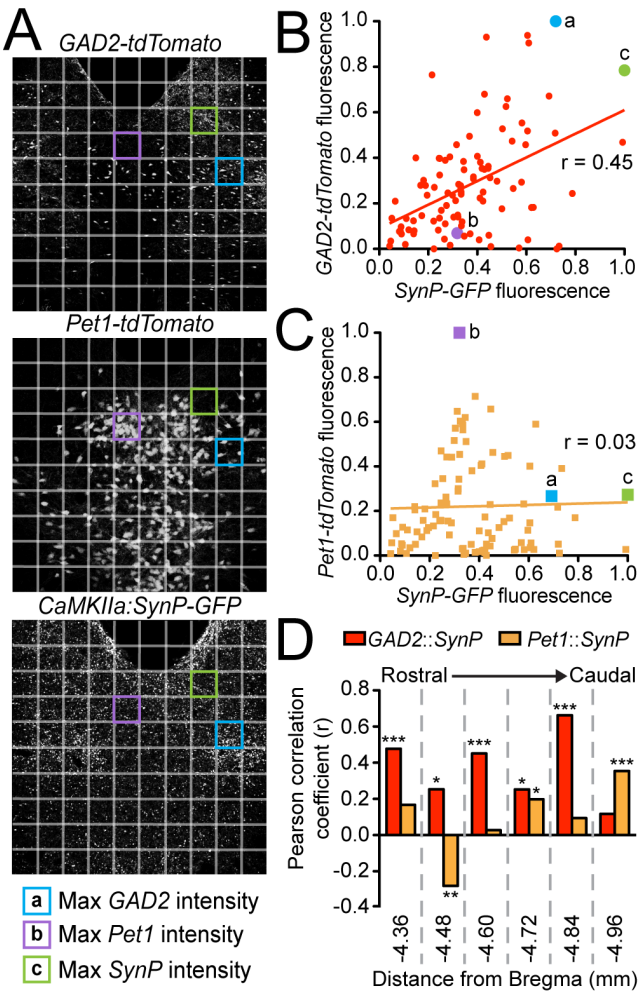

At each of the 6 rostrocaudal levels of the DRN, images of each fluorescent signal were divided into a 10 x 10 grid. Relative intensities were calculated for each of the *SynP-GFP* (vmPFC terminals), *GAD2-tdTomato* (GABA neurons) and *Pet1-tdTomato* (5-HT neurons) fluorescent signals for each box of the grid at every rostrocaudal level. **(A)** For example, depicted here are DRN slices at -4.60 mm from Bregma. Highlighted grid boxes depict areas that were calculated to have the highest (a) *GAD2-tdTomato* intensity, (b) *Pet1-tdTomato* intensity and (c) *SynP-GFP* intensity. Intensity values of *SynP-GFP* were correlated with that of **(B)** *GAD2-tdTomato* or **(C)** *Pet1-tdTomato* at each of the 6 rostrocaudal levels. These were graphed on scatter plots with (x,y) coordinates plotted as (*SynP-GFP* intensity, *tdTomato* intensity). Grid boxes highlighted in (A) are plotted in (B) and (C) as examples. Pearson's correlation coefficients (r) were calculated for *GAD2-tdTomato* or *Pet1-tdTomato* versus *SynP-GFP* with r = 1 signifying strong correlation, r = 0 signifying no correlation and r = -1 signifying strong negative correlation. **(D)** Overall there is a stronger correlation of topographic distribution of GABA neurons with vmPFC terminals than 5-HT neurons except in the most caudal DRN. (Bars with asterisks indicate Pearson coefficients that are significantly non-zero; *p < 0.05, **p < 0.005, **p < 0.001).

Descending excitatory projections from the vmPFC preferentially drive DRN *cFos* induction in GABAergic neurons

Using immediate early gene mapping, we previously established that exposure to CSDS activates DRN GABA neurons preferentially over 5-HT neurons and that the topographic distribution of these neurons overlaps with that of vmPFC terminals (Challis et al., 2013). Here, we tested whether direct activation of the terminals would increase

cFos primarily in GABA neurons. We did this by stereotaxic infusion of an AAV vector leading to *CaMKIIa*-driven expression of *YFP*-tagged *Channelrhodopsin-2* (*ChR2-YFP*) in the vmPFC (Ji and Neugebauer, 2012) (Fig. 3.4A,B). Previous studies have shown that this approach restricts expression chiefly to pyramidal neurons (Tsien et al., 1996). Twenty-eight days after surgery we observed robust expression of *ChR2-YFP* in the vmPFC that spread through infralimbic (IL) and prelimbic (PL) regions. We confirmed the expression and function of *ChR2* in the vmPFC by performing current-clamp recordings of YFP^+ neurons during exposure to trains of pulsed light (Fig. 3.4C). Photostimulation frequencies from 5 Hz up to 25 Hz resulted in pulse-locked action potentials, however at 100 Hz, a stimulation frequency similar to that of deep brain stimulation (DBS), this fidelity was lost. To then stimulate terminals directly in the DRN, we implanted cannulae targeting the DRN three weeks after injection (Fig. 3.4D). Three days before stimulation fiber optic ferrules were inserted in the cannulae and secured to the skull. The day prior to testing, mice were connected to the laser via fiber optic patch cable and remained isolated in home cages overnight. On the day of testing we performed laser stimulation without disturbing the mice to prevent activation by handling. We used a selective photoexcitation protocol of vmPFC axon terminals in the DRN similar to an approach that has previously been shown to produce robust time-locked behavioral effects dependent on the resulting local release of glutamate in the DRN (Warden et al., 2012). Here, photostimulation of the vmPFC terminals in the DRN for 20 minutes (473 nm, 10 mW, 25 Hz, 10 ms pulse width) resulted in a significant overall increase in *cFos* expression compared to unstimulated controls (Student's t-test, $t_{(10)}=14.89$, $p<0.001$; n=6-8 per group; Fig. 3.4E,F). In *GAD2-tdTomato* and *Pet1-tdTomato* mice, this stimulation

protocol led to significantly higher activation of *GAD2*- over *Pet1*-labeled neurons (Two- way ANOVA, genotype x stim, $F_{(3,13)} = 102.07$, $p < 0.001$, Fig. 3.4G,H). Control mice that were connected to the laser, but not stimulated did not display an increase in *cFos* immunoreactivity. Mice that were injected with sham virus also did not

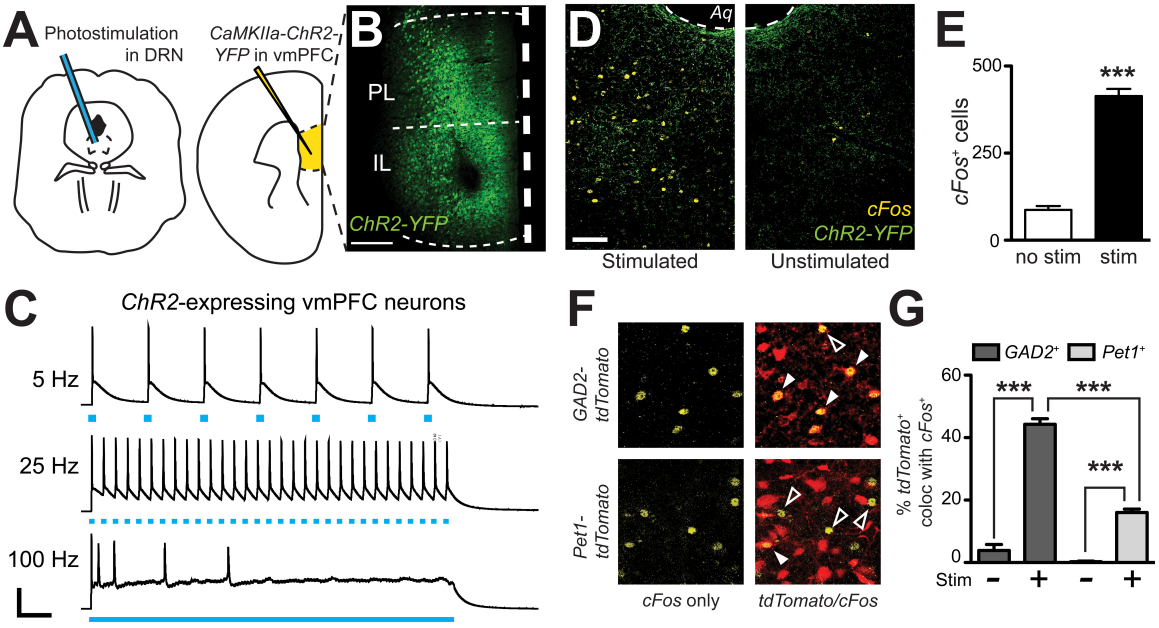

Figure 3.4. Preferential *cFos* induction in GABA neurons after photostimulation of vmPFC terminals in the DRN.

(A) *CaMKIIa*-driven *ChR2-YFP* was injected in the vmPFC of *GAD2-tdTomato* or *Pet1-tdTomato* mice.
(B) After allowing 6 weeks, robust expression of *ChR2-YFP* was achieved. Scale bar 25 µm.
(C) Fluorescent neurons in layer V of the vmPFC were recorded. Current-clamp traces of YFP^+ vmPFC neurons demonstrate temporal fidelity of *ChR2*-mediated photocurrents at 5 Hz and 25 Hz, and loss of precision at 100 Hz. Scale bar 40 pA, 0.2 s.
(D) At the same time point post-injection (6 weeks), vmPFC terminals in the DRN were photostimulated for 20 min using 473nm light (10 mW, 25 Hz, 10 ms pulse width).
(E) *cFos* immunofluorescence was evaluated after photostimulation to indicate neuronal activation. Scale bar 50µm.
(F) Photostimulation resulted in a significant increase in total *cFos* expression with no difference between genotype (Student's t-test, ***$p < 0.001$).
(G) Quantification of *cFos* colocalization with native *tdTomato* fluorescence was used to determine the neuronal populations activated. Closed arrows indicate colocalized neurons.
(H) Without laser stimulation there is minimal *cFos* expression. After photoactivation of vmPFC terminals there were increases in neuronal activation of both GABA and 5-HT neurons, however a much higher percentage of *GAD2-tdTomato* neurons colocalize with *cFos* (Two-way ANOVA, Fisher post-hoc, ***$p < 0.001$).

display an increase in *cFos* expression (data not shown). This outcome, in line with previous neuroanatomical and ultrastructural data, implicates GABAergic neurons as the primary postsynaptic targets of vmPFC afferents in the DRN.

Photostimulation of vmPFC terminals in DRN drives timed-locked AMPA-mediated postsynaptic responses in GABAergic but not 5-HT neurons

To determine if the vmPFC drives synaptic activity of GABA neurons in the DRN we again injected *CaMKIIa*-driven *ChR2* into the vmPFC of *GAD2-tdTomato* mice. After 6 weeks, we then prepared slices of the DRN for whole-cell patch clamp electrophysiology and recorded from genetically labeled $GAD2^{+}$ GABA neurons (Fig. 3.5A). Brief pulses of 473nm laser stimulation (0.5 Hz, 10 mW, 10 ms pulse width) resulted in pulse-locked EPSC events (Fig. 3.5C) that remained in high fidelity up to 25 Hz (Fig. 3.5D). In the presence of DNQX these events disappeared, indicating that the recorded excitatory events were mediated by AMPA receptors (Fig. 3.5B). Comparing laser-evoked EPSCs to spontaneous events revealed significant differences in event rise time [Student's t-test, $t_{(12)} = 4.56$, $p < 0.001$; number of mice(number of neurons) = 2(12)] and decay time (Student's t-test, $t_{(12)} = 2.16$, $p < 0.05$) and trends towards significance in event amplitude and charge transfer (Fig. 3.5B and Table 3.1). These differences indicated that the photostimulation of vmPFC fibers resulted in a unique postsynaptic response that was distinguishable from spontaneous quantal release. Using these stimulation parameters we were able to record postsynaptic responses in 25% of the recorded GABA neurons (12 total neurons). In contrast, recording from identified 5-HT neurons in *Pet1-tdTomato* mice did not yield any stimulated postsynaptic responses (12

total neurons; Fig. 3.5E). These results reinforce the premise that the vmPFC sends glutamatergic projections directly to GABAergic neurons in the DRN.

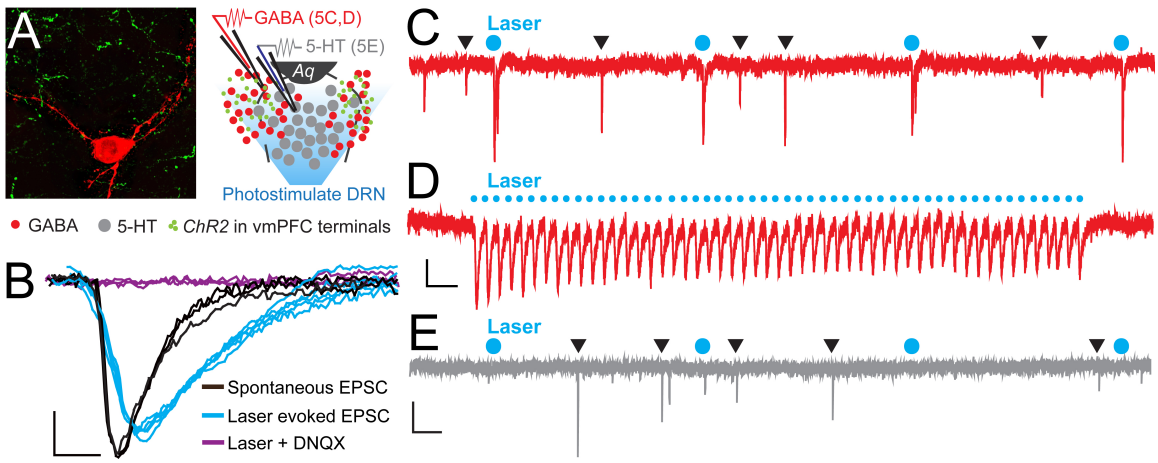

Figure 3.5. Photoactivation of vmPFC terminals results in time-locked EPSC events in DRN GABA neurons.

(A) High magnification confocal image of a biocytin-filled recorded *GAD2-tdTomato* neuron (red) in close contact with axon terminals from vmPFC neurons (green) anterogradely traced using AAV-*CaMKIIa-ChR2-YFP*. Inset displays a schematic of DRN topography in recorded slices from *GAD2-tdTomato* mice. Recorded neurons were purposely selected in ventrolateral subregions of the DRN that are rich in afferents from the vmPFC while the DRN was photostimulated. *Aq* – aqueduct.
(B) Average voltage-clamp traces of spontaneous and laser evoked EPSC events. Application of 20μM DNQX prevented laser-evoked EPSC events. Scale bar 4 pA, 3 ms.
(C) Raw voltage-clamp data trace recorded from a *GAD2-tdTomato* neuron during pulsed photoactivation of *ChR2* containing vmPFC terminals (473nm, 10mW, 0.5Hz, 10ms pulse width). Blue circles mark laser pulses. Black triangles indicate spontaneous EPSC events. Scale bar 10pA, 0.5s.
(D) EPSC events were time-locked to a 25 Hz laser stimulation train. Scale bar 5pA, 0.1s.
(E) Recordings from *Pet1-tdTomato* neurons did not display EPSC events in response to laser stimulation. Scale bar 10 pA, 0.5s.

Table 3.1. Comparison of spontaneous versus laser-evoked EPSC events in DRN GABA neurons.

	Rise (ms)	Amplitude (pA)	Decay (ms)	Area under curve (pA)
Spontaneous	1.92 ± 0.15	14.68 ± 1.61	3.74 ± 0.57	-57.68 ± 6.56
Laser-evoked	2.84 ± 0.14***	11.55 ± 1.43	4.66 ± 0.13*	-67.81 ± 9.37

Data are expressed as mean values ± SEM.
*p < 0.05, ***p < 0.001 values different from spontaneous EPSC events as determined by unpaired t-test.

Photoactivation and photoinhibition of vmPFC terminals in the DRN during post-defeat sensory contact period has opposite effects on avoidance behavior.

We have previously demonstrated that inhibition of DRN GABAergic neurons prevents the acquisition of social avoidance after defeat, but did not change expression of an already acquired avoidance phenotype (Challis et al., 2013). To determine whether vmPFC terminals that drive GABA neurons' activity in the DRN also contribute to the encoding of social aversion, we expressed optogenetic probes in *CaMKIIa-Cre* neurons in the vmPFC and photostimulated or photoinhibited terminals directly in the DRN. To activate glutamatergic vmPFC projections, we used *ChR2* (473nm) and to inhibit we expressed *Archaerhodopsin* (*Arch,* 543nm). Because we have previously shown that a period of 20 minutes of post-defeat sensory exposure is necessary and sufficient to trigger a significant avoidance response (Challis et al., 2013), mice were connected to the laser via fiber optic connector and stimulated daily during this period before returning to home cages overnight (Fig. 3.6A). This was repeated for 10 days with exposure to a novel CD1 aggressor mouse every day. On day 11, approach-avoidance choices were evaluated by performing the social interaction test using a novel social target (Fig. 3.6B).

Mice from the control group injected with a sham vector and receiving laser stimulation in the DRN displayed interaction times similar to that previously reported in defeated naïve mice indicating that the cannulation and potential thermal artifacts caused by laser manipulation do not *per se* significantly alter the development of social avoidance (Challis et al., 2013) (Fig. 3.6C). In contrast, mice whose vmPFC terminals were photoinhibited in the DRN did not display typical social avoidance and maintained high levels of approach during social interaction testing (Two-way ANOVA, virus x stim,

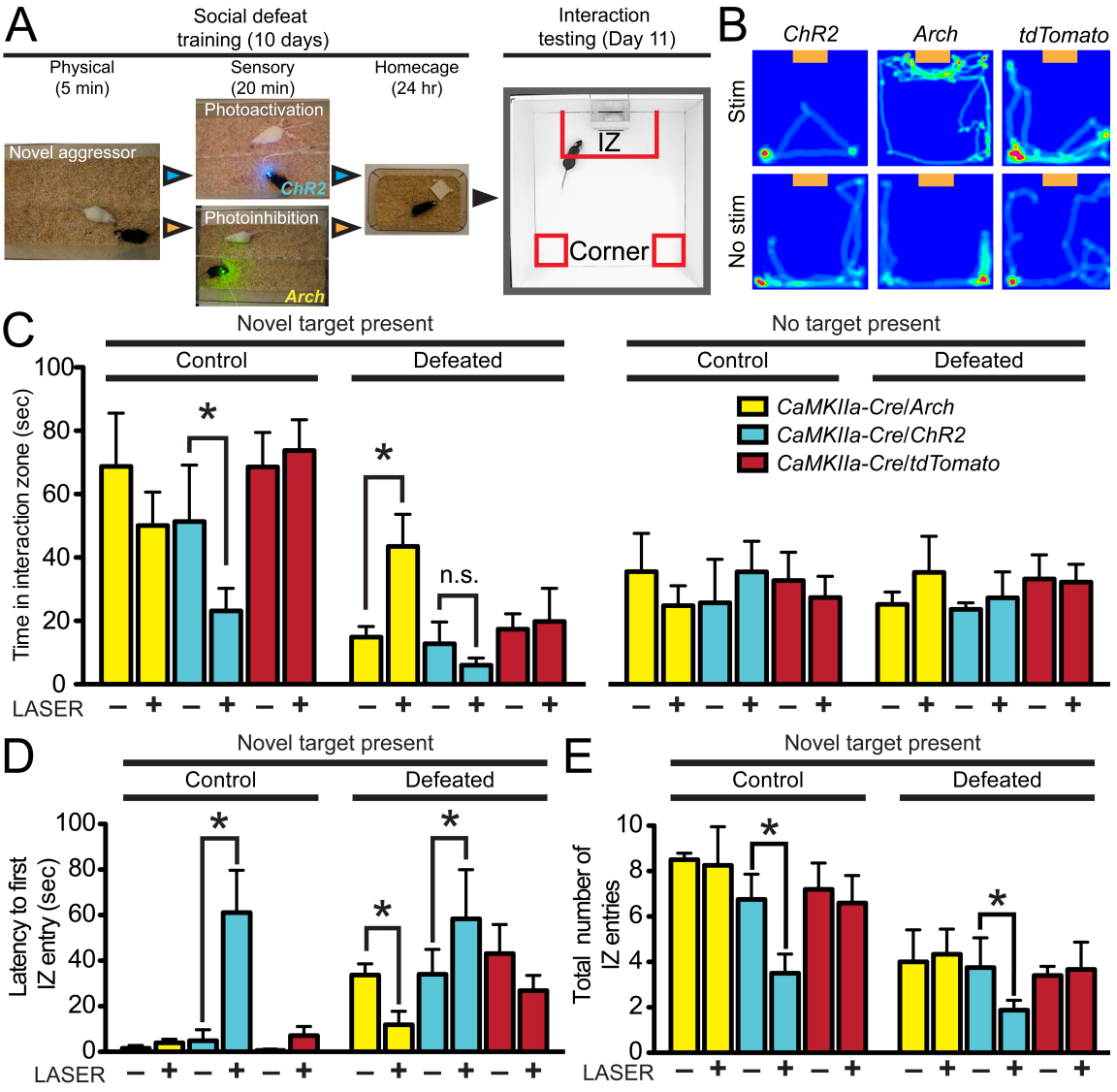

Figure 3.6. Divergent effects of vmPFC terminal photostimulation and photoinhibition in the DRN.

(A) *CaMKIIa-Cre* mice were injected in the vmPFC with *Cre*-dependent AAVs coding for the expression of *ChR2-YFP*, *Arch-GFP* or *tdTomato*. Cohorts of mice were exposed to 5 min of physical defeat followed by 20 min of sensory contact with either photoactivation by *ChR2* (473 nm, 10 mW, 25 Hz, 10 ms pulse width) or photoinhibition by *Arch* (561 nm, 10 mW) of vmPFC terminals via implanted fiber optic targeting the DRN. Mice were then placed in homecages overnight. This was repeated with exposure to a novel aggressor each day. On day 11, mice were assessed for approach or avoidance in the social interaction test. *IZ* – interaction zone.
(B) Heat maps depicting representative behavioral effects of photoactivating (C*hR2*) or photoinhibiting (*Arch*) vmPFC terminals during the sensory period of social defeat on interaction with a novel social target (orange box). Red and green areas depict areas where mice spent the most time. No effect was observed in mice injected with sham *tdTomato* virus.
(C) In defeated mice, photosilencing of vmPFC terminals prevented a decrease in social interaction (Two-way ANOVA, Fisher post-hoc, *p = 0.050) while photoactivation did not decrease interaction times

significantly from *ChR2*-expressing mice that did not receive laser stimulation. Undefeated control mice whose vmPFC terminals in the DRN were stimulated displayed a significant decrease in social interaction compared to unstimulated counterparts (Two-way ANOVA, Fisher post-hoc, *p = 0.049). No effect of virus of photostimulation was observed when a novel social target was not present.
(D) With a novel social target present, mice whose vmPFC terminals were photoactivated via *ChR2* during sensory contact displayed significant increases in latencies to first enter the IZ in both control (Two-way ANOVA, Fisher post-hoc, *p = 0.033) and defeated conditions (*p = 0.049). Defeated mice whose vmPFC terminals in the DRN were photosilenced via *Arch* during sensory contact displayed shorter latencies to first enter the IZ (*p = 0.048).
(E) Total number of entries into the IZ was decreased in both control and defeated mice whose vmPFC terminals in the DRN were photoactivated during sensory contact (Two-way ANOVA, Fisher post-hoc, control *p = 0.042, defeated *p = 0.049).

$F_{(11,50)} = 6.58$, $p < 0.001$; n = 6-10 mice per group). On the other hand, defeated mice whose vmPFC terminals were photoactivated tended to show reductions in social interaction compared to mice injected with sham virus, although this difference did not reach statistical significance due to a floor effect on the expression of social avoidance. Interestingly, control mice that did not undergo defeat, but received photoactivation of vmPFC terminals in the DRN in the presence of a CD1 social target also subsequently displayed a significant decrease in time spent (Two-way ANOVA, virus x stim, $F_{(11,50)} = 4.50$, $p = 0.002$; Fig. 3.6D) and in total entries in the social interaction zone (Two-way ANOVA, virus x stim, $F_{(11,50)} = 6.85$, $p < 0.001$; Fig. 3.6E).

Increased vmPFC drive of DRN delays decision to approach novel social target

To gain further insight into how manipulation of vmPFC-DRN during CSDS training alters subsequent avoidance behaviors, we examined the effect of this manipulation on the time-course of social approach-avoidance behaviors during the interaction test. We first characterized the temporal distribution of the bouts of interaction during the course of the tests in a large cohort (n=117) of unimplanted control and defeated mice, stratified as “resilient” or “susceptible” as previously reported (Challis et al., 2013; Golden et al., 2011; Krishnan et al., 2007). Examining the cumulative time

spent in the social interaction and corner zones we found that the behavior of susceptible mice significantly diverged from control and resilient as early as 4 seconds into the test (Repeated measures ANOVA, defeat x time, $F_{(298,15049)} = 49.894$, $p < 0.001$; Fig. 3.7A). Many mice in the latter two groups entered the social interaction zone immediately, with almost all entering under 40 seconds (Fig. 3.7B), and continued to investigate the social target throughout the entire duration of the trial such that average interaction time accrued quasi-linearly in these groups (Linear regression, slope in cumulative time in seconds/second elapsed = 0.464 ± 0.005 for control, 0.4558 ± 0.004 for resilient, $r^2 = 0.741$ for control, 0.616 for resilient; Fig. 3.7A). In contrast, susceptible mice considerably delayed their decision to first enter the social interaction zone compared to resilient mice (under 50% had entered by 40 seconds; Kolmogorov-Smirnov test, $p < 0.001$; Fig. 3.7B) and rarely returned to interaction zone after their first entry (Linear regression, slope = 0.1482 ± 0.002, $r^2 = 0.436$ for susceptible; Fig. 3.7A). Together, we interpret these data as an indication that the interindividual variability during the social interaction test reflects the execution of a binary choice between two behavioral strategies made a few seconds after the initiation of the task.

We applied the same time-course analysis to the dataset obtained from undefeated control mice receiving chronic photostimulation of vmPFC terminals during sensory exposure to novel aggressor mice. We found that the behavioral profile of undefeated mice that were implanted, but not stimulated, followed the same behavioral approach pattern as unimplanted control mice described above (Fig. 3.7C). However, in striking contrast, undefeated mice whose vmPFC axon terminals in the DRN were photoactivated

chose to remain in the distal corners from the beginning of the test (Repeated measures ANOVA, stimulation x time, $F_{(149,894)} = 16.18$, $p < 0.001$; Fig. 3.7D) and delayed their

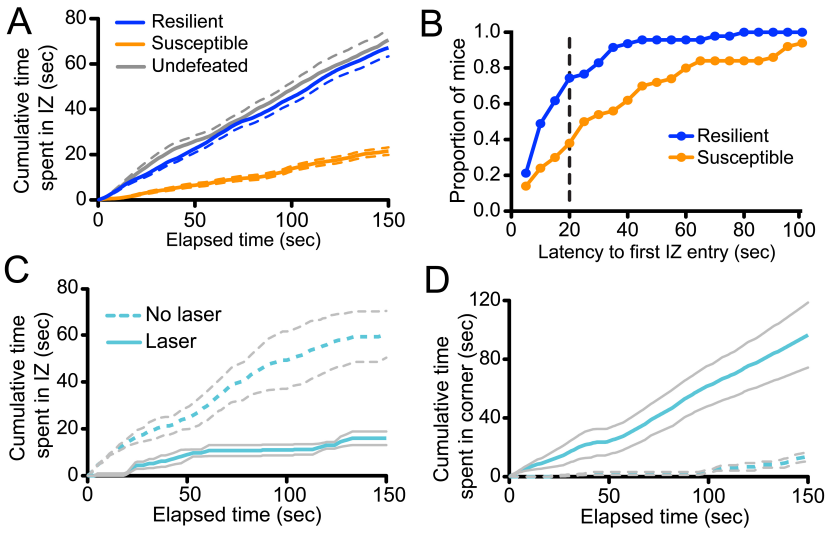

Figure 3.7. Defeat and photoactivation of vmPFC terminals in the DRN bias social approach/avoidance choices.

(A) Analysis was performed on 97 previously defeated and 20 undefeated mice. Defeated mice were characterized as resilient or susceptible based on previously described criteria (Golden et al., 2011; Challis et al., 2013). The cumulative time spent in the interaction zone (IZ) was plotted across the duration of the social interaction test. The cumulative interaction time of susceptible mice significantly diverged from that of both resilient and control mice at 4 seconds (Repeated measures ANOVA, Fisher post-hoc, $p = 0.020$ at 4 seconds). Data shown is average per group. Dashed lines represent the S.E.M.
(B) Latencies to the first IZ entry were determined in 5-second bins. Plotted are the proportions of mice within each behavioral group to display first IZ entry within the given timeframe or less. A greater proportion of resilient mice first entered the IZ faster that of susceptible mice (Kolmogorov-Smirnov test, $p < 0.001$). The dashed vertical line represents the latency at which the proportion discrepancy between the two behavioral is the largest (0.36).
(C) Cumulative time spent in the IZ is plotted across time in the social interaction test for undefeated *CaMKIIa-Cre* mice expressing *ChR2* in the vmPFC with and without laser stimulation of vmPFC terminals in the DRN. Increase in cumulative interaction time from 0 seconds did not significantly differ until 60 seconds in laser-treated mice (Repeated measures ANOVA, Fisher post-hoc within Laser group, $p = 0.045$ at 60 seconds).
(D) Cumulative time spent in the corners distal to the novel social target is plotted across time in the social interaction test. Increase in cumulative corner time from 0 seconds significantly differed at 14 seconds in laser-treated mice (Repeated measures ANOVA, Fisher post-hoc within Laser group, $p = 0.047$ at 14 seconds).

exploration of the novel social target for the majority of the trial (Repeated measures ANOVA, stimulation x time, $F_{(149,894)} = 6.79$, $p < 0.001$; Fig. 3.7C). These mice also did

not return to the social interaction zone as indicated by the plateau from 60 to 120 seconds (Linear regression, slope in cumulative time in seconds/seconds elapsed = 0.0196 ± 0.015, $r^2 = 0.007$ for Laser group from 60 to 120 seconds). These results together suggest that enhancing glutamatergic drive from vmPFC axons in the DRN, in the presence of neutral social cues, functions as an aversive compound cue that bias subsequent choice towards an avoidance strategy.

Discussion

Our results show that brief daily *ChR2*-mediated photoactivation of vmPFC inputs to the DRN temporally paired with sensory exposure to social cues in the absence of physical aggression resulted in a subsequent social avoidance phenotype, resembling that induced by social defeat. In addition, *Arch*-mediated photoinhibition of vmPFC inputs to the DRN during sensory contact phase in mice subjected to CSDS prevented the acquisition of social avoidance. Based on these results, we conclude that glutamatergic transmission within the vmPFC-DRN pathway bidirectionally modulates the valence perception of social cues. By characterizing the functional organization of DRN microcircuits underlying these biases, our results help clarify how maladaptive neuroplasticity of the vmPFC-DRN pathway could contribute to socio-emotional symptoms of affective disorders. These results also help conceptualize how somatic treatments such as DBS that target the vmPFC, may restore affective balance, partly through restoring neuroplasticty within the vmPFC-DRN pathway and altering DRN neurocircuitry (Veerakumar et al., 2013).

Top-down drive of 5-HT output may be gated by DRN GABAergic neurons

The DRN is considered the primary nucleus containing forebrain-projecting 5-HT neurons, however 5-HT neurons account for less than half of the total neuronal population (Bang and Commons, 2012; Bang et al., 2012). One major non-serotonergic cellular population in this region is comprised of GABAergic neurons and we have previously shown that *GAD2*$^{+}$ GABAergic neurons are the primarily activated neuronal population in the DRN in response to CSDS (Challis et al., 2013). In this work we show that axonal projections from the vmPFC localized in circumscribed subregions of the

DRN that we found to be rich in defeat-sensitized *GAD2*$^{+}$ cell bodies. Using whole-cell recording and *cF*os mapping after direct photoactivation of vmPFC terminals we determined that DRN GABA neurons were the direct and preferential synaptic targets of vmPFC projections in the DRN. In line with this hypothesized organization, an electrophysiological postsynaptic response in 5-HT neurons after vmPFC terminal photostimulation was not observed, however our experiments only sampled a limited population of neurons in the DRN using voltage clamp holding potentials standard for DRN 5-HT neurons (Beck et al., 2004). Recent work has also described the heterogeneity in physiological properties of 5-HT neurons in different DRN subfields that have known projections to dissimilar forebrain regions that regulate different types of behavior (Calizo et al., 2011; Crawford et al., 2011). Therefore, it will be important to probe a greater number of 5-HT neurons using various physiological conditions appropriate for the designated DRN subfield. We did observe a modest induction of *cFos* in 5-HT neurons after sustained photoactivation of vmPFC terminals, suggesting that direct excitatory influence from the vmPFC onto 5-HT neurons may exist, although the possibility that this may reflect an indirect effect cannot be excluded. The much greater percent of *cFos* induction observed in GABA neurons, though, suggests either a higher number of vmPFC projections targeting GABAergic neurons or an enhanced synaptic strength between vmPFC afferents and DRN GABA neurons.

In agreement with the findings here, previous studies had suggested preferential innervation of DRN GABA neurons by vmPFC terminals (Celada et al., 2001; Hajós et al., 2007; Jankowski and Sesack, 2004). Given these reports and our previous work showing that DRN GABA neurons locally synapse on and inhibit 5-HT neurons (Challis

et al., 2013), we are presented with a putative circuit whereby DRN GABA neurons are positioned critically to gate top-down drive of the DRN and 5-HT output that would subsequently influence affective regulation. These same DRN GABA neurons have previously been shown to receive converging inputs from both the vmPFC and lateral habenula (Varga et al., 2003) and also possibly from CRF containing neurons originating in the amygdala and BNST (Waselus et al., 2009). It will be important in future experiments to determine whether the functional impact of vmPFC is dependent upon the coincident activity of these other inputs.

Social valence choices are modulated by top-down projections from the vmPFC to the DRN

The vmPFC is classically thought of as an integrative hub that coordinates cognitive, affective and autonomic dimensions of negative emotional experiences through distributed descending inputs to subcortical regions in the limbic system and brainstem (Roy et al., 2012). Animal studies suggest this role partly involves top-down modulation of 5-HT neurons in the brainstem raphe nuclei. Multiple studies relying on pharmacological inactivation methods (Amat et al., 2005; Amat et al., 2006; Christianson et al., 2009; Slattery et al., 2011), electrical stimulation (Hamani et al., 2010; Veerakumar et al., 2013) or optogenetics (Kumar et al., 2013; Warden et al., 2012) have implicated vmPFC-DRN circuits in the regulation of behavioral response to aversive challenges. However based on the data currently available there is not a consensus as to whether activation of cortical inputs in the DRN inhibits or promotes 5-HT output. It is also controversial whether this then mediates aversion or on the contrary, facilitates anti-aversive responses. Although there is solid evidence that electrical stimulation of the

vmPFC inhibits the firing of 5-HT cells, concurrent measures of extracellular 5-HT using microdialysis have also reported corresponding enhancements of extracellular 5-HT in the DRN and forebrain (Celada et al., 2001; Hamani et al., 2010), further complicating the relationship between firing and release.

Recent computational models have posited that 5-HT codes for threat prediction signals, particularly during tasks that use behavioral inhibition as a readout for aversion in human and animals (Crockett et al., 2012; Soubrie et al., 1986). Reduction in tonic 5-HT levels after tryptophan depletion (presumably resulting in a gain in signal-to-noise for 5-HT phasic signals, see Cools et al., 2008) has been associated with enhanced neural processing and detection of social threats (Harmer and Cowen, 2013; Passamonti et al., 2012), punishment prediction (Cools et al., 2008) and increased social defensiveness (Young, 2013). Importantly, avoidance biases in response to ambiguous social cues are reported in patients suffering from depression and social phobia (Derntl et al., 2011; Heuer et al., 2007; Moser et al., 2012; Seidel et al., 2010; Volman et al., 2011). In the social interaction task we used here, mice confronting an "ambiguous" social target resembling their aggressor made a rapid binary choice between two alternative behavioral strategies (e.g. active risk assessment through social approach or social avoidance by remaining in a distal corner). Our results show that susceptible mice have a bias towards avoidance that resemble responses of depressed patients in laboratory approach-avoidance tasks. Whether this choice is effectively determined by modulation of 5-HT levels remains to be determined, however, in the context of social interactions, dishinibition of 5-HT neurons via pharmacological autoinhibition of GABA neurons in the DRN, which increases 5-HT output in the forebrain regions such as the vmPFC, has

consistently been shown to promote social approach and offensive behaviors of defeated mice (Takahashi et al., 2012; Takahashi et al., 2010). This is in general agreement with data linking enhancement of forebrain 5-HT output with resilience to social stress and maintenance of dominant social status in various species (Alekseyenko et al., 2010; Bruchas et al., 2011; Malatynska et al., 2005; Penn et al., 2010; Raleigh et al., 1991) and thus, DRN GABA neurons may pose as a key cellular population in mediating social choice through regulation of 5-HT output.

Our results demonstrate that chronically activating vmPFC inputs in the DRN is behaviorally pro-depressive, however they are at odds with results from Warden *et al* who reported time-locked antidepressant-like effects in the forced swim test (FST) upon direct, acute optogenetic activation of vmPFC glutamatergic terminals in the DRN (Warden et al., 2012). Our results are also difficult to reconcile with the model proposed by Maier and colleagues, whereby vmPFC-driven reductions in DRN 5-HT output mediate resistance to learned helplessness in rats (Amat et al., 2005). The apparent contradictions between these studies (reviewed in detail by (Lammel et al., 2014) could derive from obvious differences in the models employed, with the most likely being the different defense systems (behavioral inhibition versus flight) that are engaged during these tasks and the contradictory regulation by 5-HT (Deakin and Graeff, 1991). Nevertheless, our results clearly establish a key role of vmPFC afferents to the DRN in biasing approach-avoidance choices and begin to lay the groundwork for a mechanism of regulating 5-HT output in processing underlying affective resilience.

Chapter 4

Antidepressant-like effects of cortical deep brain stimulation coincide with pro-neuroplastic adaptations of serotonin systems

Avin Veerakumar[1,2]*, Collin Challis[1,3]*, Preetika Gupta[1,3], Jennifer Da[1], Aseem Upadhyay[1], Sheryl G. Beck[3,4], and Olivier Berton[1,3]

[1]Department of Psychiatry, [2]Department of Bioengineering, [3]Neuroscience Graduate Group, University of Pennsylvania Perelman School of Medicine, and [4]Department of Anesthesiology, Children's Hospital of Philadelphia and University of Pennsylvania Perelman School of Medicine, Philadelphia, PA 19104. *Co-authored

Acknowledgments

This work was supported by grants from the National Institute of Mental Health (MH087581 to OB and MH0754047, MH089800 to SGB), from the International Mental Health Research Organization (IMHRO) to OB, from NARSAD to OB, and by NRSA (T32MH014654 and F31MH097386) to CC.

The work in this chapter was published in *Biological Psychiatry* in 2013:

Veerakumar, A., Challis, C., Gupta, P., Da, J., Upadhyay, A., Beck, S. G., & Berton, O. (2013). Antidepressant-like effects of cortical deep brain stimulation coincide with pro-neuroplastic adaptations of serotonin systems. *Biol Psych*, 76(3), 203–212.

Abstract

Cortical deep brain stimulation (DBS) is a promising therapeutic option for treatment-refractory depression but its mode of action remains enigmatic. Serotonin (5-HT) systems are engaged indirectly upon high frequency stimulation of the ventromedial prefrontal cortex (vmPFC). Resulting neuroplastic changes in 5-HT systems could thus coincide with the long-term therapeutic activity of vmPFC DBS. We tested this hypothesis by evaluating the antidepressant-like activity of vmPFC DBS in the chronic social defeat stress (CSDS) model of depression. Circuit-wide neural activation induced by vmPFC DBS was mapped using *cFos* immunolabeling. The effects of chronic vmPFC DBS on the physiology and morphology of genetically-identified 5-HT cells from the Dorsal Raphe Nucleus (DRN) were examined using whole-cell recording, somatodendritic 3-D reconstructions and detailed morphometric analyses of presynaptic boutons along 5-HT axons. Acute DBS drove *cFos* expression locally in the vmPFC and in several distal monosynaptically-connected regions, including the DRN. Chronic DBS reversed CSDS-induced social avoidance, restored the disrupted balance of excitatory/inhibitory inputs onto 5-HT neurons, and reversed 5-HT hypoexcitability observed after CSDS. Furthermore, vmPFC DBS reversed CSDS-induced arborization of 5-HT dendrites in the DRN and increased the size and density of 5-HT presynaptic axonal varicosities in the dentate gyrus and vmPFC. We validate a new preclinical paradigm to examine cellular mechanisms underlying the antidepressant-like activity of vmPFC DBS and identify dramatic circuit-mediated cellular adaptations which correlate with this treatment. These neuroplastic changes of 5-HT neurons may contribute to the progressive mood improvements reported in patients treated with chronic courses of cortical DBS.

Introduction

Deep brain stimulation (DBS) of the subcallosal cingulate gyrus (SCG) has demonstrated promise as a somatic therapy for treatment-refractory depression (Holtzheimer et al., 2012; Lozano et al., 2008; Mayberg et al., 2005). Clinical evidence suggests that the antidepressant effects of SCG DBS are reinforced by chronic stimulation, with the fraction of remitters increasing linearly over months of DBS treatment (Holtzheimer et al., 2012), raising the possibility that long-term neuroadaptations are important contributors to its therapeutic activity. However, the existence and neurobiological nature of such changes remains enigmatic.

To date only a handful of studies have examined the behavioral and neurobiological effects of DBS of the ventromedial prefrontal cortex (vmPFC) (the rodent analog of the SCG) in preclinical models. Most of these studies have applied acute stimulation regimens and reported antidepressant-like effects in behavioral screens sensitive to pharmacological antidepressants (Hamani et al., 2012; Hamani et al., 2011). The observation that serotonin (5-hydroxytryptamine, 5-HT) depletion blocks the behavioral effects of acute and chronic DBS suggests that engagement of an intact serotonergic (5-HT) system is required for the antidepressant-like activity of DBS in rats (Hamani et al., 2010; Hamani et al., 2012; Hamani and Nóbrega, 2010).

Neuroanatomical tracing studies in rodents and primates indicate that the Dorsal Raphe Nucleus (DRN) receives projections from the vmPFC (Freedman et al., 2000; Varga et al., 2003; Varga et al., 2001; Vertes, 2004) and several preclinical studies have reported robust and immediate increases in DRN neural activity and serotonin output upon electrical or optogenetic stimulation of the vmPFC (Celada et al., 2001; Hamani et

al., 2010; Kumar et al., 2013; Varga et al., 2003; Varga et al., 2001; Warden et al., 2012). Whether and how chronic regimens of vmPFC DBS induce neuroplasticity in the 5-HT system is not known. Because previous studies have indicated that depression and suicide in humans (Budisic et al., 2010; Hercher et al., 2009; Kerman et al., 2012; Matthews and Harrison, 2012) and depressive-like symptoms in animals (Challis et al., 2013; Deneris and Wyler, 2012; Espallergues et al., 2012) are accompanied by maladaptive plasticity in the 5-HT system, we hypothesized that stable neuroplastic changes in the 5-HT system may coincide with the antidepressant-like effect of chronic vmPFC DBS.

To test this hypothesis we assessed the effects of chronic vmPFC DBS in mice in the context of a chronic social defeat stress (CSDS) paradigm that has face and predictive validity with regard to clinical depression (Berton et al., 2006; Golden et al., 2011). We first assessed the ability of chronic vmPFC DBS to suppress CSDS-induced social avoidance and used *cFos* immunolabeling to map the regions in which DBS was inducing neural activity. We then used a transgenic mouse line allowing for genetic identification and conditional viral targeting of 5-HT cells, together with an array of electrophysiological and morphological assays, to investigate whether chronic vmPFC DBS reversed defeat-induced changes in the structure and physiology of DRN 5-HT neurons. We report that chronic vmPFC DBS abolishes social avoidance behavior after CSDS and induces dramatic physiological, dendritic, and axonal neuroplastic adaptations in DRN 5-HT neurons that counteract the effects of CSDS.

Materials and Methods

Animals

8-12 week old male wild-type (for behavior and *cFos* experiments) or *Pet1-tdTomato* transgenic mice (for electrophysiology and morphology experiments) bred onto a C57BL/6 background were used for all experiments. To generate *Pet1-tdTomato* mice, BAC transgenic *Pet1-Cre* mice (*B6.Cg-Tg(Fev-cre)*1Esd/J; JAX stock number 012712) (Scott et al., 2005) were crossed to floxed-stop controlled *tdTomato* (RFP variant) mice (*B6.Cg-Gt(ROSA)26Sor*$^{tm9(CAG\text{-}tdTomato)Hze}$*/J*; JAX stock number 007908) (Madisen et al., 2010) to achieve fluorescent labeling of *Cre* containing cells.

Mice were housed on a 12 hour light/dark cycle with food and water available *ad libitum*, except during DBS or sham stimulation. All studies were conducted strictly according to protocols approved by the University of Pennsylvania Institutional Animal Care and Use Committee, and all procedures were performed in accordance with institutional guidelines.

Social Defeat and Social Interaction Testing

Social defeat and social interaction testing were conducted as previously reported (Berton et al., 2006; Challis et al., 2013; Espallergues et al., 2012). For 10 consecutive days, experimental mice were exposed to brief (5 min) physical encounters with an unfamiliar trained CD1 aggressor followed by overnight protected sensory contact with the aggressor trough a perforated plexiglass partition. Control (undefeated) animals were housed in identical cages with another mouse from the same genotype and handled daily.

For social interaction testing, mice were placed in an open field arena with a small 10 x 6 cm wire mesh target box positioned on one side of the arena. During the first 2.5

minute trial (“Target Absent”), the mouse was allowed to freely explore the arena with the empty box. During the second 2.5 minute trial (“Target Present”), the mouse freely explored the arena while the target box was occupied by an unfamiliar CD1 aggressor. Video-tracking software (Cleversys, Reston, VA) was used to measure the time each mouse spent in the “interaction zone”, a 14 x 26 cm rectangle surrounding the target box, along with total distance traveled. The social interaction ratio (IR) was calculated as the percentage time spent in the interaction zone in the target-present condition relative to the target-absent condition. Classification as susceptible (IR<100) and resilient (IR≥100) was conducted as previously reported (Espallergues et al., 2012; Golden et al., 2013). Only mice expressing social avoidance (i.e. stress-susceptible) were included in DBS experiments. Individual mice were assigned randomly to the "Defeat Sham" or "Defeat Stim" conditions such that the two groups had comparable mean avoidance scores before DBS treatment.

DBS Surgeries

Stainless steel, 125 μm diameter, 4 mm length bipolar electrodes (Plastics One, Roanoke, VA) were lowered at a 15° angle and implanted unilaterally into the left vmPFC [1.8 mm anteroposterior (AP), 0.8 mm mediolateral (ML), -0.27 mm dorsoventral (DV)] over a 5 minute time period. Coordinates were adopted from previous reports such that the electrode tips would be localized to the junction of the prelimbic and infralimbic cortex (Challis et al., 2013; Covington et al., 2010). Cyanoacrylate and dental cement (A-M Systems, Sequim, VA) were used to affix electrodes to the skull as previously described (Agterberg et al., 2010). Sham-stimulated mice were implanted identically. All mice were allowed to recover for one week following surgery. One mouse

was removed from all analyses due to electrode placement outside the vmPFC, and one mouse was removed from all analyses due to excessive tissue damage such that the electrode placement could not be determined.

DBS Experiments

After recovery from surgery, implanted electrodes were connected to a programmable stimulator (MED Associates, St. Albans, VT). Stimulation was applied at 160 Hz frequency, 60 μs pulse width, and 150 μA current, parameters which are similar to previous DBS studies in rodents and humans (Halpern et al., 2013; Hamani et al., 2010; Hamani and Nóbrega, 2010; Mayberg et al., 2005; Vassoler et al., 2008; Vassoler et al., 2013). For *cFos* expression experiments, mice were stimulated for 1 hour immediately followed by transcardial perfusion. For chronic DBS experiments, DBS was applied 5 hours per day for 7 days—a paradigm similar to prior chronic DBS studies for depression which have observed long-lasting antidepressant-like effects (Dournes et al., 2013; Falowski et al., 2011; Hamani et al., 2010; Schmuckermair et al., 2013) – while mice remained in their home cages. Sham-stimulated mice were handled and connected in an identical manner to the DBS stimulator, but no current was applied. Following 7 days of DBS, mice underwent social interaction testing 24 hours after the end of stimulation (mice were not stimulated during testing). To determine electrode placements, mice were perfused 24 hours after the conclusion of social interaction testing. For whole-cell recording experiments, mice were sacrificed 24 hours following the final social interaction test. For axonal morphology experiments, mice were perfused 24 hours following the conclusion of DBS.

Histology and Immunohistochemistry

To determine electrode placements, 30 μm thick coronal vmPFC slices were stained with hematoxylin and imaged on a stereoscope by a blinded experimenter. To visualize *cFos*, PSD-95, and Synaptophysin-Venus (SynP-Venus) by immunohistochemistry, brain slices were processed for immunohistochemistry using standard protocols (Challis et al., 2013; Espallergues et al., 2012).

The following primary antibodies were applied to samples overnight at 4°C: Rabbit anti-*cFos* (Santa Cruz Biotechnology, 1:1000), Goat anti-PSD-95 (Abcam ab12093, 1:500) and Chicken anti-GFP (AvesLab, 1:1000). Secondary antibodies (Alexa Fluor 647 or DyLight 649 fluorophores from Jackson ImmunoResearch Laboratories) were applied for 2 hours at 25°C. Slides were imaged at 200x magnification on a Leica TCS SPII Confocal Microscope and $cFos^{+}$ nuclei or PSD95 puncta were counted manually by a blinded experimenter using Leica LAS AF software. *cFos* nuclei were counted in the vmPFC, Pir, DG, LHb, BLA, and DRN at coordinates specified by the Paxinos Mouse Brain atlas (Franklin KBJ, Paxinos G (2007). The Mouse Brain in Stereotaxic Coordinates. 3rd edn Elsevier Academic Press: New York, USA.). Identified PSD-95 puncta with a diameter of under 30 nm were excluded from the analyses, consistent with typical PSD-95 puncta size minima (Dumitriu et al., 2012).

Whole-Cell Electrophysiology

200 μm coronal slices containing the DRN were used for whole cell recording and prepared as described previously (Calizo et al., 2011; Challis et al., 2013; Crawford et al., 2010; Crawford et al., 2013; Espallergues et al., 2012). 5-HT cells from the ventromedial DRN (vmDRN) were recorded (Crawford et al., 2010).

Brain slices were prepared as previously described (Calizo et al., 2011; Crawford et al., 2010; Crawford et al., 2013; Espallergues et al., 2012). The 200 μm coronal slices containing DRN were placed in aCSF (in mM, NaCl 124, KCl 2.5, NaH_2PO_4 1.25, $MgSO_4$ 2.0, $CaCl_2$ 2.5, dextrose 10, $NaHCO_3$ 26) at 37°C, aerated with 95% O_2/5% CO_2. After one hour, slices were kept at room temperature. Tryptophan (2.5 mM) was included in the holding chamber to maintain 5-HT synthesis, but was not in the aCSF perfusing the slice in the recording chamber. Individual slices were placed in a recording chamber (Warner Instruments, Hamden, CT) and perfused with aCSF at 2 ml/min maintained at 32°C by an in-line solution heater (TC-324, Warner Instruments). Neurons were visualized using a Nikon E600 upright microscope fitted with a 60X water immersion objective and targeted under DIC or fluorescent filters. Resistance of electrodes was about 8-10 MOhms when filled with a recording solution composed of (in mM) K-gluconate (130), NaCl (5), Na phosphocreatine (10), $MgCl_2$ (1), EGTA (0.02), HEPES (10), MgATP (2) and Na_2GTP (0.5) with 0.1% biocytin and a pH of 7.3. Whole-cell recordings were obtained using a Multiclamp 700B amplifier (Molecular Devices, Sunnyvale, CA). Cell characteristics were recorded using current clamp techniques as previously described (Crawford et al., 2010; Espallergues et al., 2012). Signals were collected and stored using Digidata 1320 analog-to-digital converter and pClamp 9.0 software (Molecular Devices). Collection of IPSC data was performed as previously described (Crawford et al., 2011) with bath application of 20 μM DNQX to block AMPA/Kainate synaptic activity. Frequency of EPSC activity was determined by subtracting IPSC frequency from the baseline frequency. All drugs were made in stock solutions, diluted on the day of the experiment and added directly to the ACSF.

Electrophysiology data analysis

Cellular characteristics were analyzed using Clampfit 9.0 (Molecular Devices). Synaptic properties were analyzed using MiniAnalysis (Synaptosoft, Decatur, GA) as previously described (Crawford et al., 2011; Crawford et al., 2013). Frequency-intensity plots were generated by measuring the number of action potentials generated by depolarizing current steps ranging from 0 to 120 pA in 20 pA increments. Average firing rate for each condition was determined by the number of action potentials generated over the 500 ms current pulse. Synaptic events were analyzed using parameters optimized for each cell with the detection threshold set beyond the maximum values of the all-points noise histogram for a portion of the trace containing no detectable synaptic events. This threshold generally ranged from 5 to 8 pA. MiniAnalysis generates a summary table containing the mean and median values for the frequency, amplitude, rise time (10-90%), decay time and event half width (50%). For each cell, at least 200 events were chosen at random and manually filtered to exclude multiple peaks then combined to obtain an averaged EPSC or IPSC for each cell to obtain values for decay time, event area, and event time half-width. The Kolmogorov-Smirnov test was used to determine whether the histograms and cumulative probability plots of the synaptic activity characteristics were different between each group. Additional statistical analysis is described below. Data reported are means ± SEM.

Morphometric analyses of somatodendritic structure and axonal boutons of 5-HT neurons

To analyze somatodendritic morphology, genetically identified 5-HT neurons from *Pet1-tdTomato* mice were filled with 1% biocytin during whole-cell recording and

were analyzed as described previously (Espallergues et al., 2012) using Neurolucida software (MBF Bioscience, Williston, VT). For analyses of somatodendritic structure, neurons were filled with 1% biocytin during whole-cell recording and were processed for immunohistochemical detection. A 20x objective lens and optical z-slices of 0.8 μm thickness were used to capture the entire extent of the dendritic tree. Confocal stacks were then analyzed using Neurolucida (version 9; MBF Bioscience). The cell soma and dendrites were traced using the Autoneuron feature and then manually edited by a blinded experimenter if necessary to ensure accurate tracing. Sholl analysis was performed using radial shells at 20 μm intervals.

For morphometric analyses of presynaptic boutons along 5-HT axons, we applied a cell-type specific genetic tagging approach that relies on a fluorescently-labeled form of the presynaptic protein synaptophysin (Synaptophysin-Venus) which we expressed selectively in DRN 5-HT neurons using a conditional viral vector injected seven days prior to the beginning of CSDS. Following CSDS, DBS, and perfusion, brain slices were stained with anti-GFP antibodies. In addition to the DRN, the dentate gyrus (DG), vmPFC, basolateral amygdala (BLA), were selected for a subsequent detailed morphometric analysis based on their innervation by DRN neurons and differential activation in response to vmPFC DBS. For morphometric analyses of presynaptic boutons, we used a conditional viral vector AAV2/9.CMV.Flex.Synaptophysin-Venus.WPRE.hGH (a kind gift of Anton Maximov, Scripps, La Jolla, CA) that restricts expression of SynP-Venus to Cre-recombinase-expressing neurons (Atasoy et al., 2008). The vector was packaged into viral particles to a titer of $4*10^{13}$ CG/ml by the vector core of the University of Pennsylvania. Seven days prior to the beginning of CSDS, the AAV

vector was injected stereotaxically into the DRN (from lambda, in mm: 0.0 AP, +0.8 ML,-3.3 DV, 15° angle) of *Pet1-tdTomato* mice, which express the Cre-recombinase selectively in serotonin neurons (Scott et al., 2005). Synaptophysin is a protein integral to synaptic vesicles that has been widely used both *in vitro* (Kelsch et al., 2010) and *in vivo* (Li et al., 2010) after transient viral overexpression (Grinevich et al., 2005) or constitutive expression in transgenic animals (Li et al., 2010) to identify functional synapses and assess their plasticity. Previous studies have shown that SynP transgenes tagged with variants of GFP adequately co-localize with endogenous synaptic proteins and identify functional synapses with 90% accuracy, without altering presynaptic function (Gogolla et al., 2007; Jin et al., 2011; Li et al., 2010). Time-lapse studies in live rodent neocortex showed that axonal boutons labeled with SynP are dynamic and display a turnover of 7% per day (Stettler et al., 2006). Studies also report fluctuations in the volume of stable axonal boutons. Activity-dependent increases in density and size of SynP-eGFP labeled varicosities have been validated as quantitative dynamic index for synaptic strength in neurons (Zhang et al., 2011).

To visualize boutons, slices were imaged at 630x magnification with an additional 3.5x digital zoom. Serotonergic axons were manually traced on Leica LAS AF software using tdTomato as a guide. Axons for tracing were selected randomly by an experimenter blinded to the condition of each mouse. Each trace generated a line measurement plot for Venus fluorescence intensity (Fig. 4.8). An automated bouton detection and measurement algorithm was developed in MATLAB and validated based on parallel manual analysis of a pilot dataset. Based on pilot data, boutons were defined as having a minimal intensity of 95 pixel intensity units (2 times the intensity of the maximum noise observed) and a

minimal length of 0.1 μm, which is similar to minima observed in electron microscopy studies of CA3-CA1 axons (Shepherd and Harris, 1998). Objects detected outside these boundaries were filtered out as artifacts. Bouton length was measured at the intensity threshold (Fig. 4.8). Bouton density for an axon was calculated as the total number of boutons along the axon divided by the total axon length. These two variables have been previously validated as sensitive indices of axonal plasticity, including in serotonin neurons (Rylander et al., 2010; Zhang et al., 2011). A total of 7853 boutons were analyzed out of 425 axons representing a cumulated axon length of approximately 30000 μM.

Statistical Methods

One-way, two-way, or repeated measures ANOVA's were performed, followed by post-hoc comparisons using Fisher's PLSD test. Comparisons between two groups were performed by two-tailed Student's *t*-tests. Statistical analyses were performed using Statistica software (StatSoft, Tulsa, OK). Statistical significance was defined as a p value < 0.05. All data are presented as the mean ± SEM. Outlying values (3 standard deviations from the mean) were excluded from group means.

Results

Antidepressant-like effect of chronic vmPFC DBS in stress-susceptible mice

We first investigated the behavioral effect of chronic vmPFC DBS in the CSDS paradigm, (Fig. 4.1A). Histological analyses confirmed that DBS electrodes were placed in the vmPFC during experiments (Fig. 4.1B). A social interaction test conducted on Day 11 prior to surgery verified that interaction times were decreased in defeat-susceptible mice (Main Effect of Defeat $F_{(1,36)} = 167.11$, $p = 0.00$) (Fig. 4.1C, Left). When social interaction was retested on Day 25 following 7 days of exposure to chronic vmPFC DBS or sham stimulation, defeated, sham-stimulated mice still expressed social avoidance at a level that did not differ significantly from Day 11 (Main Effect of CSDS at Day 25 $F_{(1,35)} = 4.78$, $p = 0.03$). In contrast, DBS dramatically increased social interaction scores, restoring social interaction to levels similar to unstressed controls on Day 25 (Defeat x Stimulation interaction: $F_{(1,35)} = 6.29$, $p = 0.0169$) (Fig. 4.1C,D). In the absence of a social target, DBS had no effect on interaction times, indicating that the effect of DBS was specific to social interaction (Fig. 4.2A,B). DBS non-specifically increased total distance traveled regardless of treatment condition or the presence of a social target (Day 25 Target Absent: Main effect of Stimulation $F_{(1,36)} = 6.47$, $p = 0.02$, Day 25 Target Present: Main effect of Stimulation $F_{(1,36)} = 9.80$, $p = 0.003$) (Fig. 4.2C-F). These results indicate that chronic vmPFC DBS has a nonspecific motor stimulant effect and robust antidepressant-like activity in mice susceptible to social stress.

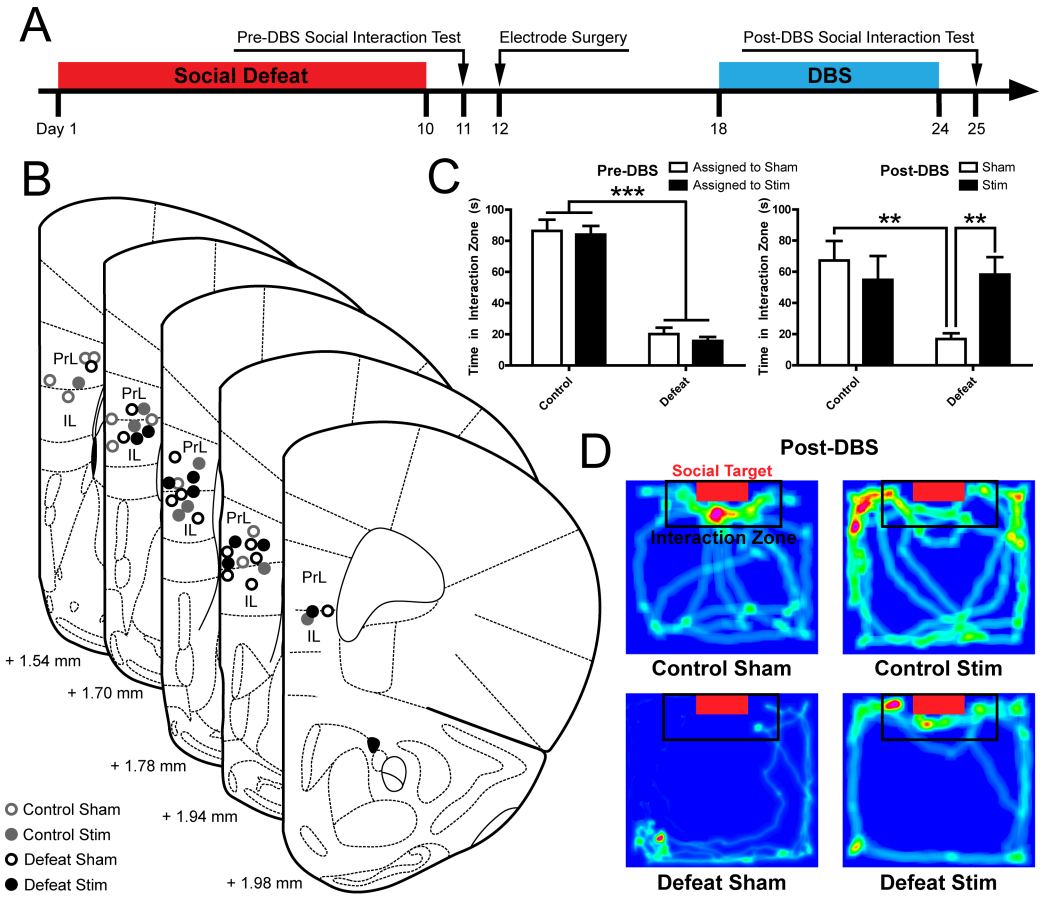

Figure 4.1. Chronic vmPFC DBS reverses sustained socioaffective deficits after defeat stress.

(A) Experimental design: Mice were implanted surgically 48 hours after the conclusion of social defeat and left undisturbed for 7 days after surgery until the beginning DBS treatment. The antidepressant-like activity of vmDBS was evaluated by comparing social interaction scores after 7 days of DBS (Day 25) to baseline avoidance levels determined 24 h after the last social defeat episode (Day 11). **(B)** Verification of unilateral DBS electrodes placements in the left vmPFC of sham-stimulated mice (open circles) and stimulated mice (solid circles). **(C)** Social defeat exposure induced a reduction in social interaction ($p < 0.001$, left panel) that was sustained in sham mice until Day 25 ($p < 0.01$ Day 25 Control Sham *vs.* Defeat Sham). Seven days of DBS resulted in a complete restoration of social interaction in defeated mice ($p < 0.01$, right panel), while there was no significant effect of DBS on social interaction in unstressed controls ($p > 0.05$, Day 25 Control Sham *vs.* Control Stim). n = 8-13 mice per condition. **(D)** Representative heat maps illustrating mouse movements relative to social target in each experimental condition. Hot colors indicate locations where the mice spent the most time. Significant differences are indicated by *$p < 0.05$, **$p < 0.01$, ***$p < 0.001$.

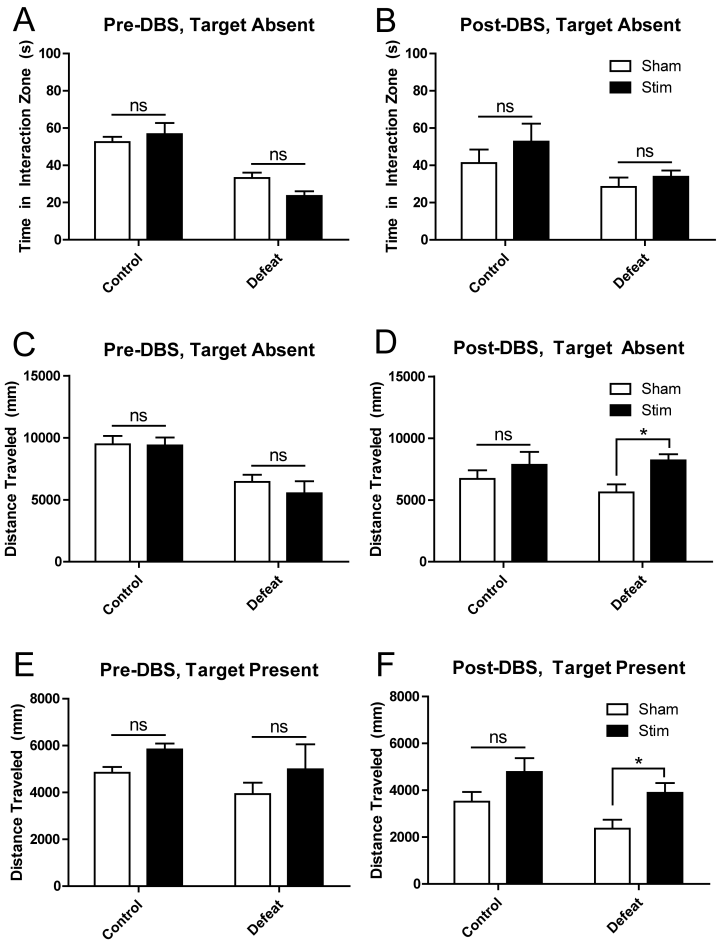

Figure 4.2. DBS behavioral data.

(**A-B**) DBS does not affect interaction time in the absence of a social target. (**C-F**) DBS increases total distanced traveled regardless of target presence. **p* < 0.05.

Acute vmPFC DBS induces *cFos* expression in brain regions with afferent and efferent monosynaptic connections

To identify distal regions modulated by vmPFC DBS, we applied 1 hour of DBS to the vmPFC of naïve mice (Fig. 4.3A) and conducted a brain wide examination of *cFos* induction. An initial survey identified several regions with marked *cFos* induction or lack thereof, a subset of which were selected for subsequent blinded quantitative assessment, including the vmPFC, the anterior piriform cortex (Pir) (an input region to the IL in mice, Fig. 4.4), the DG (which does not receive or send direct inputs to the vmPFC), the lateral habenula (LHb) (an output region of the vmPFC), and the basolateral amygdala (BLA) and DRN (two reciprocal input and ouput regions of the vmPFC) (Hoover and Vertes, 2007; Vertes, 2004). As expected, acute DBS increased *cFos*

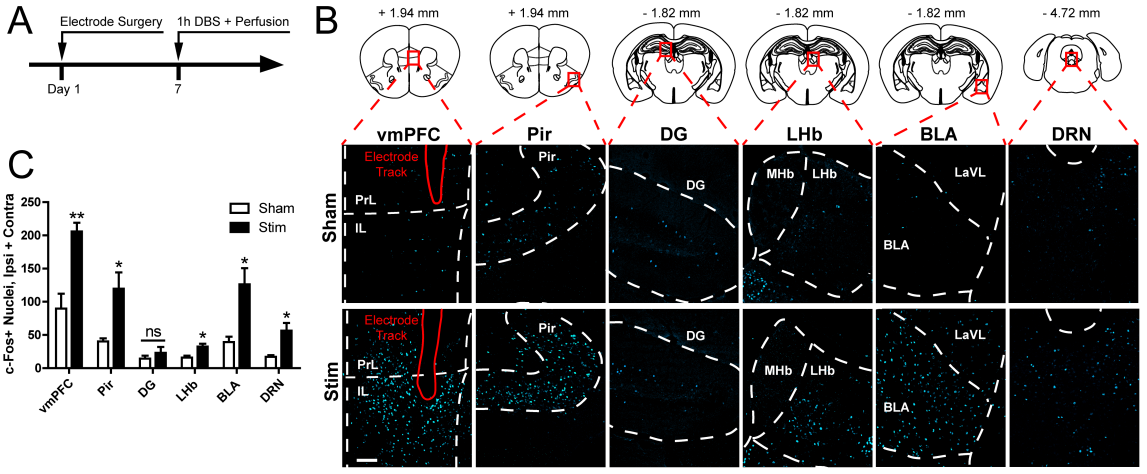

Figure 4.3. Acute DBS induces neural activation of afferent and efferent monosynaptic connections to the vmPFC.

(A) Experimental design. Mice were implanted with unilateral DBS electrodes in the left vmFPC, allowed to recover for 7 days, and underwent DBS for 1 hour immediately followed by perfusion. **(B)** Representative images of *cFos* immunoreactivity in the vmPFC, Anterior Piriform Cortex (Pir), Dentate Gyrus (DG), Lateral Habenula (LHb), Basolateral Amygdala (BLA) and Dorsal Raphe Nucleus (DRN). Scale bar, 100µm. **(C)** Corresponding counts of the number of $cFos^{+}$ nuclei reveal significant increases with DBS locally at the stimulation site (vmPFC) and in distal regions known to either receive (LHb, BLA, DRN) and/or send (Pir, BLA, DRN) projections to the vmPFC. In contrast, minor changes were seen in the DG, which has no known monosynaptic connection to the vmPFC. n = 3-4 per condition. Significant differences are indicated by $*p < 0.05$, $**p < 0.01$.

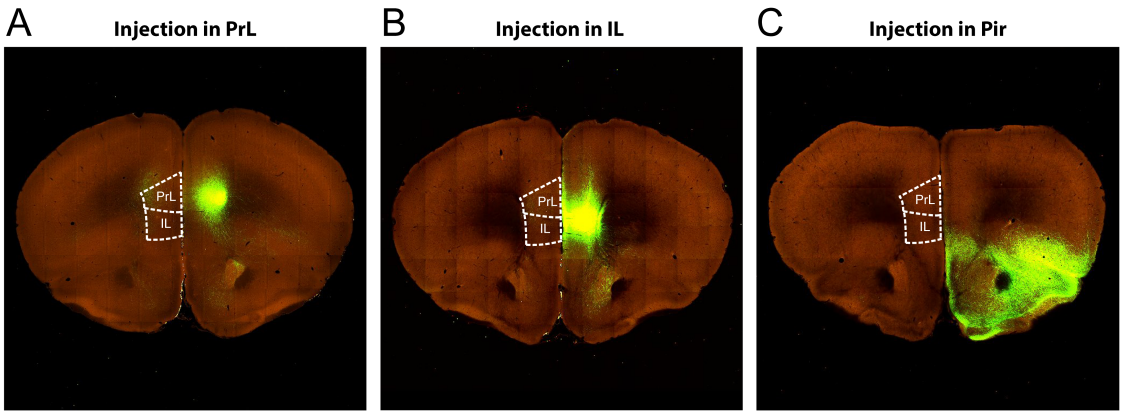

Figure 4.4. The anterior piriform cortex (Pir) projects to the ventral IL, but does not receive projections from the vmPFC.

(A) PrL injection does not result in labeled fibers in the Pir. **(B)** IL injection does not result in labeled fibers in the Pir. **(C)** Pir injection results in labeled fibers in the IL. Images obtained from the Allen Brain Atlas.

immunoreactivity locally in the vmPFC (Student's *t*-test, $p < 0.01$) (Fig. 4.3B-C). vmPFC DBS also increased *cFos* counts in the Pir, LHb, BLA, and DRN ($p < 0.05$), while *cFos* levels in the DG did not significantly increase ($p > 0.05$) (Fig. 4.3B-C). These results indicate that acute vmPFC DBS drives neural activity in several distal regions with known monosynaptic efferent and/or afferent connections to the vmPFC.

Chronic vmPFC DBS reverses CSDS-induced hypoexcitability of 5-HT neurons

We next investigated whether chronic vmPFC DBS after CSDS induces sustained neurophysiological adaptations of DRN 5-HT neurons. Our previous studies demonstrated that CSDS sensitizes synaptic inhibitory inputs and drives a state of sustained intrinsic hypoexcitability of DRN 5-HT neurons in susceptible but not resilient mice (Challis et al., 2013; Crawford et al., 2010; Espallergues et al., 2012). To determine whether chronic vmPFC DBS counteracts these stress-induced changes, we performed whole cell recordings in DRN slices collected 48 hours following the cessation of DBS administration, using a design that parallels our behavioral experiments (Fig. 4.5A-B). We used *Pet1-tdTomato* mice to genetically identify 5-HT neurons for recording. Consistent with our previous reports, we found that CSDS decreased the intrinsic excitability of DRN 5-HT neurons (Fig. 4.5C,E). DBS reversed CSDS-induced hypoexcitability, restoring intrinsic excitability of DRN 5-HT cells to the levels of unstressed sham controls. (Treatment x Input Current interaction, $F_{(6,341)} = 3.27$, $p < 0.001$; Fig. 4.5C,E). We next examined the properties of individual action potentials and found that CSDS raised the firing threshold to a more depolarized state, while DBS reverses this effect (One-Way ANOVA, $F_{(2,61)} = 4.06$, $p = 0.023$; Fig. 4.5F).

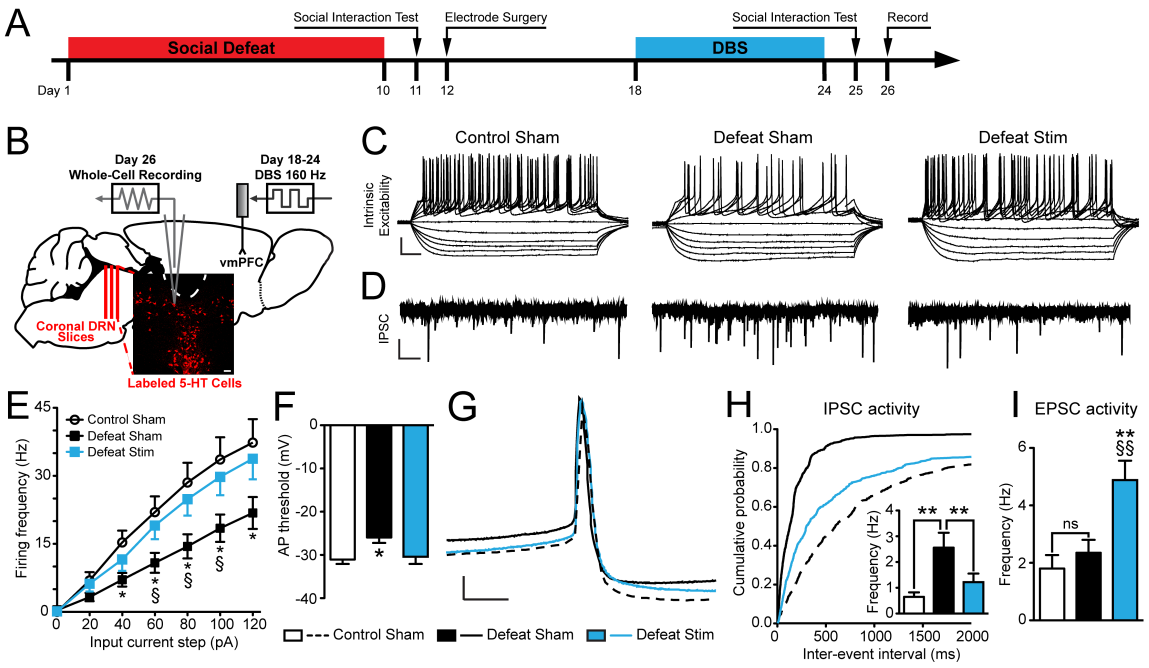

Figure 4.5. Chronic vmPFC DBS reverses social defeat-induced hypoexcitability and restores levels of inhibitory input onto DRN 5-HT neurons.

(A) Experimental timeline. **(B)** Schematic depicting electrophysiology protocol; coronal DRN slices were collected from *Pet1-tdTomato* mice 48 h following DBS and whole-cell recordings were performed from fluorescently identified 5-HT neurons in the ventromedial DRN. **(C)** Raw data traces depicting changes in membrane potential of DRN 5-HT neurons in response to 20 pA steps of depolarizing current. Scale bar, 25 mV, 50 ms. **(D)** Representative traces depicting spontaneous IPSC activity in DRN 5-HT neurons. Scale bar 20 pA, 1 s. **(E)** Frequency-current plots show a decrease in intrinsic excitability of DRN 5-HT neurons in defeated mice (*$p < 0.05$, 40-120 pA). Hypoexcitability of DRN 5-HT neurons is reversed in defeated mice treated with chronic DBS ($^{\S}p < 0.05$, 60-100 pA); intrinsic excitability is comparable to that of controls [$N(n) = 2$ mice (20 cells) for Control Sham, 4(23) for Defeat Sham, 3(20) for Defeat Stim]. **(F)** The action potential threshold of DRN 5-HT neurons is increased by social defeat ($p < 0.05$) and restored after vmPFC DBS. **(G)** Enlarged depiction of individual action potentials in DRN 5-HT neurons for each experimental condition. Scale bar 10 mV, 5 s. **(H)** Cumulative probability plots displaying the defeat-induced shift to shorter inter-event intervals of spontaneous IPSC's in DRN 5-HT neurons versus controls. DRN 5-HT neurons in DBS-treated mice display a shift back towards longer inter-stimulus intervals ($p < 0.001$). Inset: summary histogram showing increased mIPSC frequency after SD that is reversed after vmPFC DBS [$N(n) = 2(14)$ for Control Sham, 4(19) for Defeat Sham, 3(16) for Defeat Stim]. **(I)** Spontaneous EPSC frequency of DRN 5-HT neurons is unchanged in defeated mice but increased in defeated mice treated with vmPFC DBS ($^{\S\S}p < 0.01$ *vs.* Control Sham, **$p < 0.01$ *vs.* Defeat Sham). Significant differences are indicated by *$p < 0.05$, $^{\S}p < 0.05$, $^{\S\S}p < 0.01$, **$p < 0.01$.

The vmPFC sends strong excitatory projections to the DRN (Commons et al., 2005; Soiza-Reilly and Commons, 2011) that presumably establish synapses with a

mixed and interconnected population of serotonin and GABAergic neurons (Celada et al., 2001; Jankowski and Sesack, 2004; Soiza-Reilly and Commons, 2011; Varga et al., 2001). We tested whether chronic vmPFC DBS affects the excitatory and inhibitory synaptic inputs of DRN 5-HT neurons using voltage clamp techniques (Crawford et al., 2011; Crawford et al., 2013). As previously observed (Challis et al., 2013), CSDS increased spontaneous IPSC frequency of 5-HT neurons in susceptible mice (One-Way ANOVA: $F_{(2,39)} = 6.55$, $p = 0.004$, Fig. 4.5D, inset of Fig. 4.5H). DBS reversed this potentiation, returning inhibitory input to the levels of controls (Kolmogorov-Smirnov test, $Z = 11.44$, $p < 0.001$; Fig. 4.5H). We next analyzed EPSC frequency of DRN 5-HT neurons and found that CSDS did not affect this variable. Interestingly, we observed a sustained enhancement of EPSC frequency by DBS treatment (One-Way ANOVA, $F_{(2,39)} = 7.65$, $p = 0.002$; Fig. 4.5I). These results indicate that chronic vmPFC DBS opposes the effects of CSDS on the activity of DRN 5-HT neurons by increasing their intrinsic excitability and modulating inhibitory and excitatory input onto this cell population.

Chronic vmPFC DBS induces dendritic plasticity in DRN 5-HT neurons

To further investigate CSDS and DBS-induced neuroplasticity of 5-HT DRN neurons, we took advantage of the fact that 5-HT neurons were individually filled with biocytin during whole-cell recordings to obtain z-stacks of their somatodendritic arborization for morphological analyses. Consistent with our previous work (Espallergues et al., 2012), we found that CSDS increased the length and branching complexity of DRN 5-HT dendrites (Mean Dendrite Length: $F_{(2,38)} = 9.33$, $p = 0.001$, Fig. 4.6A,B; Sholl Intersections: $F_{(2,38)} = 8.49$, $p = 0.001$, Fig. 4.6A,C). DBS reversed CSDS-induced dendritic adaptations, restoring dendritic length and complexity to control levels (Defeat

Sham *vs.* Defeat Stim, $p < 0.01$ for dendrite length and $p < 0.01$ for Sholl intersections). DBS also restored total dendritic length to the level of controls ($F_{(2,38)} = 5.19$, $p = 0.01$). Furthermore, in line with our observation that DBS increases excitatory input onto DRN 5-HT neurons, immunostaining for the marker PSD-95 revealed a significant enhancement of the number of postsynaptic densities per micron of DRN tdTomato^{+} process (One-Way ANOVA, $F_{(2,45)} = 10.54$, $p < 0.001$; Fig. 4.6D,E), suggesting an increased number of functional glutamatergic synapses on the dendrites of 5-HT neurons. Importantly, the number of PSD-95 puncta per micron of 5-HT dendrite was not altered by CSDS. These results indicate that chronic vmPFC DBS reverses CSDS-induced dendritic plasticity in DRN 5-HT neurons while driving an increase in the density of excitatory synapses onto these neurons.

Social defeat and chronic vmPFC DBS induce axonal plasticity in DRN 5-HT neurons

Previous studies have implicated the stimulation of 5-HT release in DRN projection regions such as the hippocampus as a possible mechanism of action of vmPFC DBS (Hamani et al., 2010; Hamani et al., 2012). Because serotonin is released both synaptically and extrasynaptically from synaptic boutons and axonal varicosities (De-Miguel and Trueta, 2005), which are dynamic structures (De Paola et al., 2006; Stettler et al., 2006; Zhang et al., 2011), we sought to investigate whether CSDS and/or DBS induce sustained changes in the morphology or density of boutons along the axons of DRN 5-HT neurons. To visualize axons and boutons originating from DRN 5-HT neurons, *Pet1-tdTomato* mice were injected in the DRN with an adeno-associated virus (AAV) expressing SynP-Venus in a Cre recombinase-dependent manner. After a week of post-

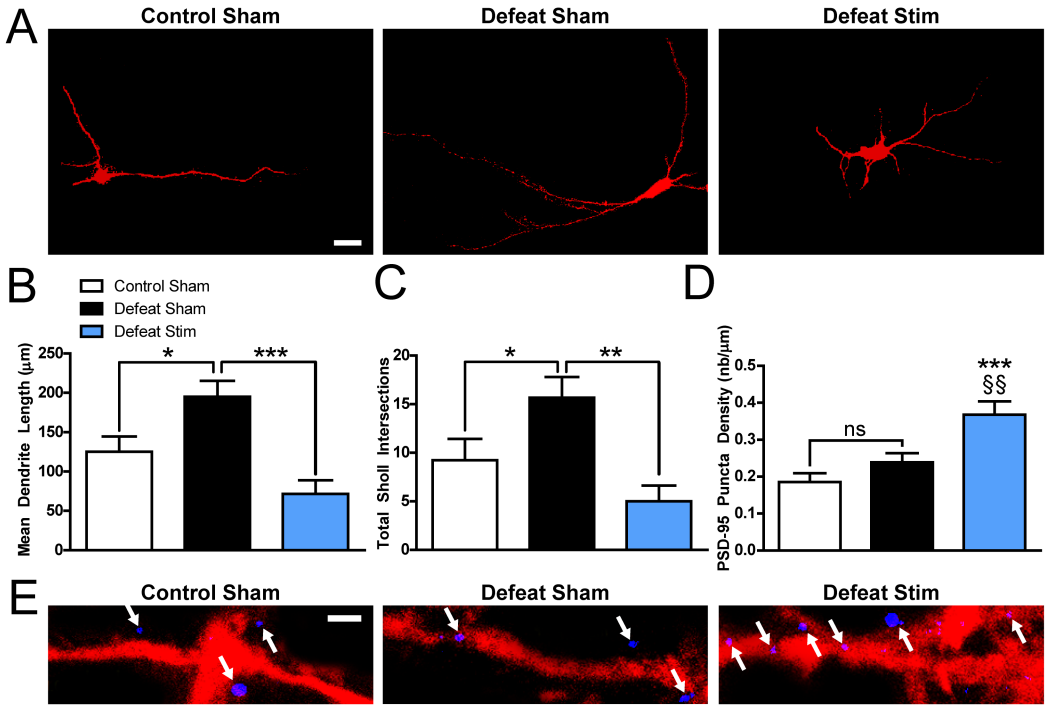

Figure 4.6. Chronic vmPFC DBS reverses social defeat-induced dendritic plasticity in DRN 5-HT neurons.

(A) Representative images of biocytin-filled 5-HT neurons. Scale bar, 30µm. **(B)** Social defeat induces a significant increase in dendritic length ($p < 0.05$), and chronic DBS restores mean dendrite length ($p < 0.001$) to levels comparable to controls ($p > 0.05$). **(C)** Social defeat induces a significant increase in dendritic complexity as assayed by Sholl analysis ($p < 0.05$), and chronic DBS restores dendritic complexity ($p < 0.01$) to levels comparable to controls ($p > 0.05$) [$N(n) = 2$ mice (13 cells) for Control Sham, 4(18) for Defeat Sham, 2(10) for Defeat Stim]. **(D)** Social defeat does not significantly change the density of PSD-95 puncta along 5-HT DRN dendrites ($p > 0.05$ Control Sham *vs.* Defeat Sham), while DBS significantly increases PSD-95 puncta density (***$p < 0.001$, Control Sham *vs.* Defeat Stim, $^{§§}p < 0.01$, Defeat Sham *vs.* Defeat Stim) [$N(n) = 2$ mice (16 dendritic segments) per condition]. **(E)** Representative images of PSD-95 puncta along 5-HT DRN dendrites. Scale bar, 1.00 µm. Significant differences are indicated by *$p < 0.05$, **$p < 0.01$, $^{§§}p < 0.01$, ***$p < 0.001$.

surgical recovery, mice were exposed to CSDS and chronic vmPFC DBS according to a timeline paralleling our behavioral and electrophysiological experiments, followed by perfusion and imaging of DRN projection regions (Fig. 4.7A,B; Fig. 4.8). Over 99% of SynP-Venus-expressing somas in the DRN also expressed tdTomato, confirming 5-HT-selective transgene expression. Approximately 40% of 5-HT neurons in the DRN were labeled at the site of injection, indicating robust transduction efficiency (Fig. 4.7C,D).

Transduction rates were not significantly different between experimental groups (One-Way ANOVA, $F_{(2,9)} = 0.554$, $p > 0.05$, Fig. 4.7D). While infected cell bodies were only observed in the DRN, fluorescent puncta typical of presynaptic labeling were observed broadly in the brainstem, outside of the site of injection, as well as widely throughout the forebrain. The regional pattern was similar to that of serotonergic innervation and co-localized with serotonin (not shown) and tdTomato in axon terminals, indicating that the tagged protein was effectively targeted to 5-HT presynaptic structures in remote regions innervated by the DRN (Fig. 4.7C).

In the DG and vmPFC of sham-treated mice, CSDS induced significant reductions of the average length and density of presynaptic boutons along DRN 5-HT axons **(**Fig. 4.7E,F**)** (Main effect on DG bouton length: $F_{(2,2000)} = 21.37$, $p < 0.001$, effect on DG bouton density: $F_{(2,119)} = 10.64$, $p < 0.001$, effect on vmPFC bouton length: $F_{(2,3046)} = 21.741$, $p < 0.001$, effect on vmPFC bouton density: $F_{(2,177)} = 6.55$, $p < 0.001$; Fig. 4.7H,I,K,L). DBS restored bouton length to levels comparable to unstressed controls in the DG and vmPFC (Figure 4.7E,F,H,I), and restored bouton density to control levels in the DG (Fig. 4.7E,K). Surprisingly, in contrast to its effects in the DG and the vmPFC, CSDS did not alter bouton length and it increased bouton density in the BLA ($F_{(2,120)} = 3.891$, $p = 0.0231$) (Fig. 4.7G,J,M). In this region, DBS increased bouton length over the level of controls, ($F_{(2,2798)} = 25.68$, $p < 0.001$) and did not change bouton density. All DBS-induced changes in bouton length were reflected in a leftward shift of cumulative probability plots after CSDS (Fig. 4.7H,I,J) (Kolmogorov-Smirnov Test, $p < 0.01$ in DG, vmPFC, and BLA). These results indicate that CSDS and chronic vmPFC DBS induce

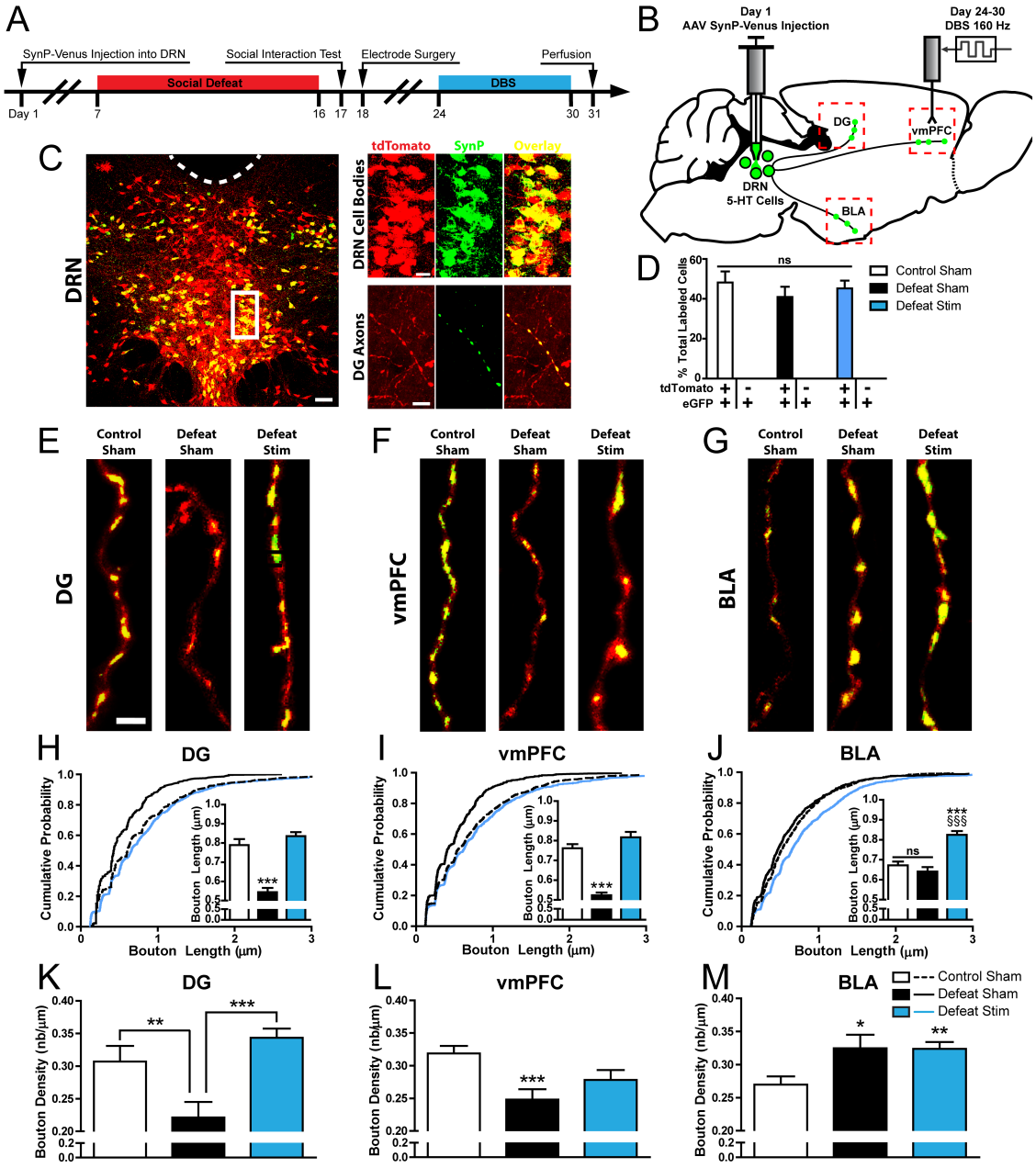

Figure 4.7. vmPFC DBS-induces structural axonal plasticity in DRN 5-HT neurons.
(A) Experimental design: An AAV vector carrying a Flex Synaptophysin-Venus (SynP-Venus) cassette was injected into the DRN of *Pet1-tdTomato* mice. Mice underwent the same social defeat and DBS paradigm as described in Figure 4.4 and were perfused 24 h after the end of stimulation. **(B)** Experimental schematic indicating AAV injection in the DRN, resulting in targeting of the SynP-Venus fusion protein to 5-HT cell bodies in the DRN and labeling of presynaptic boutons in DRN projection regions such as the dentate gyrus (DG), vmPFC, and basolateral amygdala (BLA). **(C)** Left Panel: Low magnification confocal image illustrating SynP-Venus expression (green) in the DRN of *Pet1-tdTomato* mice. 5-HT neurons are genetically identified by expression of the tdTomato reporter (red). Colocalization of SynP-Venus and tdTomato is indicated by yellow. Right Panel: High magnification images illustrate SynP-Venus localization to 5-HT somas in the DRN (top) and 5-HT axon terminals in the DG (Bottom). Note the concentration of SynP-Venus signal to axonal boutons.

Scale bars: 50 µm (left), 20 µm (top right) 5 µm (bottom left). **(D)** Validation of SynP-Venus expression efficiency and selectivity. Over 40% of all tdTomato$^+$ DRN somas expressed SynP-Venus, indicating strong transduction efficiency, and >99% of all SynP-Venus$^+$ DRN somas were tdTomato$^+$, indicating complete serotonergic selectivity. There were no significant differences in transduction rates between Control Sham, Defeat Sham, and Defeat Stim mice ($p > 0.05$). **(E-G)** Representative images of DRN 5-HT axons in the DG, vmPFC, and BLA across treatment groups. Scale bar, 2 µm. Morphometric measures of 5-HT presynaptic bouton length **(H-J)** and density **(K-M)** were derived from intensity measurements of SynP-Venus fluorescence intensity along tdTomato$^+$ traced axons segments (see **Figure S3** for example of analysis). Social defeat significantly reduced the length and density of presynaptic boutons in the DG and vmPFC while increasing the density of presynaptic boutons in the BLA. DBS restored the length and/or density of 5-HT presynaptic boutons in the DG and the vmPFC to the level of unstressed controls and increased bouton length over the level of controls in the BLA. Bouton Length: n = 291-1362 boutons per condition from 2 mice per condition, Bouton Density: n = 31-66 axons from 2 mice per condition. Significant differences are indicated by $*p < 0.05$, $**p < 0.01$, $***p < 0.001$.

region-specific and often opposing neuroplastic adaptations of DRN 5-HT axon terminals, with DBS either increasing or not changing presynaptic bouton length and density.

Taken together, the results of our electrophysiological and morphological experiments are suggestive of a sustained decrease in activity and synaptic output of DRN 5-HT neurons after CSDS and a restorative effect of vmPFC DBS through a circuit-mediated resensitization of DRN 5-HT neurons and an increase in the size and density of 5-HT release sites.

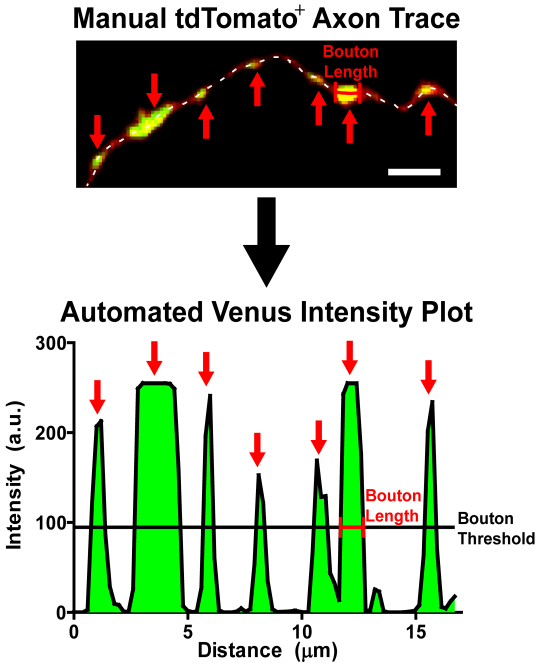

Figure 4.8. Methodology of bouton analysis and quantification.

Axons originating from DRN 5-HT neurons were identified from native tdTomato fluorescence and Venus$^+$ boutons labeled by immunohistochemistry. Axons were manually traced along tdTomato fluorescence (top panel, dashed white line) using LAS AF software to generate a Venus fluorescence intensity plot. Venus$^+$ boutons generated large fluorescent peaks, which were detected by thresholding (bottom panel). Fluorescence intensity analyses allowed for measurement of bouton length (width of peak at threshold) and bouton density (number of discrete peaks above threshold divided by total length of trace). Scale bar, 2 µm.

Discussion

In this study we have demonstrated that chronic vmPFC DBS reverses social avoidance in a mouse model of depression and induces striking neuroadaptations in brainstem 5-HT neurons. Together, these neuroadaptations reverse maladaptive plasticity induced by CSDS and point to a sustained increase in 5-HT activity upon repeated courses of DBS.

We first built on previous studies of cortical DBS in the chronic mild stress model (Dournes et al., 2013; Hamani et al., 2012) by demonstrating the efficacy of DBS in modulating CSDS-induced social avoidance, which models another symptom of human depression. In line with our previous reports (Berton et al., 2006; Challis et al., 2013; Espallergues et al., 2012) CSDS induced a persistent social withdrawal. Seven days of unilateral chronic vmPFC DBS proved sufficient to restore social approach behavior to levels comparable to unstressed mice. The finding that left unilateral DBS was sufficient to elicit an antidepressant-like responses is consistent with previous observations that stimulation of the left vmPFC or left LHb is sufficient to produce antidepressant-like responses in the forced swim test (Hamani et al., 2010) and the learned helplessness paradigm (Li et al., 2011). Furthermore, we found that chronic DBS stimulated social interaction in defeated, stress-susceptible mice while it had no effects on social interaction in unstressed mice, which is consistent with previous work indicating that the effect of DBS is observed in stressed but not control rats (Hamani et al., 2012). It should be noted that the effects of DBS on approach behavior were only observed in the presence of a social target, and these effects were superimposed on a small, non-specific locomotor stimulant effect of DBS that was seen in all animals independently of their

previous exposure to social stress, which is consistent with clinical results indicating that SCG DBS increases motor speed (Mayberg et al., 2005). An interesting recent study in rats and humans has indicated that the early effects of DBS may be attributed to inflammatory responses from insertional effects (Perez-Caballero et al., 2014). The results in the present study are unlikely to be due to this effect because interaction testing was conducted over 2 weeks following surgery, and all stimulated animals were compared to sham animals with identical electrodes implanted in the same region.

SCG DBS has been shown to modulate the activity of remote brain regions in human PET studies (Lozano et al., 2008), and prior preclinical studies report activation of the DRN, a well-characterized target of vmPFC projection neurons (Kumar et al., 2013; Warden et al., 2012). To further characterize the regions modulated by vmPFC DBS, we examined circuit-wide *cFos* expression after acute vmPFC DBS. DBS drove local neural activity in the vmPFC, which is consistent with preclinical studies showing that DBS also increased local *cFos* levels when applied in the NAc (Schmuckermair et al., 2013), NAc shell (Halpern et al., 2013; Vassoler et al., 2013), and LHb (Li et al., 2011). Consistent with DBS-induced orthodromic activation, we observed significant *cFos* activation in the LHb, BLA, and DRN. Activation of the LHb indicates that vmPFC DBS may indirectly engage a similar circuit mechanism to LHb DBS, which is also being explored as a treatment for depression (Henn, 2012). DRN activation could provide an explanation for increased hippocampal 5-HT release with vmPFC DBS (Hamani et al., 2010). We observed robust *cFos* activation in the anterior piriform cortex (Pir), an input region to the vmPFC. This activation may occur through DBS-induced antidromic transmission, which is consistent with recent findings from DBS of the NAc shell (Vassoler et al.,

2013) and a large body of data from DBS of the subthalamic nucleus (Montgomery, 2008). As expected, we did not observe significant activation in the DG, which neither receives nor sends projections to the vmPFC (Hoover and Vertes, 2007; Vertes, 2004).

In agreement with our previous findings (Challis et al., 2013; Espallergues et al., 2012), CSDS decreased cellular excitability, increased inhibitory input, and increased dendritic length and complexity in DRN 5-HT neurons. Importantly, in the present study these observations were made 14 days following the end of CSDS compared to 24 hours post-CSDS in our previous studies, indicating that CSDS-induced changes in physiology and morphology are highly stable. Chronic vmPFC DBS restored DRN 5-HT intrinsic excitability, action potential threshold, and inhibitory input to levels comparable to undefeated controls, indicating a dramatic DBS-mediated reversal of CSDS-induced maladaptive plasticity. The combined resensitization and shift in the balance of excitatory/inhibitory synaptic inputs onto 5-HT neurons may play a causal role in the restoration of social approach behaviors. Indeed, a recent study demonstrated that direct stimulation of glutamatergic vmPFC-DRN axons promoted antidepressant responses (Warden et al., 2012). Furthermore we have recently shown that optogenetic silencing of DRN GABAergic neurons that receive inputs from the vmPFC and monosynaptically inhibit nearby 5-HT cells blocks the consolidation of social avoidance during CSDS (Challis et al., 2013). Though the precise cellular mechanisms responsible for these adaptations remain unknown, our morphological analyses point to a number of possible underlying mechanisms. In other types of neurons, intrinsic excitability and firing pattern has been shown to be causally related to dendritic morphology, size and topology (van Elburg and van Ooyen, 2010). The reduction in dendritic length and complexity observed

after DBS administration may thus mediate changes in excitability. Interestingly, we also observed a strengthening of excitatory synaptic input onto DRN 5-HT neurons, a variable that was not initially altered by CSDS. This could be attributed to an increase in the number of excitatory synapses or an increased presynaptic release probability. We observed a DBS-induced increase in the density of PSD-95^{+} puncta along DRN 5-HT dendrites, indicating that the former may be the case. Indeed, it has been shown that PSD-95 overexpression increases mEPSC frequency and decreases inhibitory synaptic input (Prange et al., 2004), both of which were observed in DRN 5-HT neurons following chronic DBS in this study. The finding that inhibitory synaptic input was restored by chronic vmPFC DBS raises the possibility of DBS-induced plasticity in DRN GABA neurons; indeed, prior electrophysiological and structural evidence indicates that most vmPFC-DRN afferents synapse onto non-5-HT neurons (Celada et al., 2001; Hou et al., 2012; Jankowski and Sesack, 2004; Varga et al., 2001).

Because CSDS and chronic vmPFC DBS induced physiological and dendritic morphological adaptations in DRN 5-HT neurons, we asked whether DBS also induces adaptations in DRN 5-HT axons that may translate into altered synaptic output in innervated regions. We achieved cell-type specific anterograde labeling of DRN 5-HT axons and selectively visualized their presynaptic boutons in forebrain projections regions for morphometric analysis. This approach is advantageous over previous methods used to detect axons of 5-HT cells that rely on conventional tracers or endogenous markers such as 5-HT or 5-HTT, as such approaches may detect a large proportion of varicosities that do not form functional synapses and do not necessarily originate from the DRN.

We used our approach to demonstrate that CSDS has a significant effect on both the density and/or length of 5-HT varicosities in all regions examined. CSDS induced a dramatic decrease in the length and density of boutons in the DG and vmPFC, suggesting a decrease in the strength and number of functional 5-HT synapses. DBS restored bouton length and density in the DG and restored bouton length in the vmPFC, suggesting that repeated DBS may reinforce 5-HT output to the hippocampus and vmPFC by concomitantly increasing 5-HT firing along with the number and size of release sites. DBS-induced effects on 5-HT bouton dynamics were region- and projection-specific; we observed that CSDS exerted an opposing influence on bouton density in the BLA as compared to the DG and vmPFC. This observation is in line with previous findings that stress often induces opposing neuroplastic changes in the BLA and DG (Mitra et al., 2005).

Mechanisms leading to increased boutons are unclear. Recent studies suggest that the dynamics of varicosities reflect localized neuronal activity. After high frequency electrical stimulation, increases in bouton density were observed selectively on axons that are in the microproximity of *cFos*$^{+}$ neuronal somas (Zhang et al., 2011). Such mechanisms could explain the increases observed in the vmPFC and BLA, but would not account for changes in the DG, since this region was not noticeably activated by DBS. Axonal adaptations in the DG are suggestive of somatodendritic engagement of 5-HT neurons and consecutive effects on nuclear translation and axonal transport. Further studies will be necessary to establish the molecular underpinnings of these adaptations. This is to our knowledge the first investigation of 5-HT presynaptic bouton dynamics in the context of depression or vmPFC DBS.

Overall, our study establishes a novel experimental paradigm that may prove advantageous to assess cell-type specific mechanisms of DBS using transgenic mouse lines, and we identify DRN 5-HT neurons as a key neural substrate for further studies on the long-term mechanisms of SCG DBS in depression.

Chapter 5

General Discussion

The goal of this work was to clarify the neural circuitry underlying social approach/avoidance motivation in mice and to reveal mechanisms whereby adverse social experiences can precipitate dysfunctional neuroplasticity that underlie behavioral symptoms relevant to the socioaffective dimension of mood disorders.

Current neuroimaging-based studies of depression reveal patterns of aberrant connectivity between the prefrontal cortex and downstream structures in the limbic system, striatum and brainstem (Drevets et al., 2008; Mayberg, 1997). This dysconnectivity is thought to underlie the heterogenous deficits in socioemotional information processing and affective control that are characteristic of MDD syndromes. Several studies including recent investigations using single unit recordings and electrode-based neuromodulation in awake MDD patients point to the normalization of the vmPFC as a key process in therapeutic response (Laxton et al., 2013; Riva-Posse et al., 2014). Probabilistic tractography studies seeking to identify key downstream regions mediating DBS therapeutic activity have identified the DRN as one of the regions required (Gutman et al., 2009; Lehman et al., 2011).

Based on this data, I focused my thesis on the connection between the vmPFC and the DRN. I hypothesized that GABAergic interneurons, which are the primary non-serotonergic population in the DRN, are key mediators of top-down influences from the vmPFC onto mood regulating 5-HT neurons. Until this work this question had never been fully resolved due to the lack of tools to unequivocally identify 5-HT and non-5-HT

neurons in the DRN. For my thesis I used emerging techniques and addressed my hypothesis in 4 major ways. **1:** Using genetically labeled mice that allow for the identification of serotonergic, GABAergic and glutamatergic neurons, I characterized the neuroanatomical and functional connectivity of this pathway. My results show that GABAergic neurons are the primary targets in the DRN of excitatory vmPFC projections and that these GABA neurons locally inhibit 5-HT neurons. Thus, this GABA population is positioned to relay and translate integrated information about aversive contingencies descending from the vmPFC into inhibition of 5-HT output. **2:** I demonstrated that the social defeat paradigm induces sustained deficits in socioaffective behaviors that are triggered by stable neuroplastic adaptations in the vmPFC-DRN microcircuit that result in sensitized inhibition of 5-HT neurons. **3:** Using optogenetic techniques I tested the causal role of the vmPFC-DRN circuit by silencing DRN GABAergic neurons or vmPFC inputs to the DRN. I found that photosilencing either population prevented the acquisition of an avoidance phenotype, suggesting a key role of this pathway in experience dependent shifts in valence of social cues. Interestingly, in contrast I found that manipulation of the vmPFC-DRN microcircuit after associative avoidance was established appeared unable to restore social approach, indicating dissociation between this pathway and the execution of aversive behaviors. **4:** I used vmPFC DBS, an emerging circuit-targeted electrode-based therapeutic procedure under clinical evaluation for the treatment of MDD, to show that chronic high frequency stimulation of vmPFC descending pathways reverses the avoidance phenotype. Using this as a model for therapeutic response to antidepressant interventions, I characterized coincident changes in DRN neuroplasticity and found that DBS drove a strengthening of direct glutamatergic

inputs to 5-HT neurons while suppressing inhibitory synaptic input, thereby hypothetically restoring excitatory/inhibitory balance.

Below, I have highlighted selected key points of my work that I believe make important advances. I also discuss the possible limitations of my experiments and speculate on how these limitations might be addressed in future research.

Reinterpreting the social defeat model

Importance of sensory exposure and identification of a sensitive period

The social defeat paradigm has been adopted by many groups and is widely used to understand individual differences in depression-like behaviors. While most previous studies focus primarily on the resulting social avoidance behaviors and reversal by potential therapeutic interventions, much remains unknown about the sensory pathways and associative processes that underlie the development, stabilization and extinction of social avoidance. One of the key findings I made in this thesis was that by eliminating sensory contact after the physical encounter during social defeat, I drastically reduced the probability of mice to display avoidance during the social interaction task. Furthermore, retaining sensory contact, but limiting it to just 20 minutes was sufficient to maintain avoidance, implicating this as a key sensitive interval for associative encoding. The sensory period can be paralleled to the association phase of fear conditioning, where subjects learn to associate a neutral cue such as a tone or odor with a footshock, resulting in a fear response (i.e. freezing) to the initially neutral cue (Maren, 2001). Though, it is still unclear what actually occurs during the sensory period of social defeat, that we were able to prevent avoidance by completely removing this phase suggests that LTP-like plasticity processes or consolidation of relatively aversive valence might be occurring to

guide future behaviors. The neural pathways of fear have been well studied from the processing of sensory signals to the learned behavioral response (LeDoux et al., 1990; Rogan et al., 1997; Tsvetkov et al., 2002), but it is unknown exactly what pathways and cues contribute to acquired avoidance behaviors. Future research will characterize the sensory cues learned during the sensory phase of defeat and recalled during the social interaction test. It is likely that multiple sensory modalities are active at the same time during associative encoding as has been shown in human cognition (Chikazoe et al., 2014). We will isolate different sensory systems and titer the strength of each during the sensory phase to determine what social cues contribute to encoding of negative bias and susceptibility to social defeat stress. This will be accomplished by occluding visual, olfactory or auditory cues during the sensory contact period or social interaction testing and then determining the effect on approach or avoidance.

Avoidance behaviors reflect rapid binary choices between approach/avoidance strategies

It has been theorized that all organisms are hardwired to make approach-avoidance decisions in response to social stimuli by rapidly applying motivational valence values to social partners (Elliot and Covington, 2001; Nieh et al., 2013; Panksepp, 2005; Zajonc, 1984). For example, cognitive studies in humans have shown that we make complex unconscious judgments of others within 40 milliseconds of exposure to a social stimulus such as a picture of a face (Morris et al., 1998; Todorov, 2008). Similar behaviors in mice are apparent during the social interaction task, where subjects confront a non-threatening social target and rapidly decide to either approach or avoid, making a choice that likely maximizes survival value. Undefeated mice appear to find social interaction rewarding or safe and may attribute positive valence to their social partners,

since the majority of subjects will immediately approach the social target during the social interaction test. After defeat though, there is a spread in how animals respond to the same "ambiguous" social target that control mice unconditionally approached and it is likely that differences in the activity of neural pathways between mice underlie the heterogeneity of approach-avoidance behaviors.

For susceptible mice, defeat-induced neuroplastic adaptations might have sensitized their response to social stimuli such that seemingly neutral, or even rewarding, social partners are viewed as more threatening, resulting in an immediate decision to avoid and retreat to the distal corners from the social target. Similar behaviors have been reported in MDD and social anxiety patients who, when performing a joystick-based approach-avoidance task, pay increased attention to negative or threatening social stimuli and also tend to immediately pull a lever more often to signal withdrawal regardless of the subjective emotion (i.e. happy, neutral or sad) of the stimuli (Derntl et al., 2011; Godard et al., 2011). This is believed to be regulated by aversive (i.e. dangerous) and appetitive (i.e. safe or rewarding) motivational systems specific to the social stimulus presented (Davidson et al., 1990; Lang et al., 1990), and when dysfunctional, result in negatively biased autonomic evaluation and implicit social withdrawal (Seidel et al., 2010). The social interaction test is capable of detecting these different systems in mice that are important for motivational social processing and separate from those involved in fight or flight behaviors, such as those produced by the forced swim test.

Neuroplastic shifts in balance of excitatory/inhibitory synaptic inputs to DRN 5-HT neurons encode sustained approach/avoidance bias

One of the most striking findings made in this thesis were the neuroplastic adaptations induced in serotonergic and GABAergic neurons in the DRN. What I found was that in susceptible mice, 5-HT neurons were hypoexcitable and had sensitized inhibitory input while GABA neurons were hyperexcitable and had increased excitatory input. Having established vmPFC-DRN microcircuitry using optogenetic techniques, my results suggest that shifting excitatory/inhibitory balance to DRN 5-HT neurons mediates social avoidance and depression-like behaviors. This would be in line with human studies that have shown that altering 5-HT synthesis shifts social perception along an affiliative-agonistic axis (Bilderbeck et al., 2011; Robinson et al., 2013; Young, 2013). A recent paper from Minmin Luo's group demonstrated in great detail that the ability of 5-HT neurons to stay active during appetitive stimuli is necessary for the association between a rewarding outcome and sensory cue (Liu et al., 2014). I also demonstrated that glutamatergic vmPFC inputs to the DRN might encode aversion since activation during sensory contact in the absence of an aggressive encounter resulted in social avoidance. This would be in line with a study showing that acute microstimulation of the equivalent neural region in macaques promoted negative motivational valence (Amemori and Graybiel, 2012). Therefore, given our neurocircuitry findings, acutely activating the vmPFC in the presence of social sensory cues may be preventing appetitive encoding by negatively shifting the excitatory/inhibitory balance of 5-HT neuronal activity. Though we have yet to establish what effect activating the vmPFC-DRN pathway directly has on serotonergic output, other studies have shown that electrical activation of the vmPFC results in the silencing of putative 5-HT neurons (Celada et al., 2001). We will use

optogenetics and *in vivo* sampling techniques such as microdialysis in our future experiments to address this.

Interestingly, once social avoidance behaviors were established and consolidated, acute photoinhibition or photostimulation of the components of the vmPFC-DRN circuit did not produce immediate changes in approach or avoidance. This implicates that while socioaffective learning depends on the vmPFC-DRN microcircuit, this pathway is dispensable for the execution of learned approach-avoidance behaviors. Human imaging work from MDD patients has revealed abnormal vmPFC activity and altered synchrony with other limbic or subcortical structures such as the amygdala and hypothalamus (Johnstone et al., 2007; Kwaasteniet et al., 2013; Liao et al., 2011; Mayberg, 1997; Murray et al., 2011). Synchrony of the DRN with the vmPFC or limbic regions has not been well studied due to difficulty in measuring BOLD signal in this small and deep region, however studies combining PET and fMRI imaging show that 5-HT1_A autoreceptor binding, and therefore 5-HT release, predicts limbic activation (Fisher et al., 2006; Selvaraj et al., 2014). Work in animals from Dzirasa's group combined optogenetics and *in vivo* recording to show that low frequency stimulation of the vmPFC results in evoked potentials in numerous subcortical and limbic structures, such as the amygdala and nucleus accumbens, however they found that the response in the DRN occurred significantly faster, despite the DRN being more anatomically distal than the amygdala and other structures (Kumar et al., 2013). This was also the case with the VTA, another distal monaminergic nucleus that has been shown to modulate the encoding of avoidance and socioaffective behaviors (Chaudhury et al., 2012; Tye et al., 2012). Whether these pathways are faster due to differential modes of transmission or other

mechanisms has yet to be determined, but it is possible that the vmPFC may first be communicating with monoaminergic nuclei such as the DRN to establish threat sensitivity by synchronizing or desynchronizing limbic structures via 5-HT output and encode the appropriate behavioral response.

Clinical trials using vmPFC DBS have reversed mood deficits in treatment-resistant patients and normalized this vmPFC network activity (Haber and Brucker, 2009; Mayberg, 2009; Mayberg et al., 2005). In this thesis I present the first mouse model of vmPFC DBS in order to look at antidepressant mechanism and found that chronic high frequency stimulation of the vmPFC after avoidance behaviors were established restored social interaction. The fact that I observed an increase in excitatory input to 5-HT neurons suggests that chronic DBS of the vmPFC pathway desensitizes inhibition of 5-HT neurons, restoring the depressed excitatory/inhibitory balance after social defeat stress (Fig. 5.1). This effect was not observed when I acutely photomanipulated vmPFC terminals in the DRN, thus chronic vmPFC DBS may be inducing an LTP-like plasticity that strengthens excitation of DRN 5-HT neurons, overriding defeat-mediated inhibition, and reestablishing the ability of 5-HT neurons to reinforce rewarding behaviors in association with specific social stimuli.

Exploring vmPFC-DRN circuitry: novel insights and limitations

Though there have been a considerable number of tracing studies that establish vmPFC projections to the DRN, I further expanded on this literature by using genetically labeled mouse lines to identify specific cellular populations. By combining optogenetics with electrophysiology and *cFos* mapping in our *tdTomato* mouse lines, I started establishing a detailed wiring diagram for intra-DRN connectivity and its modulation by

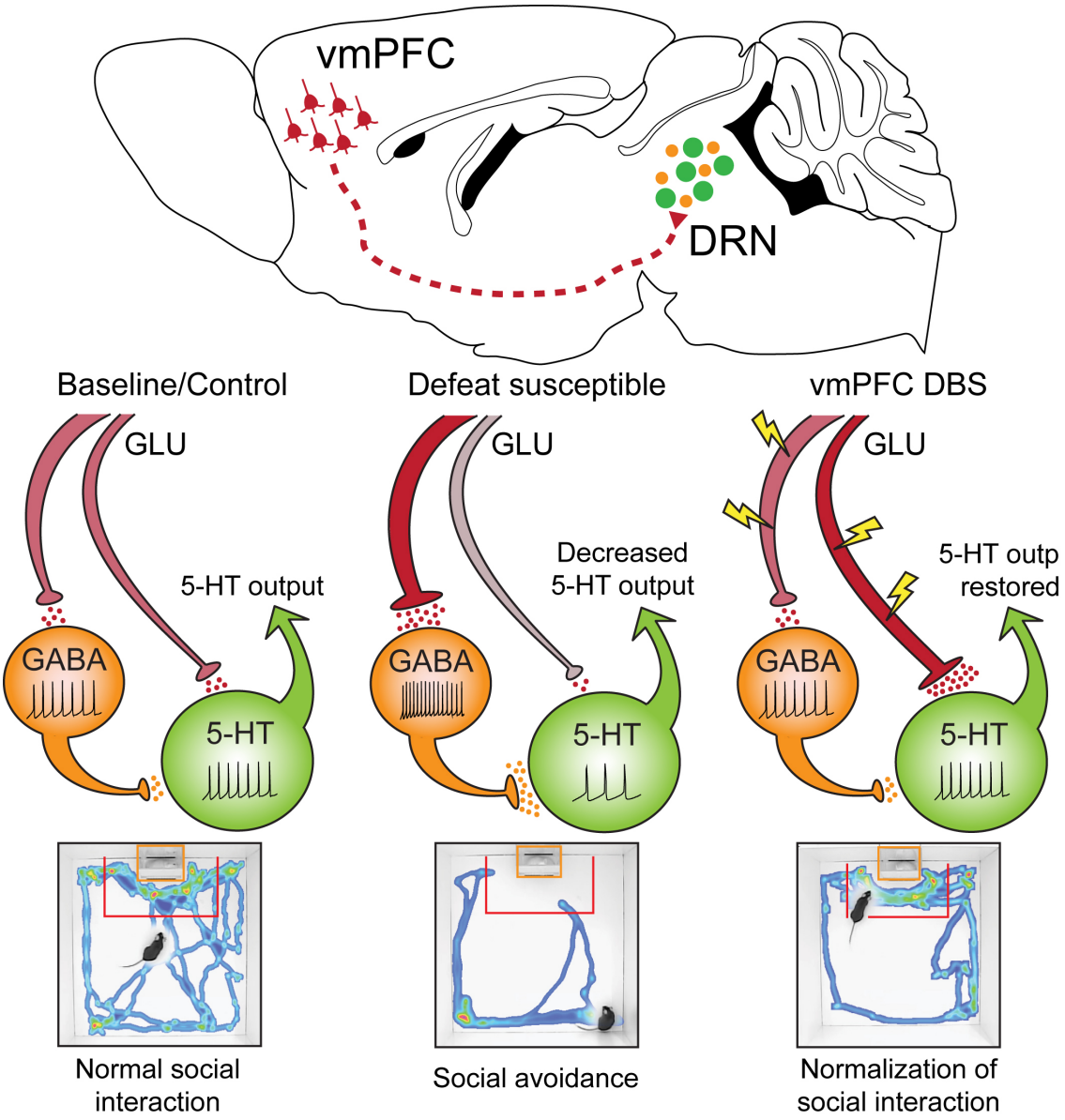

Figure 5.1. Hypothesized adaptations in the vmPFC-DRN microcircuit induced by social defeat and vmPFC DBS

Schematic summarizing the differential neuroplastic adaptations in the vmPFC-DRN microcircuit and hypothesized effect on 5-HT output. Depicted are changes in intrinsic cellular excitability, synaptic activity (EPSC, IPSC) and corresponding social approach/avoidance behavior profiles (shown as video tracking heat maps). Compared to controls, in susceptible mice we observed hyperexcitable GABA neurons that had increased glutamatergic input and hypoexcitable 5-HT neurons that had increased GABAergic input. After chronic vmPFC DBS, there was a neuroplastic remodeling of DRN microcircuitry that normalized GABA-mediated hyperinhibition of 5-HT neurons and facilitated a direct excitatory synaptic drive of 5-HT neurons. Though the direct source of synaptic adaptations was not causally determined in this work, our mapping studies provide strong evidence for this circuit and adaptive mechanisms.

a novel long-range vmPFC projection. First, I established the pivotal role of GABAergic neurons as local inhibitory relays using optogenetics, confirming a concept that had been suggested by previous work (Celada et al., 2001; Jankowski and Sesack, 2004), but never causally established. Next, although previous studies have hypothesized the existence of direct vmPFC inputs to DRN GABA neurons, we obtained the first electrophysiological evidence of such input through laser-elicited postsynaptic currents in GABA neurons from *ChR2*-expressing vmPFC terminals. Though we attempted to use the same technique to demonstrate the connection between the vmPFC and 5-HT neurons, we were unable to observe such a connection. One possibility we were unable to do so is that the direct vmPFC to 5-HT neuron connection may not rely on fast acting AMPA receptors, but rather slower NMDA receptors or metabotropic glutamate receptors (mGluR). Observation of these currents would certainly be interesting as they are shown to play a prominent role in long-term potentiation and memory formation (Anwyl, 1999; Bliss and Collingridge, 1993; Collingridge and Bliss, 1987; Malenka and Bear, 2004). *In situ* hybridization studies have localized different mGluR subtypes to the DRN (Ohishi et al., 1993; Shigemoto et al., 1992) and injection of an mGluR antagonist into the DRN does alter serotonergic activity (Palazzo et al., 2004). NMDA receptors however, are unlikely to have a major role in raphe because ketamine, a well-characterized NMDA receptor antagonist, does not seem to alter 5-HT output though direct infusion in the DRN (Nishitani et al., 2014). I did not probe for either NMDA receptor or mGluR currents in this thesis though searching for and isolating these currents in DRN 5-HT neurons is undoubtedly a focus of future experiments.

There is also a possibility that the areas in which we were probing for vmPFC connectivity with 5-HT neurons were subregions not particularly dense in these synapses. The genetic mapping experiment I performed actually reveals a rostrocaudal gradient in the overlap between glutamatergic vmPFC input and GABA or 5-HT cellular populations, with higher coincidence of terminals with GABAergic neurons in the rostral DRN and

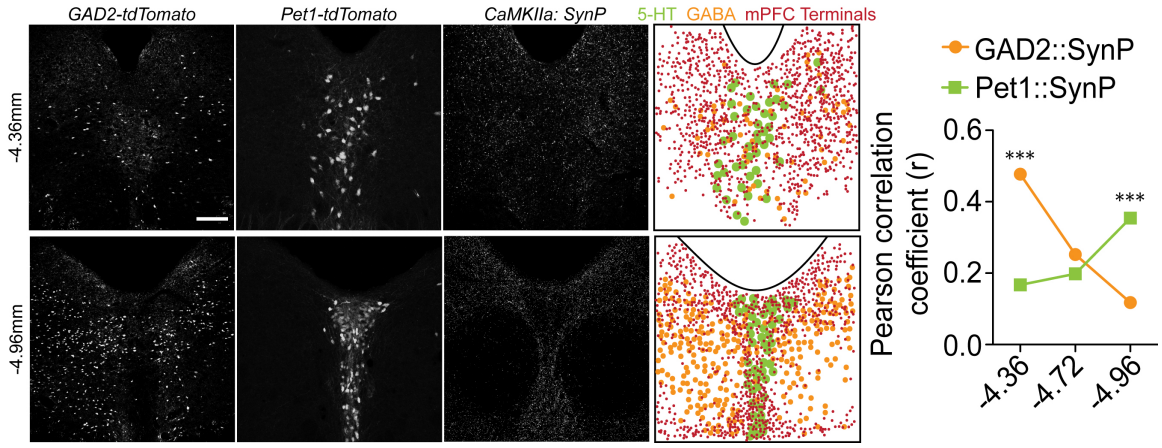

Figure 5.2. Analysis of the distribution of vmPFC axon terminals relative 5-HT and GABA neurons in the DRN

Coronal views of rostral (top row) and caudal (bottom row) DRN depict innervation by vmPFC axons visualized by AAV-based anterograde tracing. *SynP-GFP* was targeted excitatory neurons of the vmPFC by stereotaxic infusion of an AAV vector under the *CaMKIIa* promoter. After anterograde transport, *SynP-GFP* identifies excitatory vmPFC synaptic in the DRN of *Pet1-tdTomato* and *GAD2-tdTomato* mice. Renderings (fourth panel) represent the overlay of the 3 pictures on corresponding row depicting genetically identified GABA neurons, 5-HT neurons and vmPFC presynaptic terminals. Topographic cross-correlations between *SynP-GFP* fluorescent signal and *tdTomato* signals were calculated across 3 rostro-caudal levels. Plot of Pearson correlation coefficients reveals a predominant innervation of GABA neurons by vmPFC in the rostral DRN and 5-HT neurons in the caudal DRN.

with 5-HT neurons in the caudal DRN (Fig. 5.2). Given that 5-HT neurons have different cellular properties and projection targets dependent on the DRN subfield (Bang et al., 2012; Calizo et al., 2011), it is likely that where vmPFC afferents make their connections with 5-HT neurons has a functional significance that has yet to be explored. Our genetic mapping remains a low definition attempt, as we use data collected from a limited

population of 5-HT and GABA neurons that were not sampled systematically throughout the DRN and were taken from different transgenic lines of mice, making the colocalization correlations probabilistic. To address this we are focused on using new trans-synaptic viral tracing methods that allow for the quantitative mapping of synapses formed between genetically identified neurons. One such approach is based on mGRASP, a technique that uses split-GFP reassembly across a synapse and can indicate the number, location and clustering of synapses with high resolution (Feng et al., 2012; Kim et al., 2011; Yook et al., 2013). Specifically, a viral vector coding for the constitutively expressed first half of GFP will be injected into the vmPFC while virus for the *Cre*-inducible second half will be injected in the DRN of *GAD2*- or *Pet1-Cre* mice, thereby achieving specific labeling of synapses from the vmPFC to either GABAergic or serotonergic neurons. This technique would clarify the spatial distribution of specific synaptic connectivity and may indicate DRN subregions that have higher probabilities of achieving a postsynaptic response.

Conclusion and future directions

As progress is made towards determining socioaffective-relevant circuits and their dysfunction, evidence grows to suggest that social skill deficits are a symptom of MDD rather than a precipitating factor. In this thesis, I show that repeated acute, social stress causes neuroplastic adaptations in the vmPFC-DRN microcircuit that decrease 5-HT neuronal activity and result in long-lasting social avoidance. I also present data suggesting vmPFC projections to the DRN encode aversion and that high frequency stimulation of this pathway restores avoidance behaviors, likely through normalizing the balance of excitatory/inhibitory input in 5-HT neurons. Further investigation would look

more in depth at these mechanisms to understand the circuitous mechanisms during normal and pathological behaviors. Because much of the physiological work for this these was performed in slice, it would be imperative to study circuit and population dynamics *in vivo*. This can be achieved by combining *in vivo* recording techniques with optogenetic tools to genetically identify neurons in awake, freely moving mice. With this strategy and the future directions mentioned in this chapter, we would like to **1:** track acute and long-term physiological activity of GABAergic and 5-HT neurons in the DRN during social defeat and social interaction, **2:** determine the precise neurophysiological effects vmPFC DBS has on DRN neurons, and **3:** explore the activity of the vmPFC-DRN microcircuit in valence encoding and social perception. This work would expand our knowledge on social deficits in mood disorders and provide the foundation to develop more efficacious therapeutic treatments.

Appendix I

List of abbreviations used

5-HT – 5-hydroxytryptamine or serotonin

AAV – adeno-associated virus

Arch – Archaerhodopsin, optogenetic molecule that silences cells via yellow light-driven outward proton pump

BDA – biotinylated dextran amine, an anterograde tracer

BLA – basolateral amygdala

CaMKIIa – calcium/calmodulin-dependent protein kinase IIa, used to identify glutamatergic neurons

Cg – cingulate cortex

ChR2 – Channelrhodopsin, optogenetic molecule that excites cells via blue light-gated cation channel

CSDS – chronic social defeat stress

CTb – cholera toxin B subunit, a retrograde tracer

DBS – deep brain stimulation

DG – dentage gyrus of the hippocampus

DP – dorsal peduncular cortex

DRN – dorsal raphe nucleus

EPSC – excitatory postsynaptic current

EPM – elevated plus maze

fMRI – functional magnetic resonance imaging

FST – forced swim test

GABA – gamma-Aminobutyric acid

GAD1/2 – glutamic acid decarboxylase, used to identify GABAergic neurons

HRP – horseradish peroxidase, a retrograde tracer

IL – infralimbic cortex

IPSC – inhibitory postsynaptic current

LHb – lateral habenula

MDD – major depressive disorder

NAc – nucleus accumbens

OFT – open field test

PET – positron emission tomography

Pet1 – early transcription factor used to identify serotonergic neurons

PHA-L – *Phaseolus vulgaris* leukoagglutinin, an anterograde tracer

Pir – piriform cortex

PL – prelimbic cortex

PSD-95 – postsynaptic density protein 95

RDA – rhodamine-labeled dextran amine, an anterograde tracer

RES – resilient condition following social defeat

SCG – subcallosal cingulate gyrus

SUS – susceptible condition following social defeat

SynP – synaptophysin, protein that localizes to synaptic boutons

TPH – tryptohan hydroxylase, synthesizing enzyme for serotonin

vmPFC – ventromedial prefrontal cortex

VTA – ventral tegmental area

WGA – wheat germ agglutinin, a retrograde tracer

List of references

Chapter 1 references

Adolphs, R. (2014). Social attention and the ventromedial prefrontal cortex. Brain *137*, 1572-1574.

Aghajanian, G.K., and Wang, R.Y. (1977). Habenular and other midbrain raphe afferents demonstrated by a modified retrodgrade tracing technique. Brain Research *122*, 229-242.

Alekseyenko, O.V., Lee, C., and Kravitz, E.A. (2010). Targeted manipulation of serotonergic neurotransmission affects the escalation of aggression in adult male Drosophila melanogaster. PloS One *5*, e10806.

Beck, A.T. (2008). The evolution of the cognitive model of depression and its neurobiological correlates. The American Journal of Psychiatry *165*, 969-977.

Bellani, M., Dusi, N., Yeh, P.-H., Soares, J.C., and Brambilla, P. (2011). The effects of antidepressants on human brain as detected by imaging studies. Focus on major depression. Progress in Neuro-Psychopharmacology and Biological Psychiatry *35*, 1544-1552.

Berton, O., Hahn, C.-G., and Thase, M.E. (2012). Are we getting closer to valid translational models for major depression? Science *338*, 75-79.

Berton, O., McClung, C.a., Dileone, R.J., Krishnan, V., Renthal, W., Russo, S.J., Graham, D., Tsankova, N.M., Bolanos, C.a., Rios, M.*, et al.* (2006). Essential role of BDNF in the mesolimbic dopamine pathway in social defeat stress. Science *311*, 864-868.

Bilderbeck, A.C., McCabe, C., Wakeley, J., McGlone, F., Harris, T., Cowen, P.J., and Rogers, R.D. (2011). Serotonergic activity influences the cognitive appraisal of close intimate relationships in healthy adults. Biological Psychiatry *69*, 720-725.

Billeke, P., Boardman, S., and Doraiswamy, P.M. (2013). Social cognition in major depressive disorder: A new paradigm? Translational Neuroscience *4*, 437-447.

Björkqvist, K. (2001). Social defeat as a stressor in humans. Physiology & Behavior *73*, 435-442.

Boksem, M.A.S., Smolders, R., and De Cremer, D. (2012). Social power and approach-related neural activity. Social cognitive and affective neuroscience *7*, 516-520.

Boldrini, M., Underwood, M.D., Mann, J.J., and Arango, V. (2005). More tryptophan hydroxylase in the brainstem dorsal raphe nucleus in depressed suicides. Brain Research *1041*, 19-28.

Brody, A.L., Saxena, S., Stoessel, P., Gillies, L.a., Fairbanks, L.a., Alborzian, S., Phelps, M.E., Huang, S.C., Wu, H.M., Ho, M.L.*, et al.* (2001). Regional brain metabolic changes in patients with major depression treated with either paroxetine or interpersonal therapy: preliminary findings. Archives of General Psychiatry *58*, 631-640.

Brown, S.M., Henning, S., and Wellman, C.L. (2005). Mild, short-term stress alters dendritic morphology in rat medial prefrontal cortex. Cerebral Cortex *15*, 1714-1722.

Buckholtz, J.W., and Meyer-Lindenberg, A. (2012). Psychopathology and the human connectome: toward a transdiagnostic model of risk for mental illness. Neuron *74*, 990-1004.

Cahn, D.D., and Frey, L.R. (1992). Listeners' perceived verbal and nonverbal behaviors associated with communicators' perceived understanding and misunderstanding. Perceptual and Motor Skills *74*, 1059-1064.

Calizo, L.H., Akanwa, A., Ma, X., Pan, Y.-Z., Lemos, J.C., Craige, C., Heemstra, L.a., and Beck, S.G. (2011). Raphe serotonin neurons are not homogenous: electrophysiological, morphological and neurochemical evidence. Neuropharmacology *61*, 524-543.

Chang, S.W.C., Brent, L.J.N., Adams, G.K., Klein, J.T., Pearson, J.M., Watson, K.K., and Platt, M.L. (2013). Neuroethology of primate social behavior. Proceedings of the National Academy of Sciences of the United States of America *110 Suppl*, 10387-10394.

Chiba, T., Kayahara, T., and Nakano, K. (2001). Efferent projections of infralimbic and prelimbic areas of the medial prefrontal cortex in the Japanese monkey, Macaca fuscata. Brain Research *888*, 83-101.

Chourbaji, S., Zacher, C., Sanchis-Segura, C., Dormann, C., Vollmayr, B., and Gass, P. (2005). Learned helplessness: validity and reliability of depressive-like states in mice. Brain Research Protocols *16*, 70-78.

Commons, K.G., Beck, S.G., and Bey, V.W. (2005). Two populations of glutamatergic axons in the rat dorsal raphe nucleus defined by the vesicular glutamate transporters 1 and 2. European Journal of Neuroscience *21*, 1577-1586.
Cooper, M.a., and Huhman, K.L. (2007). Corticotropin-releasing factor receptors in the dorsal raphe nucleus modulate social behavior in Syrian hamsters. Psychopharmacology *194*, 297-307.
Crawford, L.K., Craige, C.P., and Beck, S.G. (2010). Increased intrinsic excitability of lateral wing serotonin neurons of the dorsal raphe: a mechanism for selective activation in stress circuits. Journal of Neurophysiology *103*, 2652-2663.
Crawford, L.K., Craige, C.P., and Beck, S.G. (2011). Glutamatergic input is selectively increased in dorsal raphe subfield 5-HT neurons: role of morphology, topography and selective innervation. European Journal of Neuroscience *34*, 1794-1806.
Crockett, M.J., Apergis-Schoute, A., Herrmann, B., Lieberman, M., Muller, U., Robbins, T.W., and Clark, L. (2013). Serotonin Modulates Striatal Responses to Fairness and Retaliation in Humans. Journal of Neuroscience *33*, 3505-3513.
Crockett, M.J., Clark, L., Apergis-Schoute, A.M., Morein-Zamir, S., and Robbins, T.W. (2012). Serotonin modulates the effects of pavlovian aversive predictions on response vigor. Neuropsychopharmacology *37*, 2244-2252.
Damasio, A.R., Tranel, D., and Damasio, H. (1990). Individuals with sociopathic behavior caused by frontal damage fail to respond autonomically to social stimuli. Behavioural Brain Research *41*, 81-94.
Delaveau, P., Jabourian, M., Lemogne, C., Guionnet, S., Bergouignan, L., and Fossati, P. (2011). Brain effects of antidepressants in major depression: a meta-analysis of emotional processing studies. Journal of Affective Disorders *130*, 66-74.
Der-Avakian, A., and Markou, A. (2012). The neurobiology of anhedonia and other reward-related deficits. Trends in Neurosciences *35*, 68-77.
Derntl, B., Seidel, E.-M., Eickhoff, S.B., Kellermann, T., Gur, R.C., Schneider, F., and Habel, U. (2011). Neural correlates of social approach and withdrawal in patients with major depression. Social Neuroscience *6*, 482-501.
Dougalis, A.G., Matthews, G.A.C., Bishop, M.W., Brischoux, F., Kobayashi, K., and Ungless, M.A. (2012). Functional properties of dopamine neurons and co-expression of vasoactive intestinal polypeptide in the dorsal raphe nucleus and ventro-lateral periaqueductal grey. European Journal of Neuroscience *36*, 3322-3332.
Drevets, W.C., Bogers, W., and Raichle, M.E. (2002). Functional anatomical correlates of antidepressant drug treatment assessed using PET measures of regional glucose metabolism. European Neuropsychopharmacology *12*, 527-544.
Drevets, W.C., Price, J.L., and Furey, M.L. (2008). Brain structural and functional abnormalities in mood disorders: implications for neurocircuitry models of depression. Brain Structure & Function *213*, 93-118.
Drevets, W.C., Price, J.L., Simpson, J., Todd, R.D., Reich, T., Vannier, M., and Raichle, M.E. (1997). Subgenual prefrontal cortex abnormalities in mood disorders. Nature *386*, 824-827.
Fava, M., and Kendler, K.S. (2000). Major Depressive Disorder. Neuron *28*, 335-341.
Finger, E.C., Marsh, A.A., Mitchell, D.G., Reid, M.E., Sims, C., Budhani, S., Kosson, D.S., Chen, G., Towbin, K.E., Leibenluft, E.*, et al.* (2008). Abnormal ventromedial prefrontal cortex function in children with psychopathic traits during reversal learning. Archives of general psychiatry *65*, 586-594.
Freedman, L.J., Insel, T.R., and Smith, Y. (2000). Subcortical projections of area 25 (subgenual cortex) of the macaque monkey. Journal of Comparative Neurology *421*, 172-188.
Frith, C.D. (2007). The social brain? Philosophical Transactions of the Royal Society of London Series B, Biological Sciences *362*, 671-678.
Fu, W., Le Maître, E., Fabre, V., Bernard, J.-F., David Xu, Z.-Q., and Hökfelt, T. (2010). Chemical neuroanatomy of the dorsal raphe nucleus and adjacent structures of the mouse brain. Journal of Comparative Neurology *518*, 3464-3494.
Fuster, J.M. (2000). Executive frontal functions. Experimental Brain Research *133*, 66-70.
Gabbott, P.L.a., Warner, T.a., Jays, P.R.L., Salway, P., and Busby, S.J. (2005). Prefrontal cortex in the rat: projections to subcortical autonomic, motor, and limbic centers. Journal of Comparative Neurology *492*, 145-177.

Geurts, D.E.M., Huys, Q.J.M., den Ouden, H.E.M., and Cools, R. (2013). Serotonin and Aversive Pavlovian Control of Instrumental Behavior in Humans. Journal of Neuroscience *33*, 18932-18939.
Gocho, Y., Sakai, A., Yanagawa, Y., Suzuki, H., and Saitow, F. (2013). Electrophysiological and pharmacological properties of GABAergic cells in the dorsal raphe nucleus. Journal of Physiological Sciences *63*, 147-154.
Golden, S.A., Christoffel, D.J., Heshmati, M., Hodes, G.E., Magida, J., Davis, K., Cahill, M.E., Dias, C., Ribeiro, E., Ables, J.L*., et al.* (2013). Epigenetic regulation of RAC1 induces synaptic remodeling in stress disorders and depression. Nature Medicine *19*, 337-344.
Gonçalves, L., Nogueira, M.I., Shammah-Lagnado, S.J., and Metzger, M. (2009). Prefrontal afferents to the dorsal raphe nucleus in the rat. Brain Research Bulletin *78*, 240-247.
Graeff, F.G., Guimarães, F.S., De Andrade, T.G., and Deakin, J.F. (1996). Role of 5-HT in stress, anxiety, and depression. Pharmacology Biochemistry and Behavior *54*, 129-141.
Gutman, D.A., Holtzheimer, P.E., Behrens, T.E.J., Johansen-Berg, H., and Mayberg, H.S. (2009). A tractography analysis of two deep brain stimulation white matter targets for depression. Biological psychiatry *65*, 276-282.
Haber, S.N., and Knutson, B. (2010). The reward circuit: linking primate anatomy and human imaging. Neuropsychopharmacology *35*, 4-26.
Hajós, M., Richards, C.D., Székely, a.D., and Sharp, T. (1998). An electrophysiological and neuroanatomical study of the medial prefrontal cortical projection to the midbrain raphe nuclei in the rat. Neuroscience *87*, 95-108.
Hamani, C., Diwan, M., Macedo, C.E., Brandão, M.L., Shumake, J., Gonzalez-lima, F., Raymond, R., Lozano, A.M., Fletcher, P.J., and Nobrega, J.N. (2010). Antidepressant-Like Effects of Medial Prefrontal Cortex Deep Brain Stimulation in Rats. Biological Psychiatry *67*, 117-124.
Hamani, C., Diwan, M., Raymond, R., Nobrega, J.N., Macedo, C.E., Brandão, M.L., Shumake, J., Gonzalez-Lima, F., Lozano, A.M., and Fletcher, P.J. (2011). Reply to: Electrical Brain Stimulation in Depression: Which Target(s)? Biological Psychiatry *69*, e7-e8.
Hamani, C., Machado, D.C., Hipólide, D.C., Dubiela, F.P., Suchecki, D., Macedo, C.E., Tescarollo, F., Martins, U., Covolan, L., and Nobrega, J.N. (2012). Deep Brain Stimulation Reverses Anhedonic-Like Behavior in a Chronic Model of Depression: Role of Serotonin and Brain Derived Neurotrophic Factor. Biological Psychiatry *71*, 30-35.
Hamilton, J.P., Etkin, A., Furman, D.J., Lemus, M.G., Johnson, R.F., and Gotlib, I.H. (2012). Functional neuroimaging of major depressive disorder: a meta-analysis and new integration of base line activation and neural response data. The American journal of psychiatry *169*, 693-703.
Harmer, C.J., Shelley, N.C., Cowen, P.J., and Goodwin, G.M. (2004). Increased positive versus negative affective perception and memory in healthy volunteers following selective serotonin and norepinephrine reuptake inhibition. The American Journal of Psychiatry *161*, 1256-1263.
Hattox, A.M., and Nelson, S.B. (2007). Layer V neurons in mouse cortex projecting to different targets have distinct physiological properties. Journal of neurophysiology *98*, 3330-3340.
Hurley, K.M., Herbert, H., Moga, M.M., and Saper, C.B. (1991). Efferent projections of the infralimbic cortex of the rat. Journal of Comparative Neurology *308*, 249-276.
Insel, T.R. (2014). The NIMH Research Domain Criteria (RDoC) Project: precision medicine for psychiatry. The American journal of psychiatry *171*, 395-397.
Ishida, Y., Hashiguchi, H., Takeda, R., Ishizuka, Y., Mitsuyama, Y., Kannan, H., Nishimori, T., and Nakahara, D. (2002). Conditioned-fear stress increases Fos expression in monoaminergic and GABAergic neurons of the locus coeruleus and dorsal raphe nuclei. Synapse *45*, 46-51.
Izquierdo, A., Wellman, C.L., and Holmes, A. (2006). Brief uncontrollable stress causes dendritic retraction in infralimbic cortex and resistance to fear extinction in mice. Journal of Neuroscience *26*, 5733-5738.
Jankowski, M.P., and Sesack, S.R. (2004). Prefrontal cortical projections to the rat dorsal raphe nucleus: ultrastructural features and associations with serotonin and gamma-aminobutyric acid neurons. Journal of Comparative Neurology *468*, 518-529.
Kaplan, J.R., Manuck, S.B., Fontenot, M.B., and Mann, J.J. (2002). Central nervous system monoamine correlates of social dominance in cynomolgus monkeys (Macaca fascicularis). Neuropsychopharmacology *26*, 431-443.

Kollack-Walker, S., Watson, S.J., and Akil, H. (1997). Social stress in hamsters: defeat activates specific neurocircuits within the brain. Journal of Neuroscience *17*, 8842-8855.
Koolhaas, J.M., De Boer, S.F., De Rutter, A.J., Meerlo, P., and Sgoifo, A. (1997). Social stress in rats and mice. Acta Physiologica Scandinavica Supplementum *640*, 69-72.
Kravitz, E.A. (2000). Serotonin and aggression: insights gained from a lobster model system and speculations on the role of amine neurons in a complex behavior. Journal of Comparative Physiology *186*, 221-238.
Krishnan, V., Han, M.-H., Graham, D.L., Berton, O., Renthal, W., Russo, S.J., Laplant, Q., Graham, A., Lutter, M., Lagace, D.C*., et al.* (2007). Molecular adaptations underlying susceptibility and resistance to social defeat in brain reward regions. Cell *131*, 391-404.
Krishnan, V., and Nestler, E.J. (2008). The molecular neurobiology of depression. Nature *455*, 894-902.
Kudryavtseva, N.N., Bakshtanovskaya, I.V., and Koryakina, L.A. (1991). Social model of depression in mice of C57BL/6J strain. Pharmacology Biochemistry and Behavior *38*, 315-320.
Lee, H.-Y., Tae, W.S., Yoon, H.-K., Lee, B.-T., Paik, J.-W., Son, K.-R., Oh, Y.-W., Lee, M.-S., and Ham, B.-J. (2011). Demonstration of decreased gray matter concentration in the midbrain encompassing the dorsal raphe nucleus and the limbic subcortical regions in major depressive disorder: an optimized voxel-based morphometry study. Journal of Affective Disorders *133*, 128-136.
Lee, H.S., Kim, M.a., Valentino, R.J., and Waterhouse, B.D. (2003). Glutamatergic afferent projections to the dorsal raphe nucleus of the rat. Brain Research *963*, 57-71.
Lehman, J.F., Greenberg, B.D., McIntyre, C.C., Rasmussen, S.A., and Haber, S.N. (2011). Rules ventral prefrontal cortical axons use to reach their targets: implications for diffusion tensor imaging tractography and deep brain stimulation for psychiatric illness. The Journal of neuroscience : the official journal of the Society for Neuroscience *31*, 10392-10402.
Liao, C., Feng, Z., Zhou, D., Dai, Q., Xie, B., Ji, B., and Wang, X. (2011). Dysfunction of fronto-limbic brain circuitry in depression. Neuroscience *201*, 231-238.
Lozano, A.M., Mayberg, H.S., Giacobbe, P., Hamani, C., Craddock, R.C., and Kennedy, S.H. (2008). Subcallosal cingulate gyrus deep brain stimulation for treatment-resistant depression. Biological Psychiatry *64*, 461-467.
Lutter, M., Sakata, I., Osborne-Lawrence, S., Rovinsky, S.A., Anderson, J.G., Jung, S., Birnbaum, S., Yanagisawa, M., Elmquist, J.K., Nestler, E.J*., et al.* (2008). The orexigenic hormone ghrelin defends against depressive symptoms of chronic stress. Nature neuroscience *11*, 752-753.
Mathews, A., and MacLeod, C. (2005). Cognitive vulnerability to emotional disorders. Annual Review of Clinical Psychology *1*, 167-195.
Mayberg, H.S. (1997). Limbic-cortical dysregulation: a proposed model of depression. Journal of Neuropsychiatry and Clinical Neurosciences *9*, 471-481.
Mayberg, H.S. (2003). Modulating dysfunctional limbic-cortical circuits in depression: towards development of brain-based algorithms for diagnosis and optimised treatment. British Medical Bulletin *65*, 193-207.
Mayberg, H.S., Lozano, A.M., Voon, V., McNeely, H.E., Seminowicz, D., Hamani, C., Schwalb, J.M., and Kennedy, S.H. (2005). Deep brain stimulation for treatment-resistant depression. Neuron *45*, 651-660.
McEwen, A.M., Burgess, D.T.A., Hanstock, C.C., Seres, P., Khalili, P., Newman, S.C., Baker, G.B., Mitchell, N.D., Khudabux-Der, J., Allen, P.S*., et al.* (2012). Increased glutamate levels in the medial prefrontal cortex in patients with postpartum depression. Neuropsychopharmacology *37*, 2428-2435.
Miller, E.K., and Cohen, J.D. (2001). An integrative theory of prefrontal cortex function. Annual Review of Neuroscience *24*, 167-202.
Morris, J.S., Ohman, A., and Dolan, R.J. (1998). Conscious and unconscious emotional learning in the human amygdala. Nature *393*, 467-470.
Muhammad, A., Carroll, C., and Kolb, B. (2012). Stress during development alters dendritic morphology in the nucleus accumbens and prefrontal cortex. Neuroscience *216*, 103-109.
Oliveira, R.F. (2009). Social behavior in context: Hormonal modulation of behavioral plasticity and social competence. Integrative and Comparative Biology *49*, 423-440.
Oliveira, R.F. (2012). Social plasticity in fish: integrating mechanisms and function. Journal of Fish Biology *81*, 2127-2150.
Oosterhof, N.N., and Todorov, A. (2009). Shared perceptual basis of emotional expressions and trustworthiness impressions from faces. Emotion (Washington, DC) *9*, 128-133.

Pan, Z.Z., and Williams, J.T. (1989). GABA- and glutamate-mediated synaptic potentials in rat dorsal raphe neurons in vitro. Journal of Neurophysiology *61*, 719-726.
Passamonti, L., Crockett, M.J., Apergis-Schoute, A.M., Clark, L., Rowe, J.B., Calder, A.J., and Robbins, T.W. (2012). Effects of acute tryptophan depletion on prefrontal-amygdala connectivity while viewing facial signals of aggression. Biological Psychiatry *71*, 36-43.
Paykel, E.S. (2008). Partial remission, residual symptoms, and relapse in depression. Dialogues in clinical neuroscience *10*, 431-437.
Peyron, C., Petit, J.M., Rampon, C., Jouvet, M., and Luppi, P.H. (1998). Forebrain afferents to the rat dorsal raphe nucleus demonstrated by retrograde and anterograde tracing methods. Neuroscience *82*, 443-468.
Phan, K.L., Wager, T., Taylor, S.F., and Liberzon, I. (2002). Functional neuroanatomy of emotion: a meta-analysis of emotion activation studies in PET and fMRI. NeuroImage *16*, 331-348.
Quirin, M., Meyer, F., Heise, N., Kuhl, J., Küstermann, E., Strüber, D., and Cacioppo, J.T. (2013). Neural correlates of social motivation: an fMRI study on power versus affiliation. International journal of psychophysiology *88*, 289-295.
Quirk, G.J., Russo, G.K., Barron, J.L., and Lebron, K. (2000). The role of ventromedial prefrontal cortex in the recovery of extinguished fear. Journal of Neuroscience *20*, 6225-6231.
Radden, J. (2003). Is This Dame Melancholy?: Equating Today's Depression and Past Melancholia. Philosophy, Psychiatry, & Psychology *10*, 37-52.
Robinson, O.J., Overstreet, C., Allen, P.S., Letkiewicz, A., Vytal, K., Pine, D.S., and Grillon, C. (2013). The role of serotonin in the neurocircuitry of negative affective bias: serotonergic modulation of the dorsal medial prefrontal-amygdala 'aversive amplification' circuit. NeuroImage *78*, 217-223.
Roche, M., Commons, K.G., Peoples, A., and Valentino, R.J. (2003). Circuitry underlying regulation of the serotonergic system by swim stress. Journal of Neuroscience *23*, 970-977.
Rogers, R.D. (2011). The roles of dopamine and serotonin in decision making: evidence from pharmacological experiments in humans. Neuropsychopharmacology *36*, 114-132.
Romera, I., Perez, V., Menchón, J.M., Delgado-Cohen, H., Polavieja, P., and Gilaberte, I. (2010). Social and occupational functioning impairment in patients in partial versus complete remission of a major depressive disorder episode. A six-month prospective epidemiological study. European Psychiatry *25*, 58-65.
Rygula, R., Abumaria, N., Flügge, G., Fuchs, E., Rüther, E., and Havemann-Reinecke, U. (2005). Anhedonia and motivational deficits in rats: impact of chronic social stress. Behavioural Brain Research *162*, 127-134.
Senn, V., Wolff, S.B.E., Herry, C., Grenier, F., Ehrlich, I., Gründemann, J., Fadok, J.P., Müller, C., Letzkus, J.J., and Lüthi, A. (2014). Long-Range Connectivity Defines Behavioral Specificity of Amygdala Neurons. Neuron *81*, 428-437.
Sesack, S.R., Deutch, A.Y., Roth, R.H., and Bunney, B.S. (1989). Topographical organization of the efferent projections of the medial prefrontal cortex in the rat: an anterograde tract-tracing study with Phaseolus vulgaris leucoagglutinin. Journal of Comparative Neurology *290*, 213-242.
Shikanai, H., Yoshida, T., Konno, K., Yamasaki, M., Izumi, T., Ohmura, Y., Watanabe, M., and Yoshioka, M. (2012). Distinct Neurochemical and Functional Properties of GAD67-Containing 5-HT Neurons in the Rat Dorsal Raphe Nucleus. Journal of Neuroscience *32*, 14415-14426.
Shively, C.A., Grant, K.A., Ehrenkaufer, R.L., Mach, R.H., and Nader, M.A. (1997). Social Stress, Depression, and Brain Dopamine in Female Cynomolgus Monkeys. Annals of the New York Academy of Sciences *807*, 574-577.
Smith, R., Chen, K., Baxter, L., Fort, C., and Lane, R.D. (2013). Antidepressant effects of sertraline associated with volume increases in dorsolateral prefrontal cortex. Journal of Affective Disorders *146*, 414-419.
Soiza-Reilly, M., and Commons, K.G. (2011). Glutamatergic drive of the dorsal raphe nucleus. Journal of Chemical Neuroanatomy *41*, 247-255.
Stevenson, P.A., and Schildberger, K. (2013). Mechanisms of experience dependent control of aggression in crickets. Current Opinion in Neurobiology *23*, 318-323.
Stockmeier, C.A., Dilley, G.E., Shapiro, L.A., Overholser, J.C., Thompson, P.A., and Meltzer, H.Y. (1997). Serotonin receptors in suicide victims with major depression. Neuropsychopharmacology *16*, 162-173.

Taborsky, B., and Oliveira, R.F. (2012). Social competence: an evolutionary approach. Trends in ecology & evolution *27*, 679-688.
Takagishi, M., and Chiba, T. (1991). Efferent projections of the infralimbic (area 25) region of the medial prefrontal cortex in the rat: an anterograde tracer PHA-L study. Brain Research *566*, 26-39.
Takahashi, A., Schilit, A.N., Kim, J., Debold, J.F., Koide, T., and Miczek, K.A. (2012). Behavioral characterization of escalated aggression induced by GABA(B) receptor activation in the dorsal raphe nucleus. Psychopharmacology *224*, 155-166.
Takahashi, A., Shimamoto, A., Boyson, C.O., DeBold, J.F., and Miczek, K.A. (2010). GABA(B) receptor modulation of serotonin neurons in the dorsal raphé nucleus and escalation of aggression in mice. Journal of Neuroscience *30*, 11771-11780.
Teles, M.C., Dahlbom, S.J., Winberg, S., and Oliveira, R.F. (2013). Social modulation of brain monoamine levels in zebrafish. Behavioural Brain Research *253*, 17-24.
Todorov, A. (2008). Evaluating faces on trustworthiness: an extension of systems for recognition of emotions signaling approach/avoidance behaviors. Annals of the New York Academy of Sciences *1124*, 208-224.
Varga, V., Székely, a.D., Csillag, a., Sharp, T., and Hajós, M. (2001). Evidence for a role of GABA interneurones in the cortical modulation of midbrain 5-hydroxytryptamine neurones. Neuroscience *106*, 783-792.
Vasic, N., Walter, H., Höse, A., and Wolf, R.C. (2008). Gray matter reduction associated with psychopathology and cognitive dysfunction in unipolar depression: a voxel-based morphometry study. Journal of affective disorders *109*, 107-116.
Vázquez-Borsetti, P., Cortés, R., and Artigas, F. (2009). Pyramidal neurons in rat prefrontal cortex projecting to ventral tegmental area and dorsal raphe nucleus express 5-HT2A receptors. Cerebral Cortex *19*, 1678-1686.
Vertes, R.P. (2004). Differential projections of the infralimbic and prelimbic cortex in the rat. Synapse *51*, 32-58.
Vinkers, C.H., Groenink, L., van Bogaert, M.J.V., Westphal, K.G.C., Kalkman, C.J., van Oorschot, R., Oosting, R.S., Olivier, B., and Korte, S.M. (2009). Stress-induced hyperthermia and infection-induced fever: two of a kind? Physiology & Behavior *98*, 37-43.
Volman, I., Roelofs, K., Koch, S., Verhagen, L., and Toni, I. (2011). Anterior prefrontal cortex inhibition impairs control over social emotional actions. Current Biology *21*, 1766-1770.
Willner, P. (2005). Chronic mild stress (CMS) revisited: consistency and behavioural-neurobiological concordance in the effects of CMS. Neuropsychobiology *52*, 90-110.
Willner, P., Scheel-Krüger, J., and Belzung, C. (2013). The neurobiology of depression and antidepressant action. Neuroscience and Biobehavioral Reviews *37*, 2331-2371.
Wilson, M.A., and Gallager, D.W. (1988). GABAergic subsensitivity of dorsal raphe neurons in vitro after chronic benzodiazepine treatment in vivo. Brain Research *473*, 198-202.
Winecoff, A., Clithero, J.A., Carter, R.M., Bergman, S.R., Wang, L., and Huettel, S.A. (2013). Ventromedial prefrontal cortex encodes emotional value. Journal of Neuroscience *33*, 11032-11039.
Wolf, R.C., Philippi, C.L., Motzkin, J.C., Baskaya, M.K., and Koenigs, M. (2014). Ventromedial prefrontal cortex mediates visual attention during facial emotion recognition. Brain.
Xie, H., Han, F., and Shi, X. (2012). Single-prolonged stress induce changes of CaM/CaMKIIα in the rats of dorsal raphe nucleus. Neurochemical Research *37*, 1043-1049.
Young, S.N. (2013). The effect of raising and lowering tryptophan levels on human mood and social behaviour. Philosophical Transactions of the Royal Society of London Series B, Biological Sciences *368*, 20110375.
Young, S.N., and Leyton, M. (2002). The role of serotonin in human mood and social interaction. Pharmacology Biochemistry and Behavior *71*, 857-865.

Chapter 2 references

Alekseyenko, O.V., Lee, C., and Kravitz, E.A. (2010). Targeted manipulation of serotonergic neurotransmission affects the escalation of aggression in adult male Drosophila melanogaster. PloS One *5*, e10806.

Amat, J., Baratta, M.V., Paul, E., Bland, S.T., Watkins, L.R., and Maier, S.F. (2005). Medial prefrontal cortex determines how stressor controllability affects behavior and dorsal raphe nucleus. Nature Neuroscience *8*, 365-371.

Bang, S.J., and Commons, K.G. (2012). Forebrain GABAergic projections from the dorsal raphe nucleus identified by using GAD67-GFP knock-in mice. Journal of Comparative Neurology *520*, 4157-4167.

Bang, S.J., Jensen, P., Dymecki, S.M., and Commons, K.G. (2012). Projections and interconnections of genetically defined serotonin neurons in mice. European Journal of Neuroscience *35*, 85-96.

Beck, A.T. (2008). The evolution of the cognitive model of depression and its neurobiological correlates. The American Journal of Psychiatry *165*, 969-977.

Berton, O., Covington, H.E., Ebner, K., Tsankova, N.M., Carle, T.L., Ulery, P., Bhonsle, A., Barrot, M., Krishnan, V., Singewald, G.M*., et al.* (2007). Induction of deltaFosB in the periaqueductal gray by stress promotes active coping responses. Neuron *55*, 289-300.

Berton, O., McClung, C.a., Dileone, R.J., Krishnan, V., Renthal, W., Russo, S.J., Graham, D., Tsankova, N.M., Bolanos, C.a., Rios, M*., et al.* (2006). Essential role of BDNF in the mesolimbic dopamine pathway in social defeat stress. Science *311*, 864-868.

Bilderbeck, A.C., McCabe, C., Wakeley, J., McGlone, F., Harris, T., Cowen, P.J., and Rogers, R.D. (2011). Serotonergic activity influences the cognitive appraisal of close intimate relationships in healthy adults. Biological Psychiatry *69*, 720-725.

Brown, R.E., McKenna, J.T., Winston, S., Basheer, R., Yanagawa, Y., Thakkar, M.M., and McCarley, R.W. (2008). Characterization of GABAergic neurons in rapid-eye-movement sleep controlling regions of the brainstem reticular formation in GAD67-green fluorescent protein knock-in mice. European Journal of Neuroscience *27*, 352-363.

Bruchas, M.R., Schindler, A.G., Shankar, H., Messinger, D.I., Miyatake, M., Land, B.B., Lemos, J.C., Hagan, C.E., Neumaier, J.F., Quintana, A*., et al.* (2011). Selective p38α MAPK Deletion in Serotonergic Neurons Produces Stress Resilience in Models of Depression and Addiction. Neuron *71*, 498-511.

Calizo, L.H., Akanwa, A., Ma, X., Pan, Y.-Z., Lemos, J.C., Craige, C., Heemstra, L.a., and Beck, S.G. (2011). Raphe serotonin neurons are not homogenous: electrophysiological, morphological and neurochemical evidence. Neuropharmacology *61*, 524-543.

Canli, T., and Lesch, K.-P. (2007). Long story short: the serotonin transporter in emotion regulation and social cognition. Nature Neuroscience *10*, 1103-1109.

Celada, P., Puig, M.V., Casanovas, J.M., Guillazo, G., and Artigas, F. (2001). Control of dorsal raphe serotonergic neurons by the medial prefrontal cortex: Involvement of serotonin-1A, GABA(A), and glutamate receptors. Journal of Neuroscience *21*, 9917-9929.

Charuvastra, A., and Cloitre, M. (2008). Social bonds and posttraumatic stress disorder. Annual Review of Psychology *59*, 301-328.

Chattopadhyaya, B., Di Cristo, G., Higashiyama, H., Knott, G.W., Kuhlman, S.J., Welker, E., and Huang, Z.J. (2004). Experience and activity-dependent maturation of perisomatic GABAergic innervation in primary visual cortex during a postnatal critical period. Journal of Neuroscience *24*, 9598-9611.

Chiba, T., Kayahara, T., and Nakano, K. (2001). Efferent projections of infralimbic and prelimbic areas of the medial prefrontal cortex in the Japanese monkey, Macaca fuscata. Brain Research *888*, 83-101.

Chow, B.Y., Han, X., Dobry, A.S., Qian, X., Chuong, A.S., Li, M., Henninger, M.a., Belfort, G.M., Lin, Y., Monahan, P.E*., et al.* (2010). High-performance genetically targetable optical neural silencing by light-driven proton pumps. Nature *463*, 98-102.

Crawford, L.K., Craige, C.P., and Beck, S.G. (2010). Increased intrinsic excitability of lateral wing serotonin neurons of the dorsal raphe: a mechanism for selective activation in stress circuits. Journal of Neurophysiology *103*, 2652-2663.

Crawford, L.K., Craige, C.P., and Beck, S.G. (2011). Glutamatergic input is selectively increased in dorsal raphe subfield 5-HT neurons: role of morphology, topography and selective innervation. European Journal of Neuroscience *34*, 1794-1806.

Crawford, L.K., Rahman, S.F., and Beck, S.G. (2013). Social stress alters inhibitory synaptic input to distinct subpopulations of raphe serotonin neurons. ACS Chemical Neuroscience *4*, 200-209.

Cusi, A.M., Nazarov, A., Holshausen, K., Macqueen, G.M., and McKinnon, M.C. (2012). Systematic review of the neural basis of social cognition in patients with mood disorders. Journal of Psychiatry & Neuroscience *37*, 154-169.

Espallergues, J., Teegarden, S.L., Veerakumar, A., Boulden, J., Challis, C., Jochems, J., Chan, M., Petersen, T., Deneris, E., Matthias, P.*, et al.* (2012). HDAC6 Regulates Glucocorticoid Receptor Signaling in Serotonin Pathways with Critical Impact on Stress Resilience. Journal of Neuroscience *32*, 4400-4416.

Ettenberg, A., Ofer, O.A., Mueller, C.L., Waldroup, S., Cohen, A., and Ben-Shahar, O. (2011). Inactivation of the dorsal raphé nucleus reduces the anxiogenic response of rats running an alley for intravenous cocaine. Pharmacology, biochemistry, and behavior *97*, 632-639.

Freedman, L.J., Insel, T.R., and Smith, Y. (2000). Subcortical projections of area 25 (subgenual cortex) of the macaque monkey. Journal of Comparative Neurology *421*, 172-188.

Fu, W., Le Maître, E., Fabre, V., Bernard, J.-F., David Xu, Z.-Q., and Hökfelt, T. (2010). Chemical neuroanatomy of the dorsal raphe nucleus and adjacent structures of the mouse brain. Journal of Comparative Neurology *518*, 3464-3494.

Golden, S.A., Covington, H.E., Berton, O., and Russo, S.J. (2011). A standardized protocol for repeated social defeat stress in mice. Nature Protocols *6*, 1183-1191.

Hamani, C., Diwan, M., Macedo, C.E., Brandão, M.L., Shumake, J., Gonzalez-lima, F., Raymond, R., Lozano, A.M., Fletcher, P.J., and Nobrega, J.N. (2010). Antidepressant-Like Effects of Medial Prefrontal Cortex Deep Brain Stimulation in Rats. Biological Psychiatry *67*, 117-124.

Hamani, C., Diwan, M., Raymond, R., Nobrega, J.N., Macedo, C.E., Brandão, M.L., Shumake, J., Gonzalez-Lima, F., Lozano, A.M., and Fletcher, P.J. (2011). Reply to: Electrical Brain Stimulation in Depression: Which Target(s)? Biological Psychiatry *69*, e7-e8.

Hames, J.L., Hagan, C.R., and Joiner, T.E. (2013). Interpersonal processes in depression. Annual review of clinical psychology *9*, 355-377.

Hou, C., Xue, L., Feng, J., Zhang, L., Wang, Y., Chen, L., Wang, T., Zhang, Q.J., and Liu, J. (2012). Unilateral lesion of the nigrostriatal pathway decreases the response of GABA interneurons in the dorsal raphe nucleus to 5-HT(1A) receptor stimulation in the rat. Neurochemistry International *61*, 1344-1356.

Jankowski, M.P., and Sesack, S.R. (2004). Prefrontal cortical projections to the rat dorsal raphe nucleus: ultrastructural features and associations with serotonin and gamma-aminobutyric acid neurons. Journal of Comparative Neurology *468*, 518-529.

Krishnan, V., Berton, O., and Nestler, E.J. (2008). The use of animal models in psychiatric research and treatment. American Journal of Psychiatry *165*, 1109.

Krishnan, V., Han, M.-H., Graham, D.L., Berton, O., Renthal, W., Russo, S.J., Laplant, Q., Graham, A., Lutter, M., Lagace, D.C.*, et al.* (2007). Molecular adaptations underlying susceptibility and resistance to social defeat in brain reward regions. Cell *131*, 391-404.

Kudryavtseva, N.N., Bakshtanovskaya, I.V., and Koryakina, L.A. (1991). Social model of depression in mice of C57BL/6J strain. Pharmacology Biochemistry and Behavior *38*, 315-320.

Kumar, S., Black, S.J., Hultman, R., Szabo, S.T., Demaio, K.D., Du, J., Katz, B.M., Feng, G., Covington, H.E., and Dzirasa, K. (2013). Cortical control of affective networks. Journal of Neuroscience *33*, 1116-1129.

Liu, C., Maejima, T., Wyler, S.C., Casadesus, G., Herlitze, S., and Deneris, E.S. (2010). Pet-1 is required across different stages of life to regulate serotonergic function. Nature Neuroscience *13*, 1190-1198.

Liu, R., Jolas, T., and Aghajanian, G. (2000). Serotonin 5-HT(2) receptors activate local GABA inhibitory inputs to serotonergic neurons of the dorsal raphe nucleus. Brain Research *873*, 34-45.

Madisen, L., Zwingman, T.a., Sunkin, S.M., Oh, S.W., Zariwala, H.a., Gu, H., Ng, L.L., Palmiter, R.D., Hawrylycz, M.J., Jones, A.R.*, et al.* (2010). A robust and high-throughput Cre reporting and characterization system for the whole mouse brain. Nature Neuroscience *13*, 133-140.

Malatynska, E., Rapp, R., Harrawood, D., and Tunnicliff, G. (2005). Submissive behavior in mice as a test for antidepressant drug activity. Pharmacology Biochemistry and Behavior *82*, 306-313.

Mattis, J., Tye, K.M., Ferenczi, E.A., Ramakrishnan, C., O'Shea, D.J., Prakash, R., Gunaydin, L.A., Hyun, M., Fenno, L.E., Gradinaru, V.*, et al.* (2012). Principles for applying optogenetic tools derived from direct comparative analysis of microbial opsins. Nature Methods *9*, 159-172.

McKenna, J.T., Yang, C., Franciosi, S., Winston, S., Abarr, K.K., Rigby, M.S., Yanagawa, Y., McCarley, R.W., and Brown, R.E. (2013). Distribution and intrinsic membrane properties of basal forebrain GABAergic and parvalbumin neurons in the mouse. Journal of Comparative Neurology *521*, 1225-1250.

Meyer-Lindenberg, A., and Tost, H. (2012). Neural mechanisms of social risk for psychiatric disorders. Nature neuroscience *15*, 663-668.
Miller, E.K., and Cohen, J.D. (2001). An integrative theory of prefrontal cortex function. Annual Review of Neuroscience *24*, 167-202.
Passamonti, L., Crockett, M.J., Apergis-Schoute, A.M., Clark, L., Rowe, J.B., Calder, A.J., and Robbins, T.W. (2012). Effects of acute tryptophan depletion on prefrontal-amygdala connectivity while viewing facial signals of aggression. Biological Psychiatry *71*, 36-43.
Paul, E.D., Hale, M.W., Lukkes, J.L., Valentine, M.J., Sarchet, D.M., and Lowry, C.a. (2011). Repeated social defeat increases reactive emotional coping behavior and alters functional responses in serotonergic neurons in the rat dorsal raphe nucleus. Physiology & Behavior *104*, 272-282.
Penn, J.K.M., Zito, M.F., and Kravitz, E.A. (2010). A single social defeat reduces aggression in a highly aggressive strain of Drosophila. Proceedings of the National Academy of Sciences of the United States of America *107*, 12682-12686.
Phan, K.L., Coccaro, E.F., Angstadt, M., Kreger, K.J., Mayberg, H.S., Liberzon, I., and Stein, M.B. (2013). Corticolimbic brain reactivity to social signals of threat before and after sertraline treatment in generalized social phobia. Biological Psychiatry *73*, 329-336.
Pollack, M.H. (2005). Comorbid anxiety and depression. The Journal of clinical psychiatry *66 Suppl 8*, 22-29.
Raleigh, M.J., McGuire, M.T., Brammer, G.L., Pollack, D.B., and Yuwiler, A. (1991). Serotonergic mechanisms promote dominance acquisition in adult male vervet monkeys. Brain Research *559*, 181-190.
Roche, M., Commons, K.G., Peoples, A., and Valentino, R.J. (2003). Circuitry underlying regulation of the serotonergic system by swim stress. Journal of Neuroscience *23*, 970-977.
Rogers, R.D. (2011). The roles of dopamine and serotonin in decision making: evidence from pharmacological experiments in humans. Neuropsychopharmacology *36*, 114-132.
Roiser, J.P., Elliott, R., and Sahakian, B.J. (2012). Cognitive mechanisms of treatment in depression. Neuropsychopharmacology *37*, 117-136.
Roy, M., Shohamy, D., and Wager, T.D. (2012). Ventromedial prefrontal-subcortical systems and the generation of affective meaning. Trends in Cognitive Sciences *16*, 147-156.
Scott, M.M., Wylie, C.J., Lerch, J.K., Murphy, R., Lobur, K., Herlitze, S., Jiang, W., Conlon, R.a., Strowbridge, B.W., and Deneris, E.S. (2005). A genetic approach to access serotonin neurons for in vivo and in vitro studies. Proceedings of the National Academy of Sciences *102*, 16472-16477.
Slavich, G.M., Way, B.M., Eisenberger, N.I., and Taylor, S.E. (2010). Neural sensitivity to social rejection is associated with inflammatory responses to social stress. Proceedings of the National Academy of Sciences of the United States of America *107*, 14817-14822.
Sunkin, S.M., Ng, L., Lau, C., Dolbeare, T., Gilbert, T.L., Thompson, C.L., Hawrylycz, M., and Dang, C. (2013). Allen Brain Atlas: an integrated spatio-temporal portal for exploring the central nervous system. Nucleic Acids Research *41*, D996-D1008.
Takahashi, A., Schilit, A.N., Kim, J., Debold, J.F., Koide, T., and Miczek, K.A. (2012). Behavioral characterization of escalated aggression induced by GABA(B) receptor activation in the dorsal raphe nucleus. Psychopharmacology *224*, 155-166.
Takahashi, A., Shimamoto, A., Boyson, C.O., DeBold, J.F., and Miczek, K.A. (2010). GABA(B) receptor modulation of serotonin neurons in the dorsal raphé nucleus and escalation of aggression in mice. Journal of Neuroscience *30*, 11771-11780.
Taniguchi, H., He, M., Wu, P., Kim, S., Paik, R., Sugino, K., Kvitsiani, D., Kvitsani, D., Fu, Y., Lu, J.*, et al.* (2011). A resource of Cre driver lines for genetic targeting of GABAergic neurons in cerebral cortex. Neuron *71*, 995-1013.
Todorov, A. (2008). Evaluating faces on trustworthiness: an extension of systems for recognition of emotions signaling approach/avoidance behaviors. Annals of the New York Academy of Sciences *1124*, 208-224.
Tsankova, N.M., Berton, O., Renthal, W., Kumar, A., Neve, R.L., and Nestler, E.J. (2006). Sustained hippocampal chromatin regulation in a mouse model of depression and antidepressant action. Nature Neuroscience *9*, 519-525.

Varga, V., Kocsis, B., and Sharp, T. (2003). Electrophysiological evidence for convergence of inputs from the medial prefrontal cortex and lateral habenula on single neurons in the dorsal raphe nucleus. European Journal of Neuroscience *17*, 280-286.

Varga, V., Székely, a.D., Csillag, a., Sharp, T., and Hajós, M. (2001). Evidence for a role of GABA interneurones in the cortical modulation of midbrain 5-hydroxytryptamine neurones. Neuroscience *106*, 783-792.

Volman, I., Roelofs, K., Koch, S., Verhagen, L., and Toni, I. (2011). Anterior prefrontal cortex inhibition impairs control over social emotional actions. Current Biology *21*, 1766-1770.

Warden, M.R., Selimbeyoglu, A., Mirzabekov, J.J., Lo, M., Thompson, K.R., Kim, S.-Y., Adhikari, A., Tye, K.M., Frank, L.M., and Deisseroth, K. (2012). A prefrontal cortex–brainstem neuronal projection that controls response to behavioural challenge. Nature *492*, 428-432.

Wierenga, C.J., Müllner, F.E., Rinke, I., Keck, T., Stein, V., and Bonhoeffer, T. (2010). Molecular and electrophysiological characterization of GFP-expressing CA1 interneurons in GAD65-GFP mice. PloS One *5*, e15915.

Young, S.N. (2013). The effect of raising and lowering tryptophan levels on human mood and social behaviour. Philosophical Transactions of the Royal Society of London Series B, Biological Sciences *368*, 20110375.

Chapter 3 references

Alekseyenko, O.V., Lee, C., and Kravitz, E.A. (2010). Targeted manipulation of serotonergic neurotransmission affects the escalation of aggression in adult male Drosophila melanogaster. PloS One *5*, e10806.

Amat, J., Baratta, M.V., Paul, E., Bland, S.T., Watkins, L.R., and Maier, S.F. (2005). Medial prefrontal cortex determines how stressor controllability affects behavior and dorsal raphe nucleus. Nature Neuroscience *8*, 365-371.

Amat, J., Paul, E., Zarza, C., Watkins, L.R., and Maier, S.F. (2006). Previous experience with behavioral control over stress blocks the behavioral and dorsal raphe nucleus activating effects of later uncontrollable stress: role of the ventral medial prefrontal cortex. Journal of Neuroscience *26*, 13264-13272.

Bang, S.J., and Commons, K.G. (2012). Forebrain GABAergic projections from the dorsal raphe nucleus identified by using GAD67-GFP knock-in mice. Journal of Comparative Neurology *520*, 4157-4167.

Bang, S.J., Jensen, P., Dymecki, S.M., and Commons, K.G. (2012). Projections and interconnections of genetically defined serotonin neurons in mice. European Journal of Neuroscience *35*, 85-96.

Beck, S.G., Pan, Y.-Z., Akanwa, A.C., and Kirby, L.G. (2004). Median and dorsal raphe neurons are not electrophysiologically identical. Journal of Neurophysiology *91*, 994-1005.

Bond, A.J. (2005). Antidepressant treatments and human aggression. European Journal of Pharmacology *526*, 218-225.

Bruchas, M.R., Schindler, A.G., Shankar, H., Messinger, D.I., Miyatake, M., Land, B.B., Lemos, J.C., Hagan, C.E., Neumaier, J.F., Quintana, A.*, et al.* (2011). Selective p38α MAPK Deletion in Serotonergic Neurons Produces Stress Resilience in Models of Depression and Addiction. Neuron *71*, 498-511.

Calhoun, M.E., Jucker, M., Martin, L.J., Thinakaran, G., Price, D.L., and Mouton, P.R. (1996). Comparative evaluation of synaptophysin-based methods for quantification of synapses. Journal of Neurocytology *25*, 821-828.

Calizo, L.H., Akanwa, A., Ma, X., Pan, Y.-Z., Lemos, J.C., Craige, C., Heemstra, L.a., and Beck, S.G. (2011). Raphe serotonin neurons are not homogenous: electrophysiological, morphological and neurochemical evidence. Neuropharmacology *61*, 524-543.

Canli, T., and Lesch, K.-P. (2007). Long story short: the serotonin transporter in emotion regulation and social cognition. Nature Neuroscience *10*, 1103-1109.

Celada, P., Puig, M.V., Casanovas, J.M., Guillazo, G., and Artigas, F. (2001). Control of dorsal raphe serotonergic neurons by the medial prefrontal cortex: Involvement of serotonin-1A, GABA(A), and glutamate receptors. Journal of Neuroscience *21*, 9917-9929.

Celada, P., Puig, M.V., Martín-Ruiz, R., Casanovas, J.M., and Artigas, F. (2002). Control of the serotonergic system by the medial prefrontal cortex: potential role in the etiology of PTSD and depressive disorders. Neurotoxicity Research *4*, 409-419.

Challis, C., Boulden, J., Veerakumar, A., Espallergues, J., Vassoler, F.M., Pierce, R.C., Beck, S.G., and Berton, O. (2013). Raphe GABAergic neurons mediate the acquisition of avoidance after social defeat. Journal of Neuroscience *33*, 13978-13988, 13988a.

Chang, S.W.C., Brent, L.J.N., Adams, G.K., Klein, J.T., Pearson, J.M., Watson, K.K., and Platt, M.L. (2013). Neuroethology of primate social behavior. Proceedings of the National Academy of Sciences of the United States of America *110 Suppl*, 10387-10394.

Christianson, J.P., Thompson, B.M., Watkins, L.R., and Maier, S.F. (2009). Medial prefrontal cortical activation modulates the impact of controllable and uncontrollable stressor exposure on a social exploration test of anxiety in the rat. Stress *12*, 445-450.

Cools, R., Robinson, O.J., and Sahakian, B. (2008). Acute tryptophan depletion in healthy volunteers enhances punishment prediction but does not affect reward prediction. Neuropsychopharmacology : official publication of the American College of Neuropsychopharmacology *33*, 2291-2299.

Crawford, L.K., Craige, C.P., and Beck, S.G. (2010). Increased intrinsic excitability of lateral wing serotonin neurons of the dorsal raphe: a mechanism for selective activation in stress circuits. Journal of Neurophysiology *103*, 2652-2663.

Crawford, L.K., Craige, C.P., and Beck, S.G. (2011). Glutamatergic input is selectively increased in dorsal raphe subfield 5-HT neurons: role of morphology, topography and selective innervation. European Journal of Neuroscience *34*, 1794-1806.

Crawford, L.K., Rahman, S.F., and Beck, S.G. (2013). Social stress alters inhibitory synaptic input to distinct subpopulations of raphe serotonin neurons. ACS Chemical Neuroscience *4*, 200-209.

Crockett, M.J., Clark, L., Apergis-Schoute, A.M., Morein-Zamir, S., and Robbins, T.W. (2012). Serotonin modulates the effects of pavlovian aversive predictions on response vigor. Neuropsychopharmacology *37*, 2244-2252.

Cusi, A.M., Nazarov, A., Holshausen, K., Macqueen, G.M., and McKinnon, M.C. (2012). Systematic review of the neural basis of social cognition in patients with mood disorders. Journal of Psychiatry & Neuroscience *37*, 154-169.

Dayan, P., and Huys, Q.J.M. (2009). Serotonin in affective control. Annual Review of Neuroscience *32*, 95-126.

Deakin, J.F., and Graeff, F.G. (1991). 5-HT and mechanisms of defence. Journal of psychopharmacology *5*, 305-315.

Derntl, B., Seidel, E.-M., Eickhoff, S.B., Kellermann, T., Gur, R.C., Schneider, F., and Habel, U. (2011). Neural correlates of social approach and withdrawal in patients with major depression. Social Neuroscience *6*, 482-501.

Espallergues, J., Teegarden, S.L., Veerakumar, A., Boulden, J., Challis, C., Jochems, J., Chan, M., Petersen, T., Deneris, E., Matthias, P.*, et al.* (2012). HDAC6 Regulates Glucocorticoid Receptor Signaling in Serotonin Pathways with Critical Impact on Stress Resilience. Journal of Neuroscience *32*, 4400-4416.

Golden, S.A., Covington, H.E., Berton, O., and Russo, S.J. (2011). A standardized protocol for repeated social defeat stress in mice. Nature Protocols *6*, 1183-1191.

Hajós, M., Allers, K.a., Jennings, K., Sharp, T., Charette, G., Sík, A., and Kocsis, B. (2007). Neurochemical identification of stereotypic burst-firing neurons in the rat dorsal raphe nucleus using juxtacellular labelling methods. European Journal of Neuroscience *25*, 119-126.

Hamani, C., Diwan, M., Macedo, C.E., Brandão, M.L., Shumake, J., Gonzalez-lima, F., Raymond, R., Lozano, A.M., Fletcher, P.J., and Nobrega, J.N. (2010). Antidepressant-Like Effects of Medial Prefrontal Cortex Deep Brain Stimulation in Rats. Biological Psychiatry *67*, 117-124.

Harmer, C.J., and Cowen, P.J. (2013). 'It's the way that you look at it'--a cognitive neuropsychological account of SSRI action in depression. Philosophical Transactions of the Royal Society of London Series B, Biological Sciences *368*, 20120407.

Heuer, K., Rinck, M., and Becker, E.S. (2007). Avoidance of emotional facial expressions in social anxiety: The Approach-Avoidance Task. Behaviour Research and Therapy *45*, 2990-3001.

Howerton, A.R., Roland, A.V., Fluharty, J.M., Marshall, A., Chen, A., Daniels, D., Beck, S.G., and Bale, T.L. (2013). Sex Differences in Corticotropin-Releasing Factor Receptor-1 Action Within the Dorsal Raphe Nucleus in Stress Responsivity. Biological Psychiatry.

Jankowski, M.P., and Sesack, S.R. (2004). Prefrontal cortical projections to the rat dorsal raphe nucleus: ultrastructural features and associations with serotonin and gamma-aminobutyric acid neurons. Journal of Comparative Neurology *468*, 518-529.
Ji, G., and Neugebauer, V. (2012). Modulation of medial prefrontal cortical activity using in vivo recordings and optogenetics. Molecular Brain *5*, 36.
Knutson, B., Wolkowitz, O.M., Cole, S.W., Chan, T., Moore, E.A., Johnson, R.C., Terpstra, J., Turner, R.A., and Reus, V.I. (1998). Selective Alteration of Personality and Social Behavior by Serotonergic Intervention. American Journal of Psychiatry *155*, 373-379.
Krishnan, V., Han, M.-H., Graham, D.L., Berton, O., Renthal, W., Russo, S.J., Laplant, Q., Graham, A., Lutter, M., Lagace, D.C.*, et al.* (2007). Molecular adaptations underlying susceptibility and resistance to social defeat in brain reward regions. Cell *131*, 391-404.
Kumar, S., Black, S.J., Hultman, R., Szabo, S.T., Demaio, K.D., Du, J., Katz, B.M., Feng, G., Covington, H.E., and Dzirasa, K. (2013). Cortical control of affective networks. Journal of Neuroscience *33*, 1116-1129.
Lammel, S., Tye, K.M., and Warden, M.R. (2014). Progress in understanding mood disorders: optogenetic dissection of neural circuits. Genes, Brain, and Behavior *13*, 38-51.
Madisen, L., Zwingman, T.a., Sunkin, S.M., Oh, S.W., Zariwala, H.a., Gu, H., Ng, L.L., Palmiter, R.D., Hawrylycz, M.J., Jones, A.R.*, et al.* (2010). A robust and high-throughput Cre reporting and characterization system for the whole mouse brain. Nature Neuroscience *13*, 133-140.
Malatynska, E., Rapp, R., Harrawood, D., and Tunnicliff, G. (2005). Submissive behavior in mice as a test for antidepressant drug activity. Pharmacology Biochemistry and Behavior *82*, 306-313.
Mattis, J., Tye, K.M., Ferenczi, E.A., Ramakrishnan, C., O'Shea, D.J., Prakash, R., Gunaydin, L.A., Hyun, M., Fenno, L.E., Gradinaru, V.*, et al.* (2012). Principles for applying optogenetic tools derived from direct comparative analysis of microbial opsins. Nature Methods *9*, 159-172.
Moser, J.S., Huppert, J.D., Foa, E.B., and Simons, R.F. (2012). Interpretation of ambiguous social scenarios in social phobia and depression: evidence from event-related brain potentials. Biological Psychology *89*, 387-397.
Munafò, M.R., Hayward, G., and Harmer, C. (2006). Selective processing of social threat cues following acute tryptophan depletion. Journal of psychopharmacology (Oxford, England) *20*, 33-39.
O'Connell, L.A., and Hofmann, H.A. (2012). Evolution of a vertebrate social decision-making network. Science *336*, 1154-1157.
Oliveira, R.F. (2012). Social plasticity in fish: integrating mechanisms and function. Journal of Fish Biology *81*, 2127-2150.
Passamonti, L., Crockett, M.J., Apergis-Schoute, A.M., Clark, L., Rowe, J.B., Calder, A.J., and Robbins, T.W. (2012). Effects of acute tryptophan depletion on prefrontal-amygdala connectivity while viewing facial signals of aggression. Biological Psychiatry *71*, 36-43.
Penn, J.K.M., Zito, M.F., and Kravitz, E.A. (2010). A single social defeat reduces aggression in a highly aggressive strain of Drosophila. Proceedings of the National Academy of Sciences of the United States of America *107*, 12682-12686.
Raleigh, M.J., McGuire, M.T., Brammer, G.L., Pollack, D.B., and Yuwiler, A. (1991). Serotonergic mechanisms promote dominance acquisition in adult male vervet monkeys. Brain Research *559*, 181-190.
Roy, M., Shohamy, D., and Wager, T.D. (2012). Ventromedial prefrontal-subcortical systems and the generation of affective meaning. Trends in Cognitive Sciences *16*, 147-156.
Scott, M.M., Wylie, C.J., Lerch, J.K., Murphy, R., Lobur, K., Herlitze, S., Jiang, W., Conlon, R.a., Strowbridge, B.W., and Deneris, E.S. (2005). A genetic approach to access serotonin neurons for in vivo and in vitro studies. Proceedings of the National Academy of Sciences of the United States of America *102*, 16472-16477.
Seidel, E.-M., Habel, U., Finkelmeyer, A., Schneider, F., Gur, R.C., and Derntl, B. (2010). Implicit and explicit behavioral tendencies in male and female depression. Psychiatry Research *177*, 124-130.
Slattery, D.A., Neumann, I.D., and Cryan, J.F. (2011). Transient inactivation of the infralimbic cortex induces antidepressant-like effects in the rat. Journal of Psychopharmacology *25*, 1295-1303.
Soubrie, P., Martin, P., El Mestikawy, S., Thiebot, M.H., Simon, P., and Hamon, M. (1986). The lesion of serotonergic neurons does not prevent antidepressant-induced reversal of escape failures produced by inescapable shocks in rats. Pharmacology Biochemistry and Behavior *25*, 1-6.

Stuhrmann, A., Suslow, T., and Dannlowski, U. (2011). Facial emotion processing in major depression: a systematic review of neuroimaging findings. Biology of Mood & Anxiety Disorders *1*, 10.

Takahashi, A., Schilit, A.N., Kim, J., Debold, J.F., Koide, T., and Miczek, K.A. (2012). Behavioral characterization of escalated aggression induced by GABA(B) receptor activation in the dorsal raphe nucleus. Psychopharmacology *224*, 155-166.

Takahashi, A., Shimamoto, A., Boyson, C.O., DeBold, J.F., and Miczek, K.A. (2010). GABA(B) receptor modulation of serotonin neurons in the dorsal raphé nucleus and escalation of aggression in mice. Journal of Neuroscience *30*, 11771-11780.

Taniguchi, H., He, M., Wu, P., Kim, S., Paik, R., Sugino, K., Kvitsiani, D., Kvitsani, D., Fu, Y., Lu, J.*, et al.* (2011). A resource of Cre driver lines for genetic targeting of GABAergic neurons in cerebral cortex. Neuron *71*, 995-1013.

Todorov, A. (2008). Evaluating faces on trustworthiness: an extension of systems for recognition of emotions signaling approach/avoidance behaviors. Annals of the New York Academy of Sciences *1124*, 208-224.

Tse, W.S., and Bond, A.J. (2004). The impact of depression on social skills. Journal of Nervous and Mental Disease *192*, 260-268.

Tsien, J.Z., Chen, D.F., Gerber, D., Tom, C., Mercer, E.H., Anderson, D.J., Mayford, M., Kandel, E.R., and Tonegawa, S. (1996). Subregion- and cell type-restricted gene knockout in mouse brain. Cell *87*, 1317-1326.

Varga, V., Kocsis, B., and Sharp, T. (2003). Electrophysiological evidence for convergence of inputs from the medial prefrontal cortex and lateral habenula on single neurons in the dorsal raphe nucleus. European Journal of Neuroscience *17*, 280-286.

Varga, V., Székely, a.D., Csillag, a., Sharp, T., and Hajós, M. (2001). Evidence for a role of GABA interneurones in the cortical modulation of midbrain 5-hydroxytryptamine neurones. Neuroscience *106*, 783-792.

Veerakumar, A., Challis, C., Gupta, P., Da, J., Upadhyay, A., Beck, S.G., and Berton, O. (2013). Antidepressant-like effects of cortical deep brain stimulation coincide with pro-neuroplastic adaptations of serotonin systems. Biological Psychiatry *76*, 203–212.

Volman, I., Roelofs, K., Koch, S., Verhagen, L., and Toni, I. (2011). Anterior prefrontal cortex inhibition impairs control over social emotional actions. Current Biology *21*, 1766-1770.

Warden, M.R., Selimbeyoglu, A., Mirzabekov, J.J., Lo, M., Thompson, K.R., Kim, S.-Y., Adhikari, A., Tye, K.M., Frank, L.M., and Deisseroth, K. (2012). A prefrontal cortex–brainstem neuronal projection that controls response to behavioural challenge. Nature *492*, 428-432.

Waselus, M., Nazzaro, C., Valentino, R.J., and Van Bockstaele, E.J. (2009). Stress-induced redistribution of corticotropin-releasing factor receptor subtypes in the dorsal raphe nucleus. Biological Psychiatry *66*, 76-83.

Young, S.N. (2013). The effect of raising and lowering tryptophan levels on human mood and social behaviour. Philosophical Transactions of the Royal Society of London Series B, Biological Sciences *368*, 20110375.

Young, S.N., and Leyton, M. (2002). The role of serotonin in human mood and social interaction. Pharmacology Biochemistry and Behavior *71*, 857-865.

Chapter 4 references

Agterberg, M.J.H., Spoelstra, E.N., van der Wijst, S., Brakkee, J.H., Wiegant, V.M., Hamelink, R., Brouns, K., Westerink, B.H., and Remie, R. (2010). Evaluation of temperature rise and bonding strength in cements used for permanent head attachments in rats and mice. Laboratory animals *44*, 264-270.

Atasoy, D., Aponte, Y., Su, H.H., and Sternson, S.M. (2008). A FLEX switch targets Channelrhodopsin-2 to multiple cell types for imaging and long-range circuit mapping. Journal of Neuroscience *28*, 7025-7030.

Berton, O., McClung, C.a., Dileone, R.J., Krishnan, V., Renthal, W., Russo, S.J., Graham, D., Tsankova, N.M., Bolanos, C.a., Rios, M.*, et al.* (2006). Essential role of BDNF in the mesolimbic dopamine pathway in social defeat stress. Science *311*, 864-868.

Budisic, M., Mislav, B., Karlovic, D., Dalibor, K., Trkanjec, Z., Zlatko, T., Lovrencic-Huzjan, A., Arijana, L.-H., Vukovic, V., Vlasta, V.*, et al.* (2010). Brainstem raphe lesion in patients with major depressive disorder and in patients with suicidal ideation recorded on transcranial sonography. European archives of psychiatry and clinical neuroscience *260*, 203-208.

Calizo, L.H., Akanwa, A., Ma, X., Pan, Y.-Z., Lemos, J.C., Craige, C., Heemstra, L.a., and Beck, S.G. (2011). Raphe serotonin neurons are not homogenous: electrophysiological, morphological and neurochemical evidence. Neuropharmacology *61*, 524-543.

Celada, P., Puig, M.V., Casanovas, J.M., Guillazo, G., and Artigas, F. (2001). Control of dorsal raphe serotonergic neurons by the medial prefrontal cortex: Involvement of serotonin-1A, GABA(A), and glutamate receptors. Journal of Neuroscience *21*, 9917-9929.

Challis, C., Boulden, J., Veerakumar, A., Espallergues, J., Vassoler, F.M., Pierce, R.C., Beck, S.G., and Berton, O. (2013). Raphe GABAergic neurons mediate the acquisition of avoidance after social defeat. Journal of Neuroscience *33*, 13978-13988, 13988a.

Commons, K.G., Beck, S.G., and Bey, V.W. (2005). Two populations of glutamatergic axons in the rat dorsal raphe nucleus defined by the vesicular glutamate transporters 1 and 2. European Journal of Neuroscience *21*, 1577-1586.

Covington, H.E., Lobo, M.K., Maze, I., Vialou, V., Hyman, J.M., Zaman, S., LaPlant, Q., Mouzon, E., Ghose, S., Tamminga, C.a.*, et al.* (2010). Antidepressant effect of optogenetic stimulation of the medial prefrontal cortex. Journal of Neuroscience *30*, 16082-16090.

Crawford, L.K., Craige, C.P., and Beck, S.G. (2010). Increased intrinsic excitability of lateral wing serotonin neurons of the dorsal raphe: a mechanism for selective activation in stress circuits. Journal of Neurophysiology *103*, 2652-2663.

Crawford, L.K., Craige, C.P., and Beck, S.G. (2011). Glutamatergic input is selectively increased in dorsal raphe subfield 5-HT neurons: role of morphology, topography and selective innervation. European Journal of Neuroscience *34*, 1794-1806.

Crawford, L.K., Rahman, S.F., and Beck, S.G. (2013). Social stress alters inhibitory synaptic input to distinct subpopulations of raphe serotonin neurons. ACS Chemical Neuroscience *4*, 200-209.

De Paola, V., Holtmaat, A., Knott, G., Song, S., Wilbrecht, L., Caroni, P., and Svoboda, K. (2006). Cell type-specific structural plasticity of axonal branches and boutons in the adult neocortex. Neuron *49*, 861-875.

De-Miguel, F.F., and Trueta, C. (2005). Synaptic and Extrasynaptic Secretion of Serotonin. Cellular and Molecular Neurobiology *25*, 297-312.

Deneris, E.S., and Wyler, S.C. (2012). Serotonergic transcriptional networks and potential importance to mental health. Nature neuroscience *15*, 519-527.

Dournes, C., Beeské, S., Belzung, C., and Griebel, G. (2013). Deep brain stimulation in treatment-resistant depression in mice: comparison with the CRF1 antagonist, SSR125543. Progress in neuro-psychopharmacology & biological psychiatry *40*, 213-220.

Dumitriu, D., Berger, S.I., Hamo, C., Hara, Y., Bailey, M., Hamo, A., Grossman, Y.S., Janssen, W.G., and Morrison, J.H. (2012). Vamping: stereology-based automated quantification of fluorescent puncta size and density. Journal of neuroscience methods *209*, 97-105.

Espallergues, J., Teegarden, S.L., Veerakumar, A., Boulden, J., Challis, C., Jochems, J., Chan, M., Petersen, T., Deneris, E., Matthias, P.*, et al.* (2012). HDAC6 Regulates Glucocorticoid Receptor Signaling in Serotonin Pathways with Critical Impact on Stress Resilience. Journal of Neuroscience *32*, 4400-4416.

Falowski, S.M., Sharan, A., Reyes, B.A.S., Sikkema, C., Szot, P., and Van Bockstaele, E.J. (2011). An evaluation of neuroplasticity and behavior after deep brain stimulation of the nucleus accumbens in an animal model of depression. Neurosurgery *69*, 1281-1290.

Freedman, L.J., Insel, T.R., and Smith, Y. (2000). Subcortical projections of area 25 (subgenual cortex) of the macaque monkey. Journal of Comparative Neurology *421*, 172-188.

Gogolla, N., Galimberti, I., and Caroni, P. (2007). Structural plasticity of axon terminals in the adult. Current Opinion in Neurobiology *17*, 516-524.

Golden, S.A., Christoffel, D.J., Heshmati, M., Hodes, G.E., Magida, J., Davis, K., Cahill, M.E., Dias, C., Ribeiro, E., Ables, J.L.*, et al.* (2013). Epigenetic regulation of RAC1 induces synaptic remodeling in stress disorders and depression. Nature Medicine *19*, 337-344.

Golden, S.A., Covington, H.E., Berton, O., and Russo, S.J. (2011). A standardized protocol for repeated social defeat stress in mice. Nature Protocols *6*, 1183-1191.

Grinevich, V., Brecht, M., and Osten, P. (2005). Monosynaptic pathway from rat vibrissa motor cortex to facial motor neurons revealed by lentivirus-based axonal tracing. Journal of Neuroscience *25*, 8250-8258.

Halpern, C.H., Tekriwal, A., Santollo, J., Keating, J.G., Wolf, J.A., Daniels, D., and Bale, T.L. (2013). Amelioration of binge eating by nucleus accumbens shell deep brain stimulation in mice involves D2 receptor modulation. Journal of Neuroscience *33*, 7122-7129.

Hamani, C., Diwan, M., Macedo, C.E., Brandão, M.L., Shumake, J., Gonzalez-lima, F., Raymond, R., Lozano, A.M., Fletcher, P.J., and Nobrega, J.N. (2010). Antidepressant-Like Effects of Medial Prefrontal Cortex Deep Brain Stimulation in Rats. Biological Psychiatry *67*, 117-124.

Hamani, C., Machado, D.C., Hipólide, D.C., Dubiela, F.P., Suchecki, D., Macedo, C.E., Tescarollo, F., Martins, U., Covolan, L., and Nobrega, J.N. (2012). Deep Brain Stimulation Reverses Anhedonic-Like Behavior in a Chronic Model of Depression: Role of Serotonin and Brain Derived Neurotrophic Factor. Biological Psychiatry *71*, 30-35.

Hamani, C., Mayberg, H., Stone, S., Laxton, A., Haber, S., and Lozano, A.M. (2011). The subcallosal cingulate gyrus in the context of major depression. Biological psychiatry *69*, 301-308.

Hamani, C., and Nóbrega, J.N. (2010). Deep brain stimulation in clinical trials and animal models of depression. European Journal of Neuroscience *32*, 1109-1117.

Henn, F.A. (2012). Circuits, cells, and synapses: toward a new target for deep brain stimulation in depression. Neuropsychopharmacology : official publication of the American College of Neuropsychopharmacology *37*, 307-308.

Hercher, C., Turecki, G., and Mechawar, N. (2009). Through the looking glass: examining neuroanatomical evidence for cellular alterations in major depression. Journal of psychiatric research *43*, 947-961.

Holtzheimer, P.E., Kelley, M.E., Gross, R.E., Filkowski, M.M., Garlow, S.J., Barrocas, A., Wint, D., Craighead, M.C., Kozarsky, J., Chismar, R.*, et al.* (2012). Subcallosal cingulate deep brain stimulation for treatment-resistant unipolar and bipolar depression. Archives of general psychiatry *69*, 150-158.

Hoover, W.B., and Vertes, R.P. (2007). Anatomical analysis of afferent projections to the medial prefrontal cortex in the rat. Brain structure & function *212*, 149-179.

Hou, C., Xue, L., Feng, J., Zhang, L., Wang, Y., Chen, L., Wang, T., Zhang, Q.J., and Liu, J. (2012). Unilateral lesion of the nigrostriatal pathway decreases the response of GABA interneurons in the dorsal raphe nucleus to 5-HT(1A) receptor stimulation in the rat. Neurochemistry International *61*, 1344-1356.

Jankowski, M.P., and Sesack, S.R. (2004). Prefrontal cortical projections to the rat dorsal raphe nucleus: ultrastructural features and associations with serotonin and gamma-aminobutyric acid neurons. Journal of Comparative Neurology *468*, 518-529.

Jin, I., Udo, H., and Hawkins, R.D. (2011). Rapid increase in clusters of synaptophysin at onset of homosynaptic potentiation in Aplysia. Proceedings of the National Academy of Sciences of the United States of America *108*, 11656-11661.

Kelsch, W., Sim, S., and Lois, C. (2010). Watching synaptogenesis in the adult brain. Annual Review of Neuroscience *33*, 131-149.

Kerman, I.A., Bernard, R., Bunney, W.E., Jones, E.G., Schatzberg, A.F., Myers, R.M., Barchas, J.D., Akil, H., Watson, S.J., and Thompson, R.C. (2012). Evidence for transcriptional factor dysregulation in the dorsal raphe nucleus of patients with major depressive disorder. Frontiers in neuroscience *6*, 135.

Kumar, S., Black, S.J., Hultman, R., Szabo, S.T., Demaio, K.D., Du, J., Katz, B.M., Feng, G., Covington, H.E., and Dzirasa, K. (2013). Cortical control of affective networks. Journal of Neuroscience *33*, 1116-1129.

Li, B., Piriz, J., Mirrione, M., Chung, C., Proulx, C.D., Schulz, D., Henn, F., and Malinow, R. (2011). Synaptic potentiation onto habenula neurons in the learned helplessness model of depression. Nature *470*, 535-539.

Li, L., Tasic, B., Micheva, K.D., Ivanov, V.M., Spletter, M.L., Smith, S.J., and Luo, L. (2010). Visualizing the distribution of synapses from individual neurons in the mouse brain. PloS One *5*, e11503.

Lozano, A.M., Mayberg, H.S., Giacobbe, P., Hamani, C., Craddock, R.C., and Kennedy, S.H. (2008). Subcallosal cingulate gyrus deep brain stimulation for treatment-resistant depression. Biological Psychiatry *64*, 461-467.

Madisen, L., Zwingman, T.a., Sunkin, S.M., Oh, S.W., Zariwala, H.a., Gu, H., Ng, L.L., Palmiter, R.D., Hawrylycz, M.J., Jones, A.R.*, et al.* (2010). A robust and high-throughput Cre reporting and characterization system for the whole mouse brain. Nature Neuroscience *13*, 133-140.

Matthews, P.R., and Harrison, P.J. (2012). A morphometric, immunohistochemical, and in situ hybridization study of the dorsal raphe nucleus in major depression, bipolar disorder, schizophrenia, and suicide. Journal of affective disorders *137*, 125-134.

Mayberg, H.S., Lozano, A.M., Voon, V., McNeely, H.E., Seminowicz, D., Hamani, C., Schwalb, J.M., and Kennedy, S.H. (2005). Deep brain stimulation for treatment-resistant depression. Neuron *45*, 651-660.

Mitra, R., Jadhav, S., McEwen, B.S., Vyas, A., and Chattarji, S. (2005). Stress duration modulates the spatiotemporal patterns of spine formation in the basolateral amygdala. Proceedings of the National Academy of Sciences of the United States of America *102*, 9371-9376.

Montgomery, E.B. (2008). Subthalamic nucleus neuronal activity in Parkinson's disease and epilepsy subjects. Parkinsonism & related disorders *14*, 120-125.

Perez-Caballero, L., Pérez-Egea, R., Romero-Grimaldi, C., Puigdemont, D., Molet, J., Caso, J.-R., Mico, J.-A., Pérez, V., Leza, J.-C., and Berrocoso, E. (2014). Early responses to deep brain stimulation in depression are modulated by anti-inflammatory drugs. Molecular psychiatry *19*, 607-614.

Prange, O., Wong, T.P., Gerrow, K., Wang, Y.T., and El-Husseini, A. (2004). A balance between excitatory and inhibitory synapses is controlled by PSD-95 and neuroligin. Proceedings of the National Academy of Sciences of the United States of America *101*, 13915-13920.

Rylander, D., Parent, M., O'Sullivan, S.S., Dovero, S., Lees, A.J., Bezard, E., Descarries, L., and Cenci, M.A. (2010). Maladaptive plasticity of serotonin axon terminals in levodopa-induced dyskinesia. Annals of neurology *68*, 619-628.

Schmuckermair, C., Gaburro, S., Sah, A., Landgraf, R., Sartori, S.B., and Singewald, N. (2013). Behavioral and neurobiological effects of deep brain stimulation in a mouse model of high anxiety- and depression-like behavior. Neuropsychopharmacology *38*, 1234-1244.

Scott, M.M., Wylie, C.J., Lerch, J.K., Murphy, R., Lobur, K., Herlitze, S., Jiang, W., Conlon, R.a., Strowbridge, B.W., and Deneris, E.S. (2005). A genetic approach to access serotonin neurons for in vivo and in vitro studies. Proceedings of the National Academy of Sciences of the United States of America *102*, 16472-16477.

Shepherd, G.M.G., and Harris, K.M. (1998). Three-Dimensional Structure and Composition of CA3right-arrowCA1 Axons in Rat Hippocampal Slices: Implications for Presynaptic Connectivity and Compartmentalization. Journal of Neuroscience *18*, 8300-8310.

Soiza-Reilly, M., and Commons, K.G. (2011). Glutamatergic drive of the dorsal raphe nucleus. Journal of Chemical Neuroanatomy *41*, 247-255.

Stettler, D.D., Yamahachi, H., Li, W., Denk, W., and Gilbert, C.D. (2006). Axons and synaptic boutons are highly dynamic in adult visual cortex. Neuron *49*, 877-887.

van Elburg, R.A.J., and van Ooyen, A. (2010). Impact of dendritic size and dendritic topology on burst firing in pyramidal cells. PLoS computational biology *6*, e1000781.

Varga, V., Kocsis, B., and Sharp, T. (2003). Electrophysiological evidence for convergence of inputs from the medial prefrontal cortex and lateral habenula on single neurons in the dorsal raphe nucleus. European Journal of Neuroscience *17*, 280-286.

Varga, V., Székely, a.D., Csillag, a., Sharp, T., and Hajós, M. (2001). Evidence for a role of GABA interneurones in the cortical modulation of midbrain 5-hydroxytryptamine neurones. Neuroscience *106*, 783-792.

Vassoler, F.M., Schmidt, H.D., Gerard, M.E., Famous, K.R., Ciraulo, D.A., Kornetsky, C., Knapp, C.M., and Pierce, R.C. (2008). Deep brain stimulation of the nucleus accumbens shell attenuates cocaine priming-induced reinstatement of drug seeking in rats. Journal of Neuroscience *28*, 8735-8739.

Vassoler, F.M., White, S.L., Hopkins, T.J., Guercio, L.A., Espallergues, J., Berton, O., Schmidt, H.D., and Pierce, R.C. (2013). Deep brain stimulation of the nucleus accumbens shell attenuates cocaine reinstatement through local and antidromic activation. Journal of Neuroscience *33*, 14446-14454.

Vertes, R.P. (2004). Differential projections of the infralimbic and prelimbic cortex in the rat. Synapse *51*, 32-58.

Warden, M.R., Selimbeyoglu, A., Mirzabekov, J.J., Lo, M., Thompson, K.R., Kim, S.-Y., Adhikari, A., Tye, K.M., Frank, L.M., and Deisseroth, K. (2012). A prefrontal cortex–brainstem neuronal projection that controls response to behavioural challenge. Nature *492*, 428-432.

Zhang, Z.-W., Kang, J.I., and Vaucher, E. (2011). Axonal varicosity density as an index of local neuronal interactions. PloS one *6*, e22543.

Chapter 5 references

Amemori, K.-i., and Graybiel, A.M. (2012). Localized microstimulation of primate pregenual cingulate cortex induces negative decision-making. Nature neuroscience *15*, 776-785.

Anwyl, R. (1999). Metabotropic glutamate receptors: electrophysiological properties and role in plasticity. Brain Research Reviews *29*, 83-120.

Bang, S.J., Jensen, P., Dymecki, S.M., and Commons, K.G. (2012). Projections and interconnections of genetically defined serotonin neurons in mice. European Journal of Neuroscience *35*, 85-96.

Bilderbeck, A.C., McCabe, C., Wakeley, J., McGlone, F., Harris, T., Cowen, P.J., and Rogers, R.D. (2011). Serotonergic activity influences the cognitive appraisal of close intimate relationships in healthy adults. Biological Psychiatry *69*, 720-725.

Bliss, T.V., and Collingridge, G.L. (1993). A synaptic model of memory: long-term potentiation in the hippocampus. Nature *361*, 31-39.

Calizo, L.H., Akanwa, A., Ma, X., Pan, Y.-Z., Lemos, J.C., Craige, C., Heemstra, L.a., and Beck, S.G. (2011). Raphe serotonin neurons are not homogenous: electrophysiological, morphological and neurochemical evidence. Neuropharmacology *61*, 524-543.

Celada, P., Puig, M.V., Casanovas, J.M., Guillazo, G., and Artigas, F. (2001). Control of dorsal raphe serotonergic neurons by the medial prefrontal cortex: Involvement of serotonin-1A, GABA(A), and glutamate receptors. Journal of Neuroscience *21*, 9917-9929.

Chaudhury, D., Walsh, J.J., Friedman, A.K., Juarez, B., Ku, S.M., Koo, J.W., Ferguson, D., Tsai, H.-C., Pomeranz, L., Christoffel, D.J*., et al.* (2012). Rapid regulation of depression-related behaviours by control of midbrain dopamine neurons. Nature *493*, 532-536.

Chikazoe, J., Lee, D.H., Kriegeskorte, N., and Anderson, A.K. (2014). Population coding of affect across stimuli, modalities and individuals. Nature neuroscience *17*, 1114-1122.

Collingridge, G.L., and Bliss, T.V.P. (1987). NMDA receptors - their role in long-term potentiation. Trends in Neurosciences *10*, 288-293.

Davidson, R.J., Ekman, P., Saron, C.D., Senulis, J.A., and Friesen, W.V. (1990). Approach-withdrawal and cerebral asymmetry: Emotional expression and brain physiology: I. Journal of Personality and Social Psychology *58*, 330-341.

Derntl, B., Seidel, E.-M., Eickhoff, S.B., Kellermann, T., Gur, R.C., Schneider, F., and Habel, U. (2011). Neural correlates of social approach and withdrawal in patients with major depression. Social Neuroscience *6*, 482-501.

Drevets, W.C., Price, J.L., and Furey, M.L. (2008). Brain structural and functional abnormalities in mood disorders: implications for neurocircuitry models of depression. Brain Structure & Function *213*, 93-118.

Elliot, A.J., and Covington, M.V. (2001). Approach and Avoidance Motivation. Educational Psychology Review *13*, 73-92.

Feng, L., Zhao, T., and Kim, J. (2012). Improved synapse detection for mGRASP-assisted brain connectivity mapping. Bioinformatics (Oxford, England) *28*, i25-31.

Fisher, P.M., Meltzer, C.C., Ziolko, S.K., Price, J.C., Moses-Kolko, E.L., Berga, S.L., and Hariri, a.R. (2006). Capacity for 5-HT1A-mediated autoregulation predicts amygdala reactivity. Nature Neuroscience *9*, 1362-1363.

Godard, J., Grondin, S., Baruch, P., and Lafleur, M.F. (2011). Psychosocial and neurocognitive profiles in depressed patients with major depressive disorder and bipolar disorder. Psychiatry Research *190*, 244-252.

Gutman, D.A., Holtzheimer, P.E., Behrens, T.E.J., Johansen-Berg, H., and Mayberg, H.S. (2009). A tractography analysis of two deep brain stimulation white matter targets for depression. Biological psychiatry *65*, 276-282.

Haber, S.N., and Brucker, J.L. (2009). Cognitive and limbic circuits that are affected by deep brain stimulation. Frontiers in Bioscience *14*, 1823-1834.

Jankowski, M.P., and Sesack, S.R. (2004). Prefrontal cortical projections to the rat dorsal raphe nucleus: ultrastructural features and associations with serotonin and gamma-aminobutyric acid neurons. Journal of Comparative Neurology *468*, 518-529.
Johnstone, T., van Reekum, C.M., Urry, H.L., Kalin, N.H., and Davidson, R.J. (2007). Failure to regulate: counterproductive recruitment of top-down prefrontal-subcortical circuitry in major depression. Journal of Neuroscience *27*, 8877-8884.
Kim, J., Zhao, T., Petralia, R.S., Yu, Y., Peng, H., Myers, E., and Magee, J.C. (2011). mGRASP enables mapping mammalian synaptic connectivity with light microscopy. Nature Methods *9*, 96-102.
Kumar, S., Black, S.J., Hultman, R., Szabo, S.T., Demaio, K.D., Du, J., Katz, B.M., Feng, G., Covington, H.E., and Dzirasa, K. (2013). Cortical control of affective networks. Journal of Neuroscience *33*, 1116-1129.
Kwaasteniet, B.d., Ruhe, E., Caan, M., Rive, M., Olabarriaga, S., Groefsema, M., Heesink, L., van Wingen, G., and Denys, D. (2013). Relation Between Structural and Functional Connectivity in Major DepressiveDisorder. Biological Psychiatry *null*.
Lang, P.J., Bradley, M.M., and Cuthbert, B.N. (1990). Emotion, attention, and the startle reflex. Psychological Review *97*, 377-395.
Laxton, A.W., Neimat, J.S., Davis, K.D., Womelsdorf, T., Hutchison, W.D., Dostrovsky, J.O., Hamani, C., Mayberg, H.S., and Lozano, A.M. (2013). Neuronal coding of implicit emotion categories in the subcallosal cortex in patients with depression. Biological psychiatry *74*, 714-719.
LeDoux, J., Cicchetti, P., Xagoraris, A., and Romanski, L. (1990). The lateral amygdaloid nucleus: sensory interface of the amygdala in fear conditioning. J Neurosci *10*, 1062-1069.
Lehman, J.F., Greenberg, B.D., McIntyre, C.C., Rasmussen, S.A., and Haber, S.N. (2011). Rules ventral prefrontal cortical axons use to reach their targets: implications for diffusion tensor imaging tractography and deep brain stimulation for psychiatric illness. The Journal of neuroscience : the official journal of the Society for Neuroscience *31*, 10392-10402.
Liao, C., Feng, Z., Zhou, D., Dai, Q., Xie, B., Ji, B., and Wang, X. (2011). Dysfunction of fronto-limbic brain circuitry in depression. Neuroscience *201*, 231-238.
Liu, Z., Zhou, J., Li, Y., Hu, F., Lu, Y., Ma, M., Feng, Q., Zhang, J.-e., Wang, D., Zeng, J.*, et al.* (2014). Dorsal Raphe Neurons Signal Reward through 5-HT and Glutamate. Neuron *81*, 1360-1374.
Malenka, R.C., and Bear, M.F. (2004). LTP and LTD: an embarrassment of riches. Neuron *44*, 5-21.
Maren, S. (2001). Neurobiology of Pavlovian fear conditioning. Annual review of neuroscience *24*, 897-931.
Mayberg, H.S. (1997). Limbic-cortical dysregulation: a proposed model of depression. Journal of Neuropsychiatry and Clinical Neurosciences *9*, 471-481.
Mayberg, H.S. (2009). Targeted electrode-based modulation of neural circuits for depression. Journal of Clinical Investigation *119*, 717-725.
Mayberg, H.S., Lozano, A.M., Voon, V., McNeely, H.E., Seminowicz, D., Hamani, C., Schwalb, J.M., and Kennedy, S.H. (2005). Deep brain stimulation for treatment-resistant depression. Neuron *45*, 651-660.
Morris, J.S., Ohman, A., and Dolan, R.J. (1998). Conscious and unconscious emotional learning in the human amygdala. Nature *393*, 467-470.
Murray, E.A., Wise, S.P., and Drevets, W.C. (2011). Localization of dysfunction in major depressive disorder: prefrontal cortex and amygdala. Biological Psychiatry *69*, e43-54.
Nieh, E.H., Kim, S.-Y., Namburi, P., and Tye, K.M. (2013). Optogenetic dissection of neural circuits underlying emotional valence and motivated behaviors. Brain research *1511*, 73-92.
Nishitani, N., Nagayasu, K., Asaoka, N., Yamashiro, M., Shirakawa, H., Nakagawa, T., and Kaneko, S. (2014). Raphe AMPA receptors and nicotinic acetylcholine receptors mediate ketamine-induced serotonin release in the rat prefrontal cortex. The international journal of neuropsychopharmacology / official scientific journal of the Collegium Internationale Neuropsychopharmacologicum (CINP) *17*, 1321-1326.
Ohishi, H., Shigemoto, R., Nakanishi, S., and Mizuno, N. (1993). Distribution of the mRNA for a metabotropic glutamate receptor (mGluR3) in the rat brain: an in situ hybridization study. The Journal of comparative neurology *335*, 252-266.
Palazzo, E., Genovese, R., Mariani, L., Siniscalco, D., Marabese, I., De Novellis, V., Rossi, F., and Maione, S. (2004). Metabotropic glutamate receptor 5 and dorsal raphe serotonin release in inflammatory pain in rat. European journal of pharmacology *492*, 169-176.

Panksepp, J. (2005). Affective consciousness: Core emotional feelings in animals and humans. Consciousness and cognition *14*, 30-80.

Riva-Posse, P., Sueng Choi, K., Holtzheimer, P.E., McIntyre, C.C., Gross, R.E., Chaturvedi, A., Crowell, A.L., Garlow, S.J., Rajendra, J.K., and Mayberg, H.S. (2014). Defining Critical White Matter Pathways Mediating Successful Subcallosal Cingulate Deep Brain Stimulation for Treatment-Resistant Depression. Biological Psychiatry.

Robinson, O.J., Overstreet, C., Allen, P.S., Letkiewicz, A., Vytal, K., Pine, D.S., and Grillon, C. (2013). The role of serotonin in the neurocircuitry of negative affective bias: serotonergic modulation of the dorsal medial prefrontal-amygdala 'aversive amplification' circuit. NeuroImage *78*, 217-223.

Rogan, M.T., Stäubli, U.V., and LeDoux, J.E. (1997). Fear conditioning induces associative long-term potentiation in the amygdala. Nature *390*, 604-607.

Seidel, E.-M., Habel, U., Finkelmeyer, A., Schneider, F., Gur, R.C., and Derntl, B. (2010). Implicit and explicit behavioral tendencies in male and female depression. Psychiatry Research *177*, 124-130.

Selvaraj, S., Mouchlianitis, E., Faulkner, P., Turkheimer, F., Cowen, P.J., Roiser, J.P., and Howes, O. (2014). Presynaptic Serotoninergic Regulation of Emotional Processing: A Multimodal Brain Imaging Study. Biological psychiatry.

Shigemoto, R., Nakanishi, S., and Mizuno, N. (1992). Distribution of the mRNA for a metabotropic glutamate receptor (mGluR1) in the central nervous system: an in situ hybridization study in adult and developing rat. The Journal of comparative neurology *322*, 121-135.

Todorov, A. (2008). Evaluating faces on trustworthiness: an extension of systems for recognition of emotions signaling approach/avoidance behaviors. Annals of the New York Academy of Sciences *1124*, 208-224.

Tsvetkov, E., Carlezon, W.A., Benes, F.M., Kandel, E.R., and Bolshakov, V.Y. (2002). Fear Conditioning Occludes LTP-Induced Presynaptic Enhancement of Synaptic Transmission in the Cortical Pathway to the Lateral Amygdala. Neuron *34*, 289-300.

Tye, K.M., Mirzabekov, J.J., Warden, M.R., Ferenczi, E.A., Tsai, H.-C., Finkelstein, J., Kim, S.-Y., Adhikari, A., Thompson, K.R., Andalman, A.S.*, et al.* (2012). Dopamine neurons modulate neural encoding and expression of depression-related behaviour. Nature *493*, 537-541.

Yook, C., Druckmann, S., and Kim, J. (2013). Mapping mammalian synaptic connectivity. Cellular and molecular life sciences *70*, 4747-4757.

Young, S.N. (2013). The effect of raising and lowering tryptophan levels on human mood and social behaviour. Philosophical Transactions of the Royal Society of London Series B, Biological Sciences *368*, 20110375.

Zajonc, R.B. (1984). On the primacy of affect. American Psychologist *39*, 117-123.